UNDERSTANDING THE NON-COVALENT INTERACTIONS IN MACROIONS AND HYBRID MACROMOLECULES

A Dissertation

Presented to

The Graduate Faculty of The University of Akron

In Partial Fulfillment

of the Requirements of the Degree

Doctor of Philosophy

Jing Zhou

December, 2015

UNDERSTANDING THE NON-COVALENT INTERACTIONS IN MACROIONS AND HYBRID MACROMOLECULES

Jing Zhou

Dissertation

Approved:	Accepted:
_____	_____
Advisor Dr. Tianbo Liu	Department Chair Dr. Coleen Pugh
_____	_____
Committee Member Dr. Mesfin Tsige	Dean of the College Dr. Eric Amis
_____	_____
Committee Member Dr. Matthew Becker	Dean of the Graduate School Dr. Chand Midha
_____	_____
Committee Member Dr. Toshikazu Miyoshi	Date
_____	
Committee Member Dr. Alamgir Karim	

ABSTRACT

Self-assembly is known as a route to achieve order from disorder at various length scales, ubiquitously in nature, science and technology. Noncovanlent interactions such as electrostatic interactions, hydrophobic interactions, metal coordination and hydrogen bonding have been utilized extensively in past decades to build and control macromolecular self-assemblies.

Hydrophilic macroions, with sizes ranging between simple ions (point charges valid for the Debye-Hückel Theory) and colloidal suspensions (usually described by the DLVO theory), demonstrate unique solution behavior by self-assembling into ordered, single layer, hollow, spherical "blackberry" structures. Counterion mediated attraction is considered as the main driving force for the self-assembly behavior. Herein, we investigated the solution behavior of ionic polyhedral oligomeric silsesquioxane (POSS) and cyclodextrin (CD) which have well-defined size, shape and charge density by laser light scattering (LLS). Sub-nanometer sized ionic POSS provides a valuable opportunity to explore the unknown size boundary between simple ions and macroions. Whereas studying ionic CD, a fully organic macroion, expands our understanding beyond inorganic macroion.

Macroion-polymer based giant surfactant with smart responsiveness was design and fabricated. The novel hybrid can self-assemble in pure water and response to temperature and salt stimuli. We found different types of counterions impact the vesicle formation at room temperature. The development of such stimulative vesicles provides new and useful means for catalytic and biomedical applications.

ACKNOWLEDGEMENTS

This dissertation would not have been possible without the help of so many people in so many ways. It's also a product of tremendous serendipity and encounters with people who have significant effect on my career.

First of all, I would like to thank my advisor, Dr. Tianbo Liu, for his encouragement, support and guidance to my research. He gave me the chance to fulfill my dream and enjoy the scientific exploration. Dr. Liu was very suggestive and supportive during my researches. It was my great honor to work with him. I am also very grateful to Dr. Mesfin Tsige, Dr. Matthew Becker, Dr. Toshikazu Miyoshi and Dr. Alamgir Karim for their help, discussions, advices and comments during my research.

I appreciate all of my group members in particular Dr. Panchao Yin, Dr. Fadi Haso, and Yunyi Gao for discussing and sharing their knowledge with me. They have been a critical source of support and encouragement for me to accomplish several projects within two and half years. We had a great time collaborating and working together in Dr. Liu's group.

I am very grateful to my parents, who give me all the love and encouragement forever. They have instilled in me the importance of education, working hard, and caring for others. With everything they made available to me, I could pursue my dream without any burden.

I also appreciate all of my friends in Akron for their kind friendship, trust and support. In particular, I want to thank my best friend Panpan Lin for sharing

happiness and pain with me in the past five years. They gave me good memories in Akron.

Finally, I would like to express my immense gratitude to my boyfriend Fei Lin for his love and care. He never stopped supporting me even in the most difficult time. This achievement would not have been possible without him.

TABLE OF CONTENTS

Page

LIST OF TABLES

LIST OF FIGURES

CHAPTER I

INTRODUCTION

Hydrophilic macroions, with sizes ranging between simple ions (point charges valid for the Debye-Hückel Theory) and colloidal suspensions (usually described by the DLVO theory), demonstrate unique solution behavior by self-assembling into ordered, single layer, hollow, spherical "blackberry" structures. Counterion mediated attraction is considered as the main driving force for the self-assembly behavior. Changing parameters such as the solvent polarity, the effective charge of macroions and the solution pH, can strongly influence the transition from discrete macroions to blackberries, as well as the blackberry size. The study of macroions is being expanded to different areas, *e.g.* polyoxometalates, metal-organic nanocages, charged nanoparticles and biomacromolecules. The development of synthetic methods in recent years enable people to functionalize macroions with organic ligands and explore other non-covalent interactions in these hybrid materials in additional to counterion mediated attraction.

In Chapter II of the dissertation a broad overview of macroions will be presented. The Debye-Hückel Theory and the DLVO theory governing the solution behavior of simple ions and colloids will be discussed. The solution behaviors of Macroion, as a missing gap between the two major theories, will be addressed with a focus on polyoxometalate inorganic clusters. The possible driving forces of the macroionic self-assembly process will be discussed in detail. This chapter also

includes a description on how to control the blackberry size and the mechanism of blackberry formation. The current studies of macroion-organic hybrids will also be discussed.

In Chapter III all the experimental techniques that were used in my research will be discussed with a major focus on laser light scattering and zeta potential analysis. Both static and dynamic light scattering were used to characterize the assembly structures in solution and provide information such as hydrodynamic radius and radius of gyration. Zeta potential measurements were conducted to provide the charge states of molecules in solution. Further information regarding transmission electron microscopy, conductivity analysis, and etc. will also be provided.

A detailed study of both positively and negatively charged polyhedral oligomeric silsesquioxane (POSS) electrolytes will be included in Chapter IV. POSS macroions were observed to self-assemble into blackberry-type supramolecular structures in water/acetone mixed solvents, driven by the counterion-mediated attraction. Laser light-scattering studies revealed that the sizes of the blackberry structures increase with increasing acetone content, which suggests a charge-regulated process. These POSS ions further decrease the lower size limit of macroions that can self-assemble in polar solvents reported to date.

In Chapter V the behavior of phosphate-functionalized γ-cyclodextrin macroanions in dilute solution will be discussed. The hydrophilic macroions in mixed solvents show strong attraction between each other, mediated by the counterions, and consequently self-assemble into blackberry-type hollow spherical structures. Time-resolved laser light scattering (LLS) measurements at high temperature ruled out the possibility of hydrogen bonding as the main driving force in the self-assembly and indicated the good thermodynamic stability of assemblies regulated by the charge.

The transition from single macroions to blackberries can be tuned by adjusting the content of organic solvent. The sizes of blackberries vary with the charge density of γ-cyclodextrin by adjusting pH. It is the first report that organic macroions that can generate supramolecular structures by themselves.

In Chapter VI my study was extended from macroions to macroion-polymer hybrids. Polyoxometalates (POMs) as polar head groups were covalently functionalized with Poly (N-isopropylacrylamide) (PNIPAM) tails. The macromolecular hybrid demonstrated the solution behavior of hydrophilic macroions by self-assembling into blackberry structures at room temperature. It behaved like the amphiphilic surfactant by forming vesicular structure when the temperature is above the phase transition of PNIPAM. The reversible self-assembly was also salt sensitive and the salt-induced smaller vesicular formation is a result of counterion-association.

CHAPTER II

BACKGROUND:

MACROIONS AND SOLUTION BEHAVIORS OF MACROIONS

2.1 Introduction

Studying solution behavior of electrolytes is always challenge. In terms of the size of electrolytes, those solutions can be classified into two categories, including simple ions' (<1nm, e.g. NaCl) solutions and colloidal suspensions (~10 to ~1000 nm, e.g. highly charged gold nanoparticles dispersed in the aqueous solution). Debye-Hückel theory proposed by Peter Debye and Erich Hückel in 1923 was widely used to describe dilute solutions of simple ions which can be treated as point charges. (*1*) On the other hand, colloids with much larger size behave fundamentally different in the solution. Derjaguin-Landau-Verwey-Overbeek (DLVO) theory was established to relate the stability of colloid suspensions to the competition between attractive van der Waals force and repulsive electrostatic interaction. (*2, 3*) However, these two theories failed to deal with ions with size between ~1 to ~10 nm. In this range, ions are large enough that they cannot be treated as point charges, and they are soluble by forming homogeneously real solutions. We named these ions as macroions with their unique features. "How macroions behave in the solution" is a quite intriguing question and explore this area can fill the missing gap between simple ions and colloidal particles. (Figure 2.1-1) Currently investigated macroions are mainly

composed of several groups: polyoxometalates (POMs), charged nanoparticles and bio-macroions.

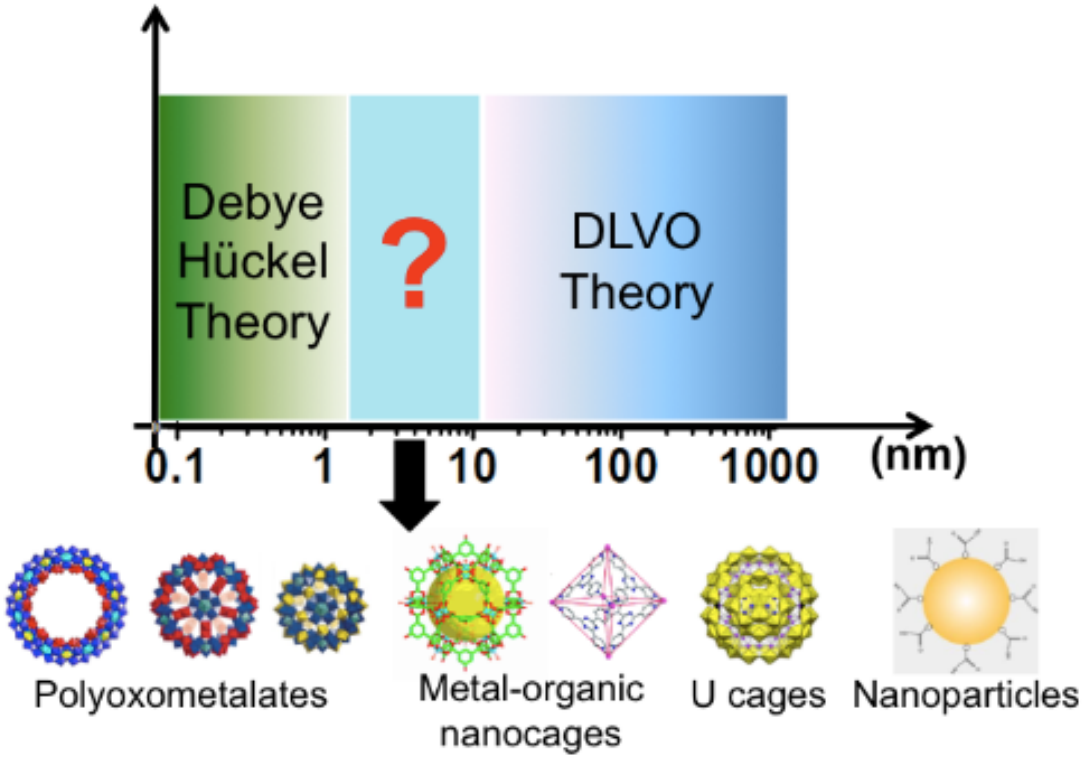

Figure 2.1-1. The schematic presentation of areas for simple ions, macroions and colloids. Macroion is a missing gap between Debye–Hückel theory and DLVO theory.

2.2 Polyoxometalates type macroions and functionalized hybrid POMs

Polyoxometalates are a large class of polyatomic ions consisting of multiple transition metal (Mo, W, V, Cr, Fe, etc.) oxide polyhedra. (*4-6*) These giant clusters have well defined three-dimensional frameworks by connecting oxygen atoms. Although POM clusters has been known since the late 19th century, they still attract extensive interests in virtue of their fascinating electronic, magnetic and optical properties and practical applications in catalysis, pharmacy, etc. (*7, 8*) Owning to tunable valence and coordination geometry, POMs with various sizes, shapes and

charges have been synthesized. The family of POM molecular clusters was expanded from early transition metal POMs (Mo, W, V, Cr, Fe, Mn, etc.) to late transition metal POMs (U, Nb, Au, Pd, etc.), and can be divided into three categories: heteropolyoxometalates, isopolyoxometalates, and the large POMs. (*9, 10*) Figure 2.2-1 represents several examples of well-characterized POM molecular clusters. Most of POMs are negatively charged in solutions. According to the nature of their charges, POM clusters can be regarded as strong or weak electrolytes. In the first category, POMs carry inherent charges balanced by small ions in crystals and exist as macroanions in solutions. POMs in the second category are neutral molecules in crystals, but they can become charged in solutions because of the deprotonation of water ligands which are attatched to clusters. Moreover, the charge density of POMs can be tuned by substituting the central transition metals, changing the oxidation state of the metal ions, or simply changing the solution pH.

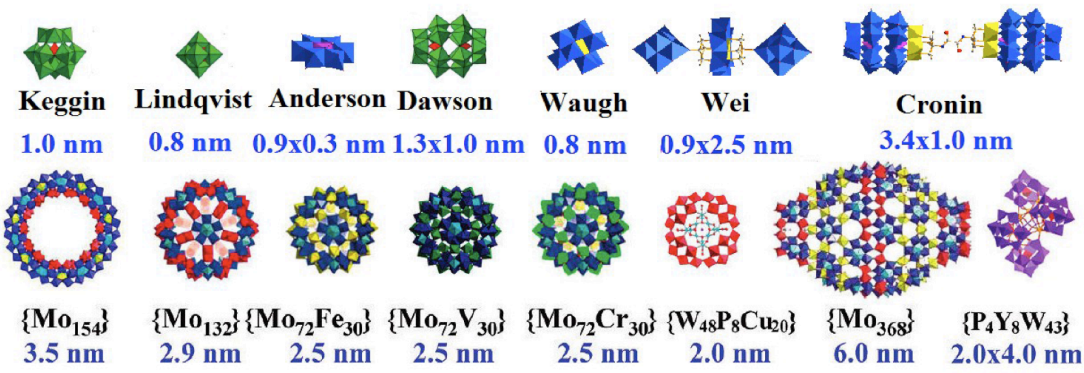

Figure 2.2-1. POMs with different topologies and sizes. Reprinted with permission from ref. 6. Copyright 2011 Wiley-VCH.

POMs, generally speaking, are not compatible with organic media because of its high hydrophilicity, which hinders the development of POM-based functional materials. In past decades, a novel type of amphiphilic hybrid materials has been

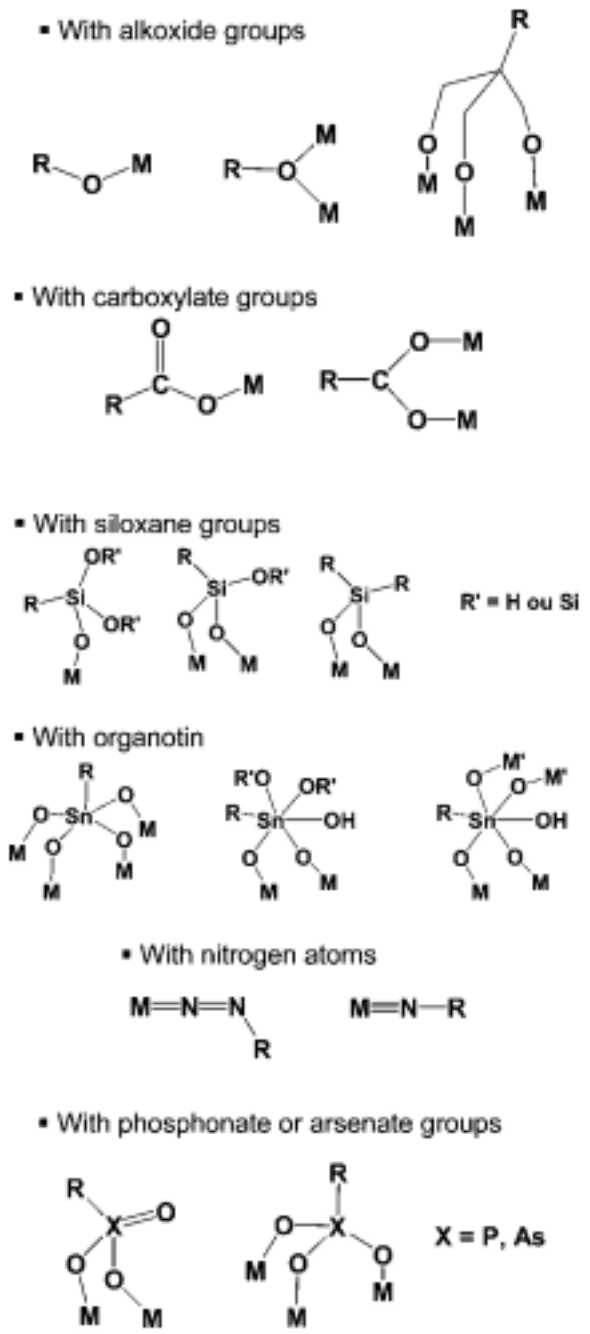

Figure 2.2-2. Main coordination modes of organic groups covalently linked to POM units via p-block elements. Reprinted with permission from ref. 10. Copyright 2010 American Chemical Society.

created by grafting organic functional motifs onto POM clusters. Two major ways are applied for functionalizing POMs: 1) non-covalently grafting organic ligands onto POMs via electrostatic interaction, hydrogen bonding, or van der Waals interactions, etc.; 2) covalently connecting organic motifs to POMs (Figure 2.2-2). (*10*) The

inorganic-organic molecular hybrids rendering amphiphilic properties can form micelles, vesicles, and reverse-vesicles in appropriate solvents, as well as improves their potential applications because of the enhanced compatibility in organic media. The study of the unique solution behaviors of a functionalized POM hybrid material will be discussed in Chapter 6.

2.3 Charged nanoparticles type macroions

Molecular Nanoparticles (MNPs) are a family of particles with their size around nanometer scale. They are shape- and volumepersistent and have well-defined molecular structure and specific symmetry. (*11*) Typical MNPs include folded globular proteins, POMs, fullerene (C_{60}) and polyhedral oligomeric silsesquioxanes (POSSs). Their overall shape can be held either by noncovalent bonds or covalent bonds. (*12-20*)

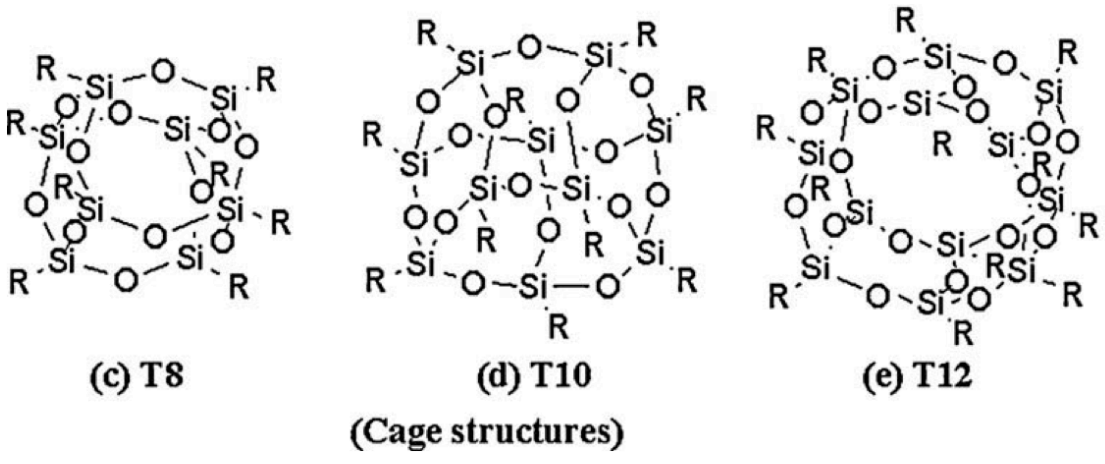

Figure 2.3-1. Structures of polyhedral oligomeric silsesquioxanes. Reprinted with permission from ref. 22. Copyright 2011 Elsevier.

POSSs as the smallest silica nanoparticles are structurally well-defined, cage-shaped clusters that have many attractive advantages owing to their nontoxic, biocompatible, chemically inert, and mechanically stable features. Usually POSS is prepared via the condensation of a silane or silanol precursor, resulting in the covalently conneting $RSiO_{3/2}$ unites at regular intervals through Si-O-Si bonds (Figure 2.3-1). (*21, 22*) The low dielectric constant of POSS materials makes them good thin-film insulators. Moreover, their three-dimensionality, high symmetry, and size make them promising building blocks for nanocomposites. The family of cage compounds has a variety of sizes and symmetries among which Octa-silsesquioxane ($R_8Si_8O_{12}$, T_8) is the most common type with a cubic shape (0.87 nm as the diagonal distance) and eight corner groups that can be chemically modified to achieve desired solubility and functionality. One distinct advantage of the POSS system is the facile tuning of its surface functional groups by either selective monofunctionalization or simultaneous multisite functionalization. (*23-26*) Many POSS derivatives prepared by these methods have been commercialized. Recently, POSS molecular clusters were successfully integrated into various architectures such as polymer-based hybrid materials (Figure 2.3-2), with applications in electronics, light-emitting diodes (LEDs), catalysis, and superhydrophobic and antimicrobial coatings. (*27-34*) The self-assembly of amphiphilic POSS–organic hybrids driven by noncovalent interactions (e.g., hydrophobic interactions, metal coordination, hydrogen bonding) has been studied extensively in past decades. (*11, 35-40*) However, POSS molecular nanoparticles with ionic domains as surface groups can be treated as a novel type of charged nanoparticle type macroions which haven't been included in any previous literature. The solution behavior of ionic POSS molucules will be discussed in Chapter 4.

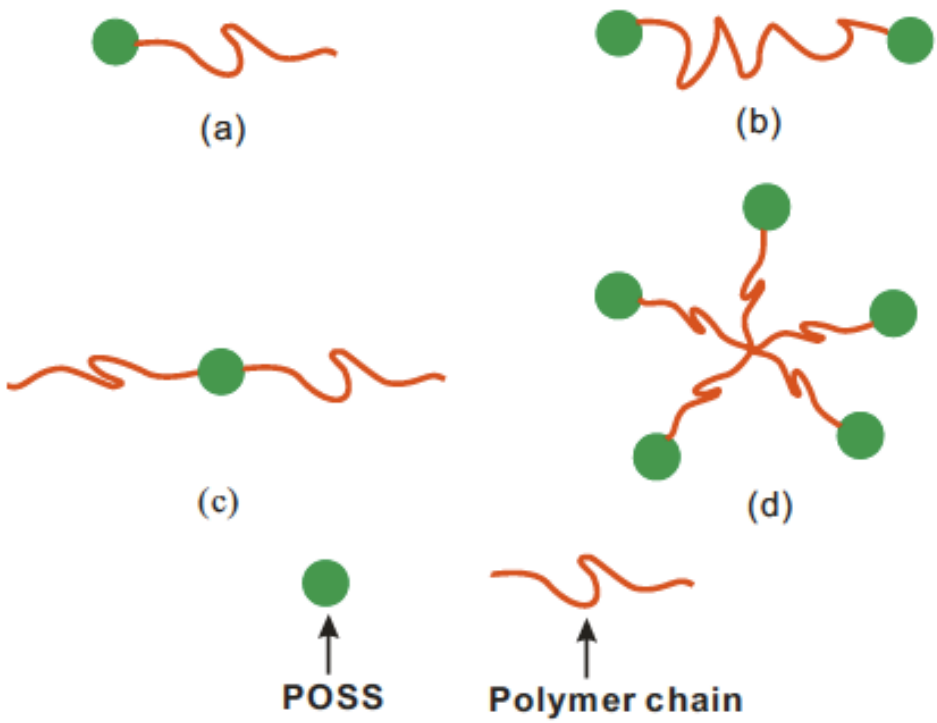

Figure 2.3-2. Hemi-telechelic, di-telechelic, eso-telechelic and penta-telechelic POSS-containing hybrid polymers. Reprinted with permission from ref. 27. Copyright 2013 Elsevier.

2.4 Charged biomolecular type macroions

Highly charged bio-macromolecules, such as DNA, RNA, proteins, virus, etc., with size in nanometer scale can also be treated as macroions. Electrostatic interactions are critical to various phynomena in these bio-macroionic systems, e.g. DNA condensation and the formation of virus capsids. However, hydrophobic interactions, hydrogen bonding, and salt bridges are also possibly involved in interactions between these bio-macroions, which make their solutions very complex. Ideal models are needed for understanding the solution behavior of biomacromolecules.

Cyclodextrins (CDs) are a class of cyclic oligosaccharides consisting of six, seven, or eight glucose entities, which are called α-, β-, or γ-CDs. CD molecules show a toroidal shape, forming by α-1,4-linked d-glucopyranosides, (*41-43*) with the diameter of the primary hydroxyl rim narrower than that of the secondary hydroxyl rim (Figure 2.4-1). (*42, 44, 45*) Due to the abundant OH groups, the external surface of CD toroid is highly hydrophilic, whereas the internal cavity is relatively hydrophobic, which enables CDs to host various guests. (*46, 47*) By virtue of its water-solubility, biocompatibility, and strong ability of incorporating guest molecules, CD has applications in areas such as food, pharmaceutical, drug delivery, and chemical industries. (*41, 43*) The inclusion complexation between CDs and guests, as well as its impacts on the assembly of these systems, has been extensively investigated. (*46, 48*) Previous work demonstrated that CDs crucially participate in the self-assembly of amphiphilic systems (either as a modulator or as a building block), as well as realize the reversibility and stimuli-responsiveness of assemblies and materials, particularly hydrogels that use inclusion complexes as crosslinks. (*49-51*) Furthermore, the involvement of CDs in macromolecular assemblies provided many other applications, such as controlling solution properties, DNA decompaction, and protein reconstruction. (*51*) Recently, it was found that CDs and CDs/surfactants complexes could self-assemble in aqueous solution driven by CD–CD H-bonds, instead of hydrophobic interactions in amphiphilic systems. (*52-57*) However, it is still, to our knowledge, unknown in dilute solutions how the pure, hydrophilic CDs themselves behave. Currently, many CD derivatives were obtained by a wide variety of synthetic methods. (*58-60*) Ionic CDs (*61*) such as phosphate, sulfate, and carboxylate sodium salts are readily commercialized. Since CD has much simpler chemical structure than other biomacromolecules, it can be treated as an ideal model

of macroions for studying charge-related solution behavior as discussed in Chapter 5.

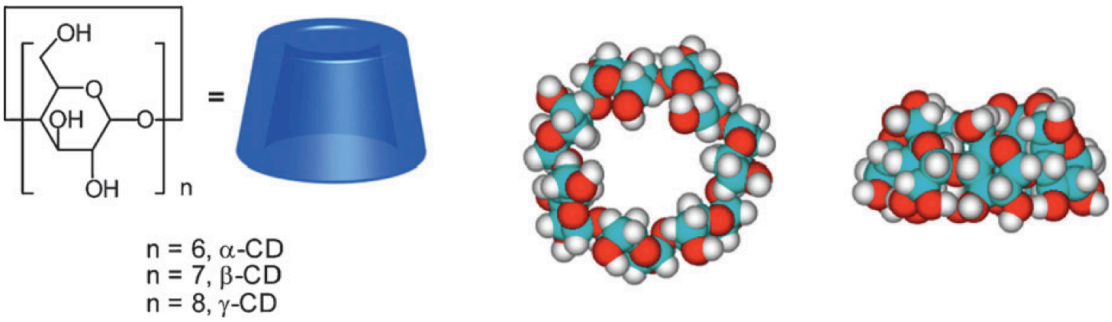

Figure 2.4-1. Chemical structure and space-filling model of cyclodextrins. Reprinted with permission from ref. 48. Copyright 2010 Royal Society of Chemistry.

2.5 Solution behaviors of macroions: theories and experimental observations

Table 2.5-1. Information on the structure, charge density, and self-assembly behavior of macro-polyoxoanions in aqueous solutions. Reprinted with permission from ref. 150. Copyright 2012 Royal Society of Chemistry.

Polyoxoanion	$\{Mo_{72}Fe_{30}\}$			$\{Mo_{72}Cr_{30}\}$	$\{Mo_{154}\}$	$\{Cu_{20}P_8W_{48}\}$	$\{P_4Y_9W_{43}\}$	$\{Mo_{132}\}$	$\{Mo_{72}V_{30}\}$
Molecular structure		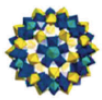		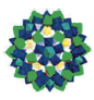	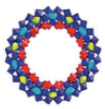	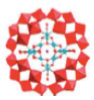			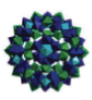
Negative charge	0–1	1–29		5	15	25	30	42	31
Size (nm)	2.5			2.5	3.6 × 1.2	2.2 × 1.1	4 × 2 × 2	2.9	2.5
Charge density (nm^{-2})	0–0.051 pH < 2.9	0.051–1.477 2.9 < pH < 6.6	Unstable pH > 6.6	0.255	0.543	1.291	1.08	1.590	1.579
Self-assembly in aqueous solution	No	Yes	Unstable	Yes	Yes	Yes	Yes	Yes at high conc.	No
R_h of Blackberry (nm)		48–15		60	45	38	46		

	Formula	Ref.
$\{Mo_{72}Fe_{30}\}$	$[Mo^{VI}{}_{72}Fe^{III}{}_{30}O_{252}(CH_3COO)_{12}\{Mo_2O_7(H_2O)\}_2\{H_2Mo_2O_8(H_2O)\}(H_2O)_{91}]\cdot ca.\ 150H_2O$	21
$\{Mo_{72}Cr_{30}\}$	$[\{Na(H_2O)_{12}\}\subset\{Mo^{VI}{}_{72}Cr^{III}{}_{30}O_{252}(CH_3COO)_{19}(H_2O)_{94}\}]\cdot ca.\ 120H_2O$	25
$\{Mo_{154}\}$	$Na_{15}[Mo_{154}O_{462}H_{14}(H_2O)_{70}]_{0.5}[Mo_{152}O_{457}H_{14}(H_2O)_{68}]_{0.5}\cdot ca.\ 400H_2O$	18
$\{Cu_{20}P_8W_{48}\}$	$K_{12}Li_{13}[Cu_{20}Cl(OH)_{24}(H_2O)_{12}(P_8W_{48}O_{184})]\cdot 22H_2O$	24
$\{P_4Y_9W_{43}\}$	$K_{15}Na_6(H_3O)_9[(PY_2W_{10}O_{38})_4(W_3O_{14})]\cdot 39H_2O$	23
$\{Mo_{132}\}$	$(NH_4)_{42}[\{(Mo^{VI})Mo^{V}{}_{15}O_{21}(H_2O)_6\}_{12}\{Mo_2O_4(CH_3COOH)\}_{30}]\cdot ca.\ 300H_2O\cdot ca.\ 10CH_3COONH_4$	19
$\{Mo_{72}V_{30}\}$	$Na_8K_{14}(VO)_2[\{(Mo^{VI})Mo^{VI}{}_5O_{21}(H_2O)_3\}_{10}\{(Mo^{VI})Mo^{VI}{}_5O_{21}(H_2O)_3(SO_4)\}_2\{V^{IV}O(H_2O)\}_{20}\{V^{IV}O\}_{10}(\{KSO_4\}_5)_2]\cdot ca.\ 150H_2O$	22

In the past decades, people achieved significant development of synthesizing various POMs with their sizes from 2 nm to 6nm (Table 2-1). (*62-69*) In contradiction to classic theories, these POM clusters don't homogeneously distribute to form real and stable solutions like what simple ions usually do nor behave similarly with

colloids by forming temporal suspensions. Instead, these highly charged macroions started to be full soluble in the aqueous solution and then slowly self-assembly into spherical, hollow, single-layered vesicular structures, which are named as “blackberry” type structures. Their solution behavior is valuable to help fill the missing gap between simple ionic solution and colloidal suspensions. For understanding this unique phenomenon, it’s necessary to exam two classic (Debye–Hückel theory and DLVO theory) theories which were widely applied to describe electrolyte solutions.

2.5.1 Debye–Hückel Theory

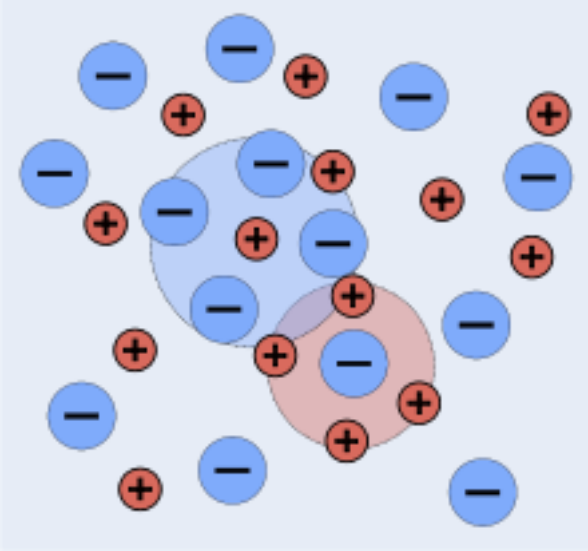

Figure 2.5-1. A snapshot of 2D section of an idealized solution of a 1:1 electrolyte.

The fundamental idea of the Debye–Hückel Theory is that ions in solution are not uniformly distributed. Overall, the ionic solution is neutral, but near any given ion there is a higher concentration of counterions. A snapshot of 2D section of an idealized electrolyte solution will regard ions as spheres with unit electrical charge

and the solvent as a uniform medium without structure (Figure 2.5-1). A given ion is surrounding by an excess of its counterions. The time-averaged "spherical cloud", which is called ionic atmosphere, includes those counterions with a net opposite charge equal to that on the central ion. If considering the ionic atmosphere around a given ion in solution, we will find the concentration of counterions C decreases exponentially as they depart from the ion with distance r.

$$C \sim e^{-\kappa r} \tag{2.1}$$

where the inverse of the decay rate κ^{-1} is called the Debye length which is thought to be the radius of the ionic atmosphere. Physically, it is the distance from the central ion over which ions do not fell each other.

In an electrolyte solution, the Debye length is shown as equation 2.2.

$$\kappa^{-1} = \sqrt{\frac{\varepsilon_r \varepsilon_0 k_B T}{2 N_A e^2 I}} \tag{2.2}$$

where ε_r is the relative permittivity of a medium, ε_0 is the permittivity of free space, k_B is Boltzmann's constant, T is the temperature of the solution, N_A is Avogadro's number, e is the elementary charge, I is the ionic strength of the solution.

The Debye–Hückel theory includes a very detailed discussion of the assumptions and their limitations. (*70*) The principal assumption is that departure from ideality is due to electrostatic interactions between ions, mediated by Coulomb's law: the force of interaction between two electric charges is given by, (*70*)

$$Force = \frac{z_1 z_2 e^2}{4\pi\varepsilon_0 \varepsilon_r r^2} \tag{2.3}$$

where z_1, z_2, r are the charge number of ionic species 1 and species 2, and the separated distance of two ionic species, respectively.

The non-ideal behaviors of an electrolyte solution can be expressed by the chemical potential of an i^{th} ion as

$$\mu_i = \mu_i^{ideal} + \Delta\mu_i^{el} \tag{2.4}$$

For an ideal solution,

$$\mu_i^{ideal} = \mu_i^0 + RT \ln x_i \tag{2.5}$$

For an electrolyte solution,

$$\mu_i = \mu_i^0 + RT \ln x_i + RT \ln \gamma_i \tag{2.6}$$

where γ_i is the activity coefficient of the i^{th} ion. Thus the deviation due to the electrostatic interaction is

$$\Delta\mu_i^{el} = RT \ln \gamma_i \tag{2.7}$$

The Debye–Hückel limiting law enables us to determine the activity coefficient of an ion in a dilute solution of known ionic strength as the equation below.

$$\ln \gamma_i = -\frac{z_i^2 e^2 \kappa}{8\pi\varepsilon_0\varepsilon_r k_B T} = -\frac{z_i^2 e^3 N_A^{1/2}}{4\pi(\varepsilon_0\varepsilon_r k_B T)^{3/2}}\sqrt{\frac{I}{2}} = -Az_i^2\sqrt{I} \tag{2.8}$$

$$I = \frac{1}{2}\sum_i z_i^2 \frac{n_i}{n_0} \tag{2.9}$$

where z_i is the charge number of ion species i, A is a constant that depends on temperature, and n_i and n_0 are number density of i species and the bulk.

There are also assumptions for Debye–Hückel theory beyond which the theory will not hold.

1. Electrolytes completely dissociate into ions in solution.
2. Ions are treated as point charges with no polarizability.
3. The solvent plays no role other than providing a medium of constant relative permittivity (or dielectric constant).

Debye–Hückel limiting law is only applicable for electrolyte solution with $I<10^{-2.3}$. Chemists extended D-H equation for solution with higher ionic strength by adding a term which is called the ion size parameter *a* as shown in Equation 2.10. This term is supposed to take into account that ions have a finite radius and are not point charges. Values are given in Table 2-2. A and B are constants with values of respectively 0.5085 and 0.3281×10^8 at 25 °C in water. The extension of Debye–Hückel theory is empirically applicable for electrolyte solution with I<0.1. (*70*)

$$\log \gamma_i = -Az_i^2 \frac{\sqrt{I}}{1 + Ba\sqrt{I}} \tag{2.10}$$

Table 2.5-2. Parameters *a* and individual ion activity coefficients.

Ion Size Parameter, *a* (Å)[a]	Ion	Activity Coefficients Calculated with (2) of Table 3.3 for Ionic Strength				
		10^{-4}	10^{-3}	10^{-2}	0.05	10^{-1}
9	H^+	0.99	0.97	0.91	0.86	0.83
	Al^{3+}, Fe^{3+}, La^{3+}, Ce^{3+}	0.90	0.74	0.44	0.24	0.18
8	Mg^{2+}, Be^{2+}	0.96	0.87	0.69	0.52	0.45
6	Ca^{2+}, Zn^{2+}, Cu^{2+}, Sn^{2+}, Mn^{2+} Fe^{2+}	0.96	0.87	0.68	0.48	0.40
5	Ba^{2+}, Sr^{2+}, Pb^{2+}, CO_3^{2-}	0.96	0.87	0.67	0.46	0.39
4	Na^+, HCO_3^-, $H_2PO_4^-$, CH_3COO^-	0.99	0.96	0.90	0.81	0.77
	SO_4^{2-}, HPO_4^{2-}	0.96	0.87	0.66	0.44	0.36
	PO_4^{3-}	0.90	0.72	0.40	0.16	0.10
3	K^+, Ag^+, NH_4^+, OH^-, Cl^- ClO_4^-, NO_3^-, I^-, HS^-	0.99	0.96	0.90	0.80	0.76

[a] After J. Kielland, *J. Am. Chem. Soc.*, **59**, 1675 (1937). Reproduced with permission from American Chemical Society.

2.5.2 Derjaguin, Landau, Verwey, and Overbeek (DLVO) Theory

A colloidal particle has a Brownian motion in solution. Upon approaching another particle, it is affected not only the surrounding solvent, but also the interactions with other particles. Particle-particle interaction is a result of the static forces. During the 1940s, two groups of scientists (Boris Derjaguin and Lev Landau in the Soviet Union, and Evert Verwey and Theo Overbeek in the Netherlands) independently published a quantitative theoretical analysis of colloidal stability, which made a major advance in colloid science. The theory became known as DLVO theory.

DLVO theory assumes that the more long-ranged interparticle interactions, including two types of force van der Waals force and double-layer force, mainly control colloidal stability. (*71*) A van der Waals force is regardless of the chemical

nature of the particles or the medium. In simple words, that is if the particles are similar, this force is always attractive. Moreover, most colloidal particles carry charges either from their surface charge groups or by specific ion adsorption from the solution. This surface charge leads to a repulsive double-layer force which becomes significant when two colloids approach each other and their electrical double layers begin to interfere. Thus, the total interaction potential Φ as a function of distance h can be written as

$$\Phi(h) = \Phi_A(h) + \Phi_R(h) \tag{2.11}$$

and the corresponding force equals

$$F = -\frac{dV}{dh} = -\frac{d\Phi_A}{dh} - \frac{d\Phi_R}{dh} \tag{2.12}$$

Let's illustrate the typical properties of the interaction potentials and the corresponding force by considering the interaction between two identical half-planes separated by a distance h. The attractive van der Waals interaction Φ_A is

$$\frac{V_A(h)}{area} = \frac{-A}{12\pi h^2} \tag{2.13}$$

where A represents the Hamaker constant.

At large separations, the double-layer interaction force is

$$\frac{F}{area} \simeq 32(kT)^2 \frac{\varepsilon_r \varepsilon_0}{z^2 e^2} \kappa^2 \Gamma_0^2 \exp(-\kappa h) \tag{2.14}$$

$$= 64 kT c_0^* \Gamma_0^2 \exp(-\kappa h)$$

where c_0^* represents the bulk electrolyte concentration and Γ_0=tan(zeΦ_0/4kT) depending on the potential at the charge surface Φ_0. The distance dependence is solely determined by the Debye screening in the solution.

We obtain the corresponding potential by integrating Equation 2.14

$$\frac{\Phi_R(h)}{area} = \frac{64 kT c_0^* \Gamma_0^2}{\kappa} \exp(-\kappa h) \tag{2.15}$$

Thus the total interaction potential and force can be written as

$$\frac{\Phi(h)}{area} = -\frac{A}{12\pi h^2} + \frac{64 kT c_0^* \Gamma_0^2}{\kappa} \exp(-\kappa h) \tag{2.16}$$

$$\frac{F}{area} = -\frac{A}{6\pi h^3} + 64 kT c_0^* \Gamma_0^2 \exp(-\kappa h) \tag{2.17}$$

As shown in Figure 2.5-2, we can plot the DLVO potential Φ as a function of the distance between two particles. (*71*) The attractive term Φ_A dominates the repulsive term Φ_R when h is very large or very small. The potential curve displays two minima, a deep primary minimum at shorter separations and a shallow secondary minimum farther out. A potential energy barrier separates the two minima when the surface is sufficiently charged and the electrolyte ions do not screen too much. If the

system reaches the primary minimum, the irreversible coagulation process takes place. If the energy barrier is far away from kT, the primary minimum becomes inaccessible and the whole system is kinetically stable. The depth of the secondary minimum is quite sensitive to the salt concentration, and if it's deep enough, the colloidal particles can flocculate and form colloidal crystallites, which is a reversible process.

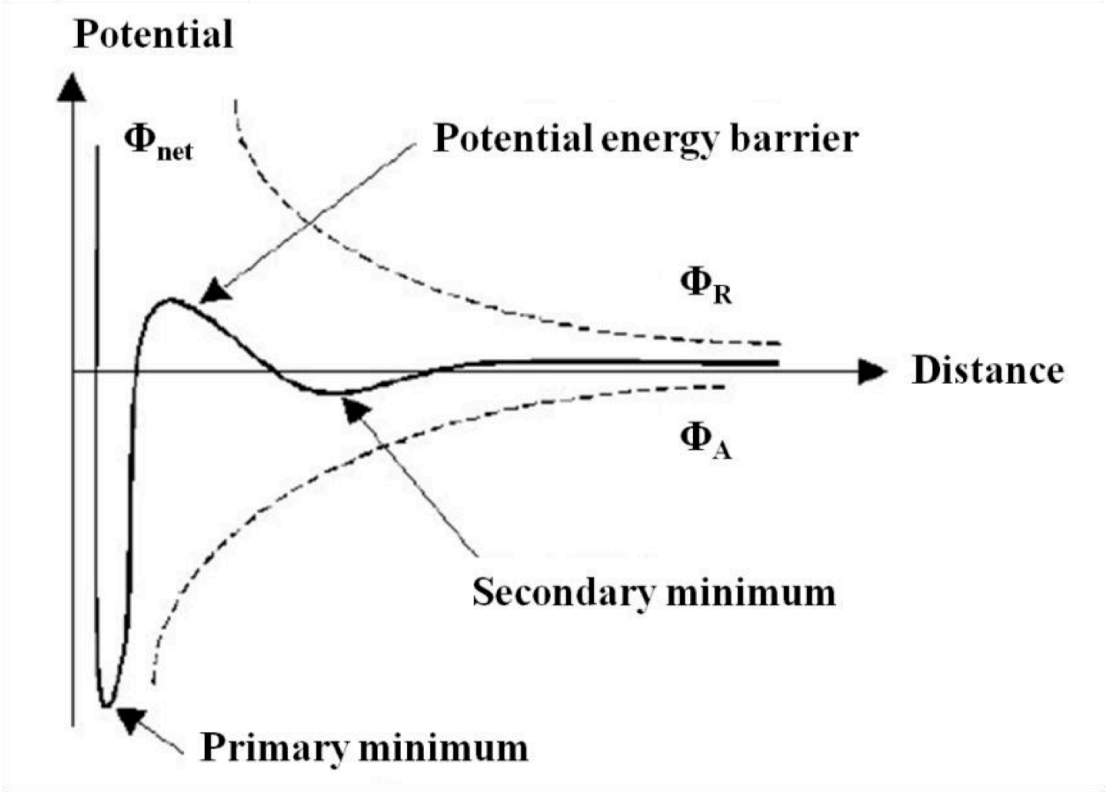

Figure 2.5-2. Plot the DLVO potential Φ_{net} versus the distance between two colloidal particles.

Although the DLVO theory successfully provided explanation and prediction of some important solution behaviors in colloidal systems, within the last 40 years, people observed new experimental phenomena beyond the application of DLVO theory. For example, Ise and co-workers noticed large void regions exist in equilibrium with densely packed regions for highly charged silica latex particles. (*72*)

In 1973, Hachisu found that increasing the salt concentration resulted in melting of colloidal crystals, which is however opposite to DLVO theory as people believed higher salt concentration should deepen the secondary minimum and therefore stabilize the colloidal crystals. (*73*) Moreover, Schurr and co-workers reported a strange "ordinary-extraordinary phase transition" when studying the dynamics of poly-L-lysine upon addition of salt. Over a narrow ionic strength range, they found the apparent diffusion coefficient Dapp decreased by 20 times, which indicated the formation of clusters in solution. (*74, 75*) Failures of applying DLVO theory to explain these results could be caused by the fundamental assumption that the short-range van der Waals force is the only attraction in the colloidal systems.

2.5.3 Blackberry type structures formed by $\{Mo_{154}\}$ POM

$\{Mo_{154}\}$ giant anions $((NH_4)_{28}[Mo_{154}(NO)_{14}O_{448}H_{14}(H_2O)_{70}]\cdot nH_2O)$ with wheel-like shape was first identified by Dr. Achim Müller and his colleagues. (*76*) Instead of staying as discrete ion, this anionic POM was observed to slowly aggregate to form larger structures in the aqueous solution. Laser light scattering (LLS), commonly applied for analyzing particles in solutions, was used to monitor the dilute POM solutions. Static light scattering (SLS) can give information such as weight-average mass (M_w), radius of gyration (R_g), as well as the nature of interparticle interactions of the studied solute (the second virial coefficient A_2) through measuring the angular dependence of scattered intensity from sample solutions at different concentrations. Dynamic light scattering (DLS) can measure the intensity-intensity time correlation function of the scattered light which can be related to the average hydrodynamic radius (R_h) of the particles and the particle size distribution. We found

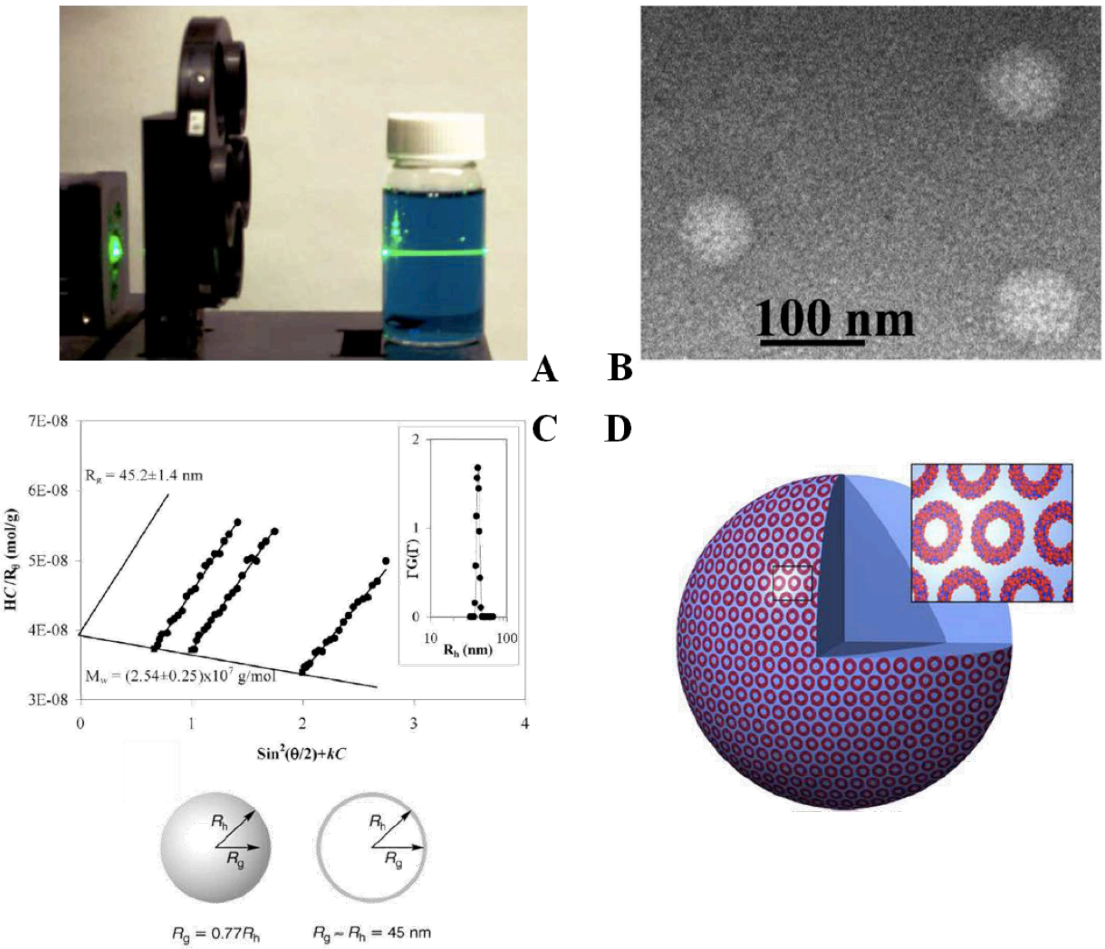

Figure 2.5-3. (A) Tyndall effect of a {Mo154} aqueous solution when a green laser passes through the solution. (B) TEM image on dilute aqueous solution of $\{Mo_{154}\}$ macroions showing the existence of spherical, ~45 nm radius assemblies. (C) Zimm plot based on the SLS study of the $\{Mo_{154}\}$ aqueous solutions at pH=3; (inset) CONTIN analysis on the DLS study of the same solution. (D) Schematic plot showing the supramolecular blackberry structure formed by $\{Mo_{154}\}$ macroions in aqueous solution. Reprinted with permission from ref. 77. Copyright 2003 Nature Publishing Group.

the POM solution forming large aggregates took a long time to reach equilibrium with no precipitation at room temperature. (*77*) A typical CONTIN analysis of DLS measurements of $\{Mo_{154}\}$ dilute solution at pH=3.0 indicated that those large assemblies have an average R_h of 45±1 nm and a narrow size distribution. SLS measurements analyzed by the Zimm plot demonstrated that the assemblies had an average M_w of 2.54×10^7 g/mol and an average R_g of 45.2±1.4 nm. As shown in Fig. 2.5-3, the transmission electron microscopy (TEM) study showed that a lot of

spherical assemblies with a relatively uniform size around 90 nm were formed in $\{Mo_{154}\}$ aqueous solution. The ratio of R_h/R_g is approximate to 1 for spherical objects, suggesting the formation of hollow vesicular structure. The average M_w is equivalent to ~1165 single $\{Mo_{154}\}$ macroions also supports the hollow interior of the assemblies since a solid 45 nm radius $\{Mo_{154}\}$ nanocrystal would contain a much more individual macroions. These evidences proved that these giant clusters were distributed to form a single layer on the surface of assembled spheres with an average intermolecular distance around 0.9 nm. We gave the novel assemblies a nickname "blackberry" due to the similarities between these two species. Similar self-assembly are also observed in other systems of POM macroanions and nanocage macroanions in various polar solvents.

2.5.4 Driving forces of the self-assembly behavior

It's worthy to notice that the formation of blackberry structures is fundamentally different from those bilayer vesicular micelles or liposomes because based on the chemical structure of POM macroions there is no hydrophobic regions that can cause possible hydrophobic interactions. Since macroions are highly charged in the aqueous solution, we expected that they would like to repel each other because of the strong electrostatic repulsion. To trigger the self-assembly, certain attractive forces should overcome the repulsive force to bring these macroions coming close to each other. In our systems, van der Waals force, hydrogen bonding and counterion-mediated attraction were taken into account as possible driving forces.

One simple experiment was done by mixing acetone with $\{Mo_{132}\}$ water solution (Figure 2.5-4) to help clarify driving forces and distinguish macroions from

other types of solutes. (*78*) In pure water, $\{Mo_{132}\}$ clusters exist as discrete ions because of strong electrostatic repulsion. When adding acetone more than 3 vol.% to the aqueous solution, blackberries began to form. With introducing more acetone, the blackberry size became bigger. When acetone was more than 70%, blackberries dissociated back into single molecules. During the whole process, the magnitude of attractive van der Waals forces basically does not change. On the other hand, the estimated inter-POM distance on the blackberry surface (close to 1 nm) also suggests that the van der Waals attraction should be weak. Therefore, these observations confirm that the van der Waals forces are not the major driving forces for the blackberry formation.

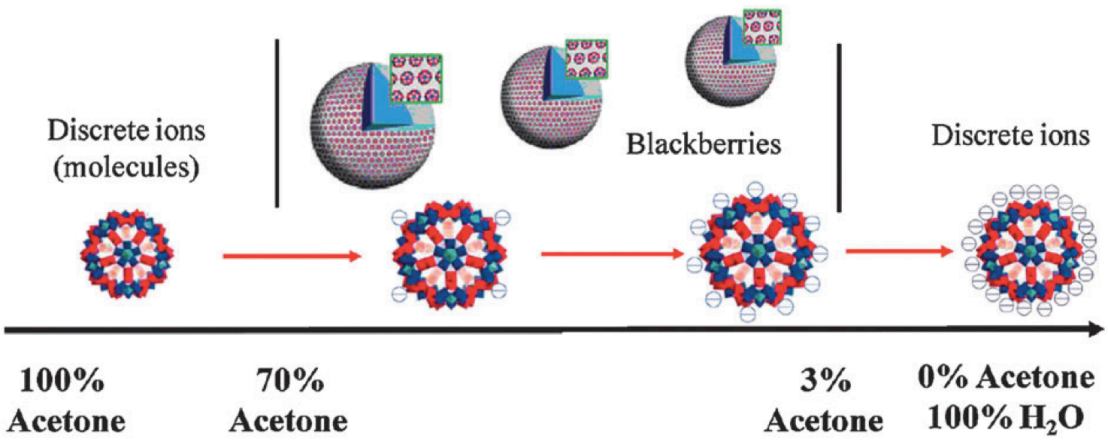

Figure 2.5-4. Transition from discrete macroions (molecules) to blackberries, then to discrete macroions due to the change of solvent content for 1.0 $mgmL^{-1}$ $\{Mo_{132}\}$ in water-acetone mixed solvents. Reprinted with permission from ref. 176. Copyright 2007 American Chemical Society.

Hydrogen bonds formed between macroions may be one of the important forces for stabilizing blackberries, which is indicated by recent experimental results form our group and other groups. For example, $\{Mo_{72}Fe_{30}\}$ and $\{Mo_{72}Cr_{30}\}$ are two types of POMs with the same size and morphology, and their charge density can be the same by carefully tuning their solution pHs (shown in Table 2-1). (*69, 79*)

Meanwhile, their assembly sizes vary with each other when they possess the same charge density, implying the charge interaction is not the only driving force existed in the system and other forces must play a role in regulation the blackberry size. (*80*) Oleinikova et al. conducted dielectric relaxation measurements during the self-assembly of $\{Mo_{154}\}$, and noticed that "the strength of the hydration extends as cluster aggregation takes place with more water molecules being more strongly bound between the wheels and the presence of relatively fewer less strongly bound water molecules". (*81*) In other words, water molecules staying between macroions show higher viscosity and act as "glue" to help attract adjacent POMs together by forming hydrogen bonds. Schmitz et al. provided an interesting hypothesis of hydrogen bonded water molecule "fingers" to explain the spherical geometry of blackberries. (*82*) However, the self-assembly of two POM macroions $\{Mo_{72}Fe_{30}\}$ and $\{Mo_{72}Cr_{30}\}$ in aqueous solution is pH-dependent, in which no self-assembly at low pH, suggesting that water-bridged hydrogen bonding might not be the major driving force for the blackberry formation, but the force to strengthen the interaction between macroions. (*80, 83*)

It's worthy to notice that in various maroionic solutions the blackberry size increases linearly with the inverse of the dielectric constant of the solvent, implying the blackberry formation process is charge-regulated. This assumption was further confirmed by the pH dependent self-assembly of $\{Mo_{72}Fe_{30}\}$. $\{Mo_{72}Fe_{30}\}$ belongs to weak electrolyte-type POMs which surface charges come from the partial deprotonation of water ligands attached to its 30 Fe^{III} centers. (*81*) Thus, its charge density can be reversibly tuned by changing the solution pH and consequently the deprotonation equilibrium. As shown in Figure 2.5-5, the $\{Mo_{72}Fe_{30}\}$ clusters are almost non-charged and stay as discrete molecules in solution when pH<2.9, while at

pH>2.9, clusters self assemble into blackberry structures with smaller sizes as pH increase. The transition from single clusters to blackberries amplifies the importance of charges in blackberry formation. (*84*)

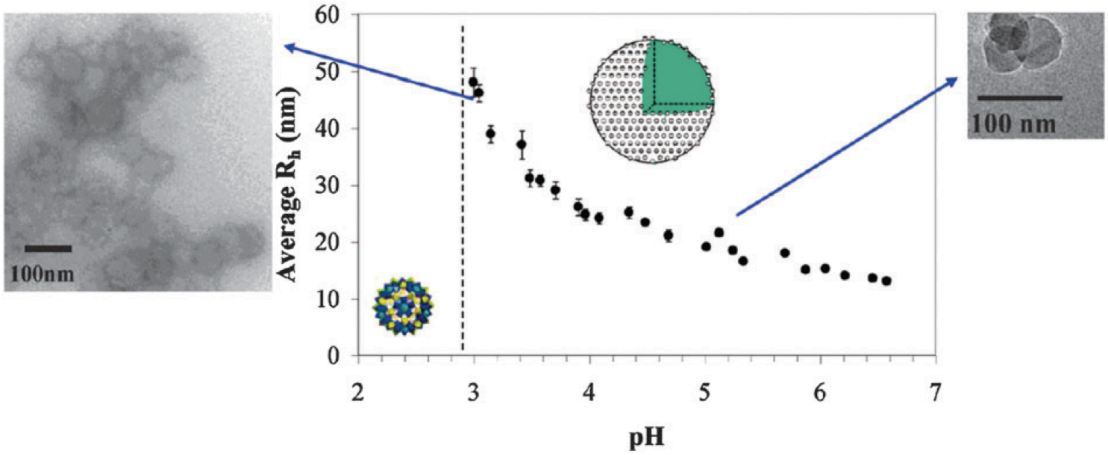

Figure 2.5-5. Average hydrodynamic radii (R_h) of the blackberries formed in 0.5mgmL^{-1} aqueous solutions of {$Mo_{72}Fe_{30}$} at different pH (adjusted by NaOH or HCl), as measured by DLS at 90° scattering angle. TEM images of aggregates on carbon films formed at pH~3.0 (left; conventional TEM) and pH~4.6 (right; more appropriate cryo-TEM). Reprinted with permission from ref. 84. Copyright 2006 American Chemical Society.

All of experimental results have raised our attention that the counterion-mediated attraction might be the possible reason to realize the blackberry formation of the macroionic solution. Actually, the counterion-mediated attraction was early proposed by Ise and Sogami who thought there exist long-range weak attractions between charged colloids because of counterions. (*85*) (Although it is still controversial in the colloid community since van der Waals force among colloidal particles are dominant) Moreover, in biomacromolecular systems, divalent or multivalent counterions were reported to induce the self-association of proteins and DNAs longtime ago. (*86-88*) Couterions with high valence can strongly associate with biomacromolecules and may even reverse the sign of their surface charges. Those biomacroions attract each other with a layer of counterions in between, which

is called counterion condensation. (*89, 90*) However, monovalent counterions can rarely trigger counterion condensation in colloidal or biomacromolecular systems. In macroionic system, the blackberry formation can take place in the presence of only monovalent counterions, which indeed indicates the uniqueness of solution behaviors of macroions.

2.5.5 Interactions between macroions and counterions

Since we have realized the importance of counterions on triggering the self-assembly of macroions, the experimental proofs of interactions between macroions and counterions are necessary.

2.5.5.1 Counterions association with macroions

Inorganic chemists started to explore the role of counterions and their interaction with POMs on the catalytic properties of POM clusters over a decade ago. Pope noticed that counterions could interact with some POMs at special binding site. (*91*) For midsize POMs, Weinstock and co-workers observed close ion pairing in the dilute solution of 1nm size Keggin anions via electrochemical studies. (*92, 93*) Using molecular dynamics simulations, Leroy et al. revealed direct, contact ion pairing between monovalent cations and Keggins in more concentrated solutions, while Antonio et al. experimentally detected contact ion pairing between Lindqvist POM $[Nb_6O_{19}]^{8-}$ and monovalent counterions in aqueous solution. (*94*) More significant counterion-macroion interactions were expected to exist in large POMs' systems. The conductivity measurement can be applied to evaluate the macroion-counterion

interaction by comparing the measured and theoretic values. Counterions even monovalent ions (such as NH_4^+ and Na^+) were found to closely associate with macroanions (such as $\{W_{148}\}$ and $\{Mo_{132}\}$), and thus they didn't contribute to the total solution conductivity. We also found the degree of counterion-association is concentration dependent which is stronger at higher concentration.

Another way to investigate the counterion asscociation with macroions is small angle X-ray scattering (SAXS). SAXS is a powerful technique to determine characteristic distances of partially ordered materials, pore sizes, and the microscale or nanoscale structure of particle systems in terms of such parameters as averaged particle sizes, shapes, distribution and surface-to-volume ratio. SAXS is appropriate for studying POMs' dilute solution when those clusters are very stable in the aqueous solution with simple and highly symmetrically structures; they have a reasonable amount of metal counterions to generate a detectable X-ray scattering contrast; they don't have any specific surface sites for interacting cations; they do not have co-ions or excess salts so that the true physical picture of counterions can be revealed. (*95*) Based on POM clusters form factors, scattering curve can be calculated for comparison with the experimental results. The scattering curve will obviously change if counterion association or the self-assembly of POMs takes place.

The dilute solution of $\{Mo_{72}V_{30}\}$ (2.5 nm size Keplerate cluster carrying 31 charges with the counterions being 14 K^+, 8 Na^+, 2 VO^{2+}, and 5 H^+) was explored in the first SAXS experiment. The distance pair distribution p(r), generated from the Moore analysis of the SAXS curve, corresponds to the probability of finding the vector length r in a molecule and can provide a physically meaningful description of the particle morphology. (*78*) For $\{Mo_{72}V_{30}\}$ in dilute aqueous solution, the p(r) curves shown in Figure 2.5-6 (top) correspond to discrete cluster with no counterion

association (a core-shell spherical particle with a maximum linear dimension of ~26 Å). When certain amount of acetone was introduced into the solution, another isolated small peak which is centered at ~30 Å and extends the effective distribution to ~34 Å appeared in the p(r) plot (Figure 2.5-6 (bottom)). The peak of $\{Mo_{72}V_{30}\}$ macroanions remained unchanged, indicating that the macroanions still existed as discrete ions since blackberry formation is a very slow process. The additional peak is caused by

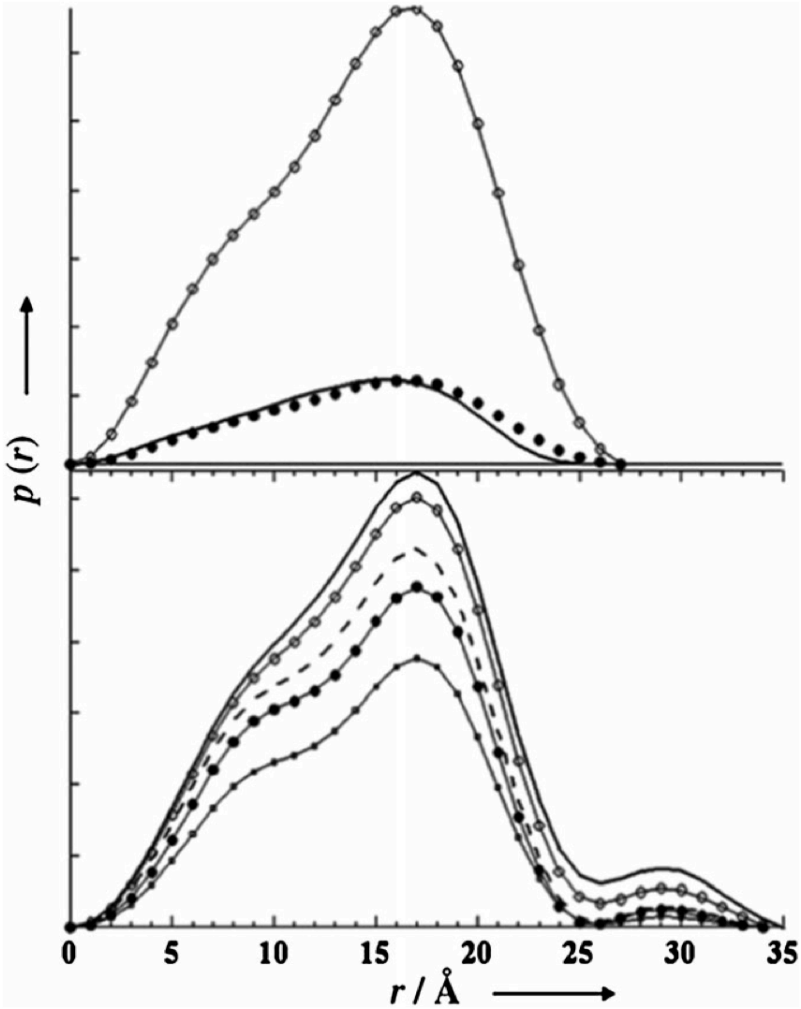

Figure 2.5-6. Top: distance distribution functions based on calculated and experimental scattering data for {Mo72V30} obtained by using an indirect Fourier transform of the primary SAXS data. (o): 0.052 mm $\{Mo_{72}V_{30}\}$, (•): 0.013 mm $\{Mo_{72}V_{30}\}$, (—): $\{Mo_{72}V_{30}\}$ calculated. Bottom: experimental distance distributions for 0.26 mm $\{Mo_{72}V_{30}\}$ in water and acetone–water mixed solvents with various acetone contents (in vol%). (—): 75% acetone–water, (o): 65% acetone–water, (---): 45% acetone–water, (•): 10% acetone–water, (■): in pure water. Reprinted with permission from ref. 78. Copyright 2009 Wiley-VCH.

higher electron density found around the $\{Mo_{72}V_{30}\}$ macroanions, suggesting that some metal counterions are closely associated with the macroions and distributed in the range of 0.2-0.9 nm to the surface of macroions. With increasing acetone content, the peak due to the counterion association became more and more distinct, and the average R_g of $\{Mo_{72}V_{30}\}$ macroions also increases according to Guinier plots. The apprearance of the peak due to associated couterions coexisted with the apprearance of the blackberry structures, indicating the direct connection between these two issues and the role of counterions in the blackberry formation.

2.5.5.2 Counterions exchange around macroions

Macroions can not only associate with couterions, but also distinguish couterions owning different hydrated sizes by interacting with them according to a corresponding preference sequence. In other words, the exchange of counterions around macroions can be achieved.

For $\{Mo_{72}Fe_{30}\}$ dilute solution, the original counterions were protons, and the blackberry size was observed to change due to adding a small amount of extra salts (Figure 2.5-7). By adding 1-20 mM LiCl or NaCl into the original solution, the blackberry size remained the same as the salt-free solution. By adding 0.1-10 mM KCl or a tiny amount of RbCl, the blackberry size significantly increase. A possible explanation was proposed as that ions with smaller hydrated sizes such as K^+ and Rb^+ ions could replace protons around $\{Mo_{72}Fe_{30}\}$, which consequently increased the attractive force between macroions and lead to larger blackberries, while ions with larger hydrated sizes such as Li^+ and Na^+ ions could not replace protons because of their lower priority. (*96*) Isothermal titration calorimetry (ITC) measurements was

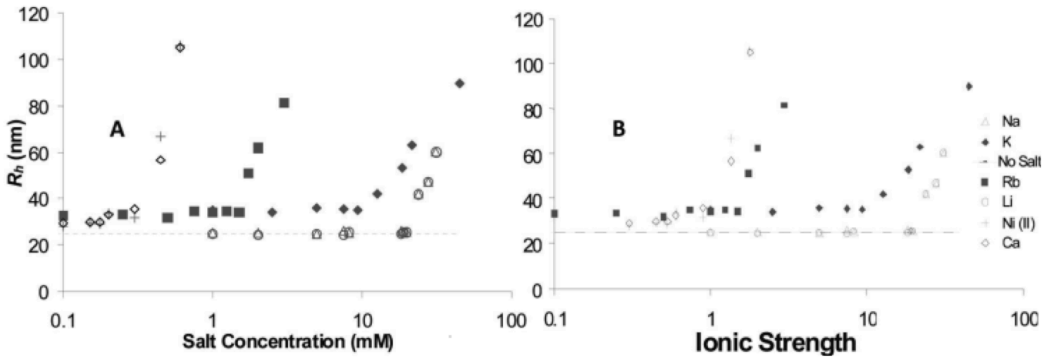

Figure 2.5-7. Change of blackberry size (in R_h) with added chloride salt concentration (A) and total ionic strength (B) for 0.5 mgmL^{-1} $\{Mo_{72}Fe_{30}\}$ solutions. For each added cation salt there is a CSC (critical salt concentration), above which the blackberry size increases with increasing salt concentration. Reprinted with permission from ref. 96. Copyright 2010 American Chemical Society.

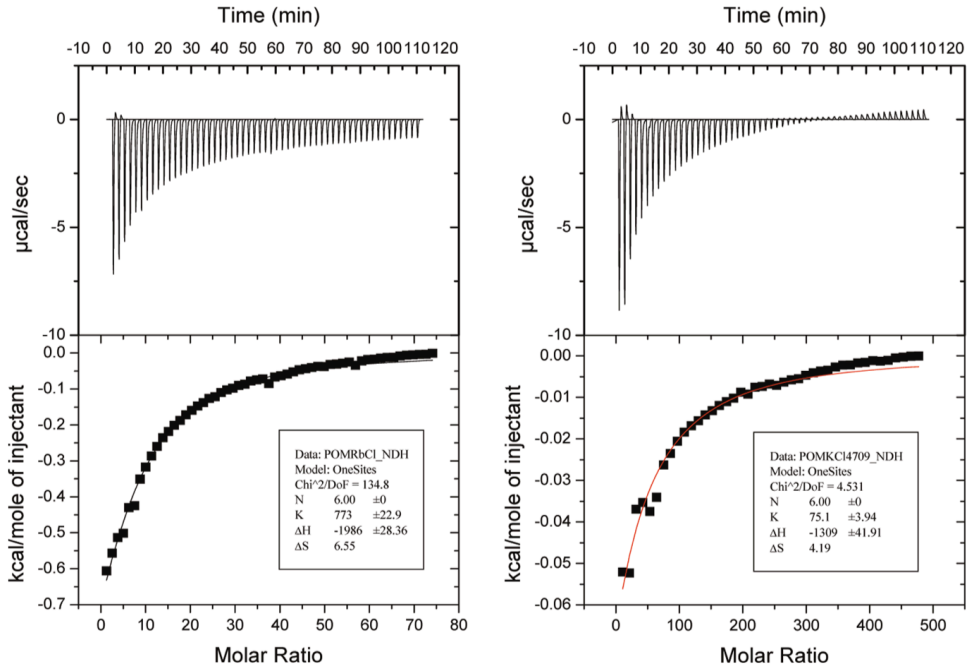

Figure 2.5-8. ITC results obtained when adding RbCl (left) and KCl (right) into 2.0mgmL^{-1} $\{Mo_{72}Fe_{30}\}$ solutions. Concentrations of 40mM for RbCl and 334mM for KCl were used. The molar ratio needed for saturation of the $\{Mo_{72}Fe_{30}\}$ binding sites is ~50-60:1 for K^+ and ~10:1 for Rb^+. Reprinted with permission from ref. 96. Copyright 2010 American Chemical Society.

applied for proving this hypothesis (Figure 2.5-8). When titrating NaCl to the aqueous solution of $\{Mo_{72}Fe_{30}\}$, there was no noticeable binding between Na^+ ions and $\{Mo_{72}Fe_{30}\}$ clusters even the molar ratio of Na^+ to POM was extremely high as

1000:1. However, the titration curves showed the binding between K^+/Rb^+ with macroions, in which 50-60 K^+ were needed for saturating the binding sites (~6) on each $\{Mo_{72}Fe_{30}\}$ cluster, and <10 Rb^+ ions were needed for saturating. This result also suggested the binding strength of Rb^+ ions to $\{Mo_{72}Fe_{30}\}$ is much stronger than that for K^+ ions. The ITC study confirmed that macroions can interact with counterions following the preference sequence of (Li^+, Na^+) < H_3O^+ < K^+ < Rb^+ < Cs^+. The counterion exchange can also be supported by the decrease of pH value (~0.2) after adding a 10:1 molar ratio of RbCl or CsCl to the $\{Mo_{72}Fe_{30}\}$ aqueous solution. This evidence indicated that the original protons disassociated with $\{Mo_{72}Fe_{30}\}$ clusters and became free in solution.

2.5.6 Controlling the assembly/disassembly and blackberry size

Previous studies indicate that the charge density of macroions plays an important role in the blackberry formation. The transition between single ions to blackberries, as well as tuning the blackberry size can be realized by adjusting the macroionic charge density from several aspects such as solvent polarity, solution pH, extra salt concentration, al et.

For the weak electrolyte POMs, the surface charge comes from the partial deprotonation of water ligands attached to it, which can be easily tuned by changing the solution pH. When the pH of 0.5 mg/mL $\{Mo_{72}Fe_{30}\}$ aqueous solution is below 2.9, the clusters stay as single molecules since the charge density is too low for them to self-assemble. The self-assembly process can be triggered by adding base into the solution. $\{Mo_{72}Cr_{30}\}$ anions demonstrate the similar pH-controlling assembly behavior with the switch point at pH=2.7. $\{Mo_{72}Fe_{30}\}$ with ammonium ions as

counterions are able to capture those counterions in the nano-pores on its surface, and thus macroions with appropriate charge density can self-assemble driven by the counterion-mediated attraction. However, after mildly heating of the solution to 40 °C, the total scattered intensity decreases as a result of disassembly of blackberries. The "power off" process can be attributed to the temperature induced release of ammonium ions from the pores into the bulk solution, leading to the enhanced charge density of macroions. (*97*) For the strong electrolyte macroions such as $\{Mo_{132}\}$ and $Pd_6L_4(NO_3)_{12}$ nanocages, the blackberry formation can be triggered only when the appropriate amount of less polar solvent is added into solutions. Moreover, a small amount of water soluble surfactants (with different chain length such as cetyltrimethylammonium bromide surfactant (CTAB), trimethyltetradecylammonium chloride surfactant (CTAT), dodecyltrimethylammonium bromide surfactant (DTAB), and octyltrimethylammonium bromide surfactant (OTAB)) were also introduced into macroionic solution such as $\{Mo_{72}V_{30}\}$ for decreasing the charge density, and consequently weakening the electrostatic repulsion between macroions. (*98*) The long-chain surfactants such as CTAB and CTAT were found to stoichiometrically interact with $\{Mo_{72}V_{30}\}$ clusters and could trigger the blackberry formation when the molar ratio of $\{Mo_{72}V_{30}\}$ to surfactant is 1:1.2. The average R_h of blackberries continuously increases with increasing surfactant concentration.

It's worthy to notice that the average blackberry size (for different POMs water/organic mixed solutions such as $\{Mo_{132}\}$, $\{Mo_{72}V_{30}\}$ and $\{W_{72}Mo_{60}\}$) is inversely proportional to the dielectric constant ε, suggesting that the self-assembly process is charge regulated. (*80, 99-101*) A general expression of blackberry sizes can be related with several parameters (as shown in Equation (2.18) and (2.19)).

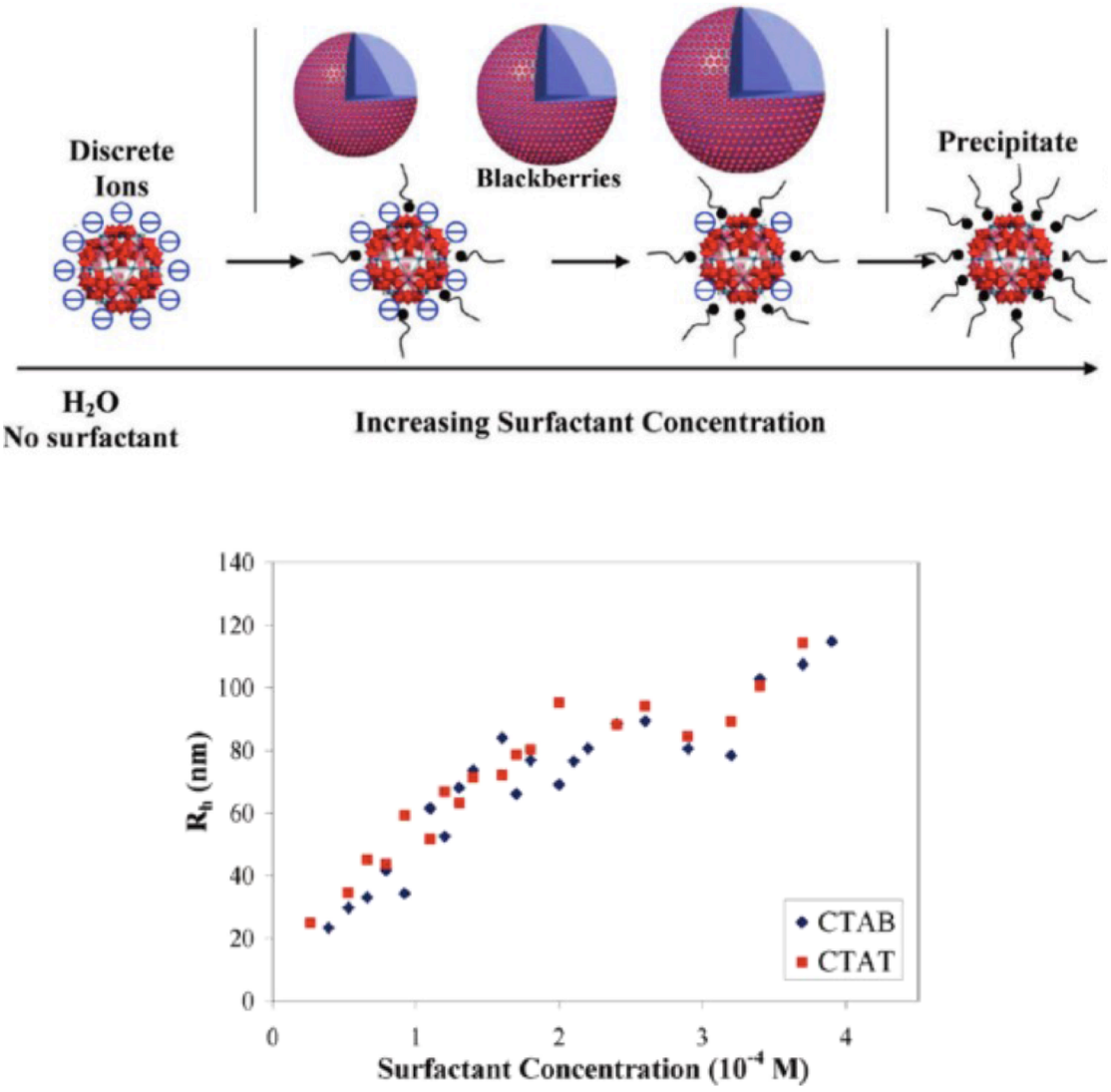

Figure 2.5-9. Top: Charge density on $\{Mo_{72}V_{30}\}$ decreases with the increment of surfactant concentration, which leads to the increment of blackberries size. Bottom: Average hydrodynamic radius (R_h) of the $\{Mo_{72}V_{30}\}$ blackberries in aqueous solution increases with surfactant (CTAB or CTAT) concentration. The concentration of $\{Mo_{72}V_{30}\}$ is 0.026 mM. Reprinted with permission from ref. 98. Copyright 2010 American Chemical Society.

$$R \approx -48\lambda_b u/\zeta^2 \tag{2.18}$$

$$\lambda_b = e^2/4\pi\varepsilon_o\varepsilon_r k_B T \approx 56/\varepsilon_r \tag{2.19}$$

in which ζ is the zeta potential, u is the cohesive bond energy (which reveals the magnitude of the attractive forces among the macroions on the blackberry shell), λ_b is

the Bjerrum length, ε_o is the vacuum permittivity, ε_r is the relative dielectric constant of the medium, e is the electron charge, k_B is the Boltzmann constant, and T is the absolute temperature.

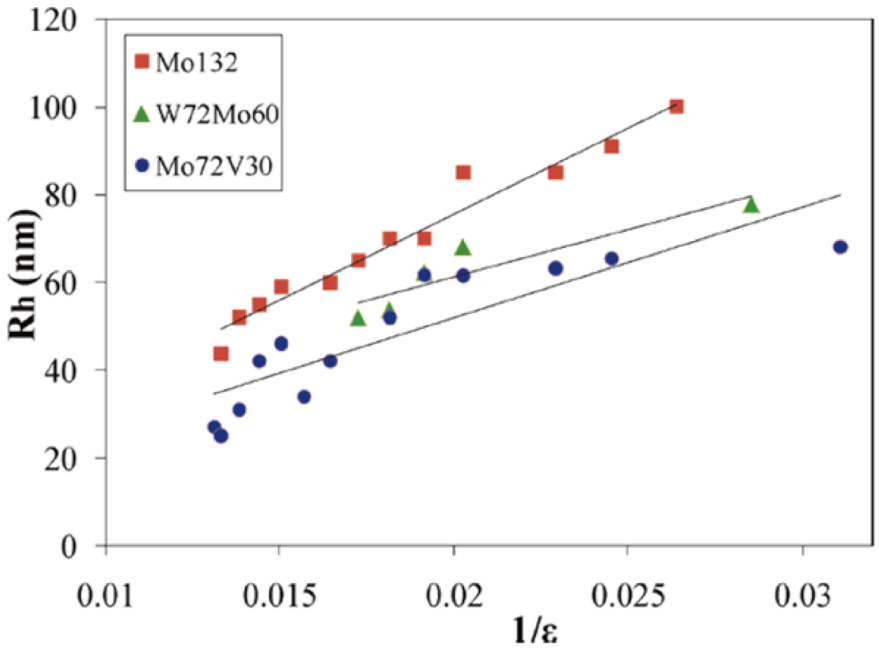

Figure 2.5-10. Plot of the average blackberry radius versus the inversed dielectric constant (1/ε) of the solvent for different POMs in water/acetone mixed solvents, demonstrating a linear relationship for these systems. Reprinted with permission from ref. 101. Copyright 2009 American Chemical Society.

The critical size of macroions is also an important issue for the unique self-assembly behavior. Different from colloidal suspensions, in macroionic solutions counterions cannot be treated as point charges and the hydrated size of counterions affects their affinity to macroions. Therefore, the size disparity between highly charged particles and counterions is considered to play a key role in ion-pairing and like charge attraction. As an important but unclear question, what is the lower critical size limit of macroions that tend to attract each other and form blackberry structures? Currently, the smallest macroions that were proved to be able to self-assemble are

ionic POSSs with their size smaller than 1 nm and highest charge density (>4 per nm^2). (*102*)

2.5.7 The mechanism of the self-assembly: connection to the virus capsid formation

Different from relatively fast self-assembly of amphiphilic systems, the transition from single macroions to blackberry structures takes a long period of time, sometimes even several months, to reach the equilibrium. The kinetic studies of the slow self-assembly process have been conducted by monitoring solutions for long time, which shared similarities with the self-assembly of virus capsid proteins.

2.5.7.1 The kinetic properties of the self-assembly

The slow blackberry formation process under certain circumstances enables detailed study on the mechanism of the self-assembly. Both typical SLS and DLS studies were performed for investigating the formation of $\{Mo_{72}Fe_{30}\}$ blackberries in aqueous solution at different macroionic concentrations. (*103*) Figure 2.5-11 demonstrates that at room temperature the self-assembly process takes months to reach equilibrium. The scattered intensity monitored by SLS increased continuously with time, suggesting the continuous formation of assembly structures in solution. Meanwhile, two types of particles were observed by the CONTIN analysis from DLS Measurements in solution: one with $R_h \approx 1.2$ nm which could be assigned to $\{Mo_{72}Fe_{30}\}$ unimers and the other with average $R_h \approx 25$ nm which was attributed to large assemblies. The small-size peak became smaller and smaller while the big-size one grew larger with time, indicating that the discrete macroions were continuously

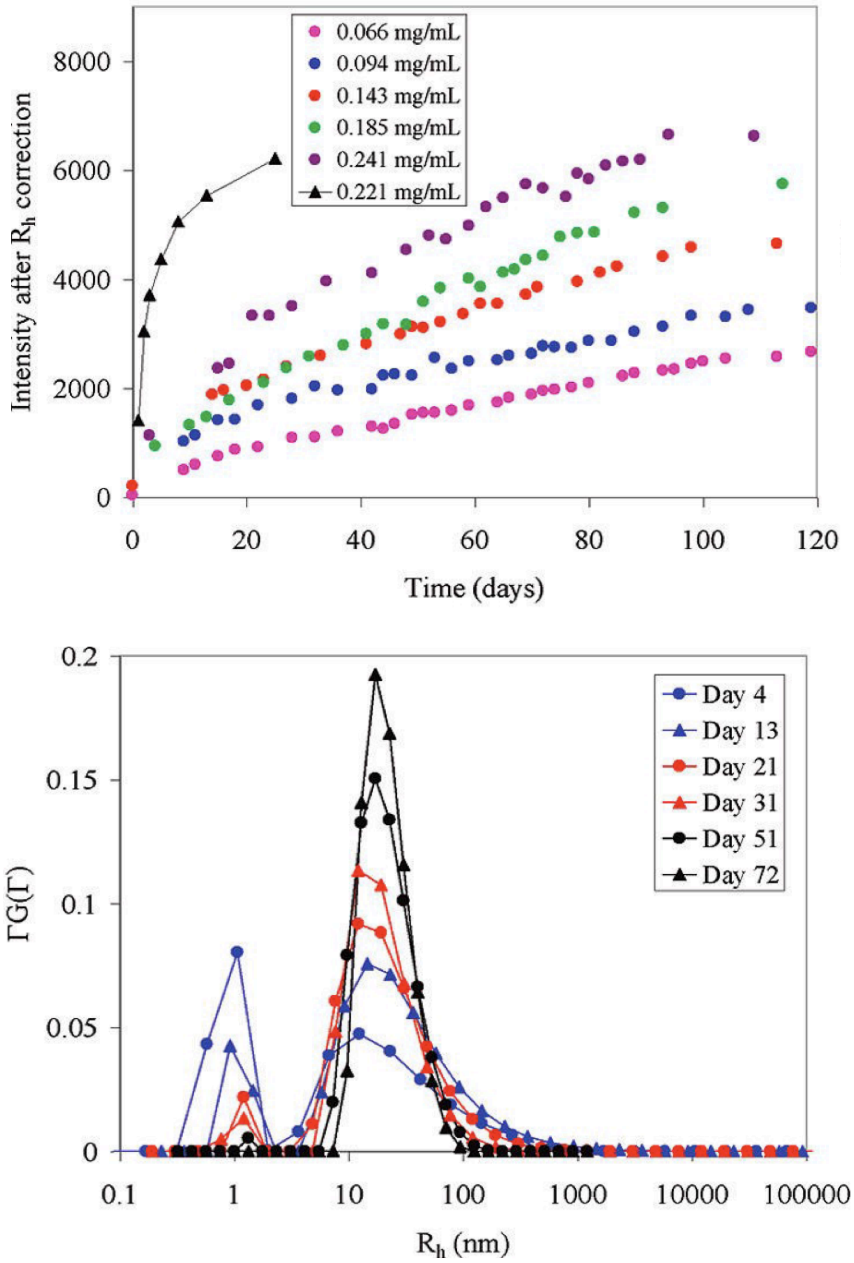

Figure 2.5-11. Top: Change of total scattered intensity of $\{Mo_{72}Fe_{30}\}$ solutions at 90˚ scattering angle. All solutions were kept at 25 ˚C except one at 45 ˚C (the data shown by black triangle). Bottom: CONTIN analysis of DLS study on {Mo72Fe30} aqueous solution at different times. Reprinted with permission from ref. 103. Copyright 2005 American Chemical Society.

self-assembling into blackberries. More importantly, the average R_h of blackberry structures remained almost unchanged during the whole process, suggesting us the formation mechanism of blackberries should follow upper route in Figure 2.5-12. (*104*) That is, at the beginning, the unimers slowly associated into dimmers (or

oligmers), which was the rate-determining step. Once the amount of oligmers exceeded the critical concentration, they quickly assembled into large blackberries. This step is fast so that no "smaller" blackberries could be observed during the whole process.

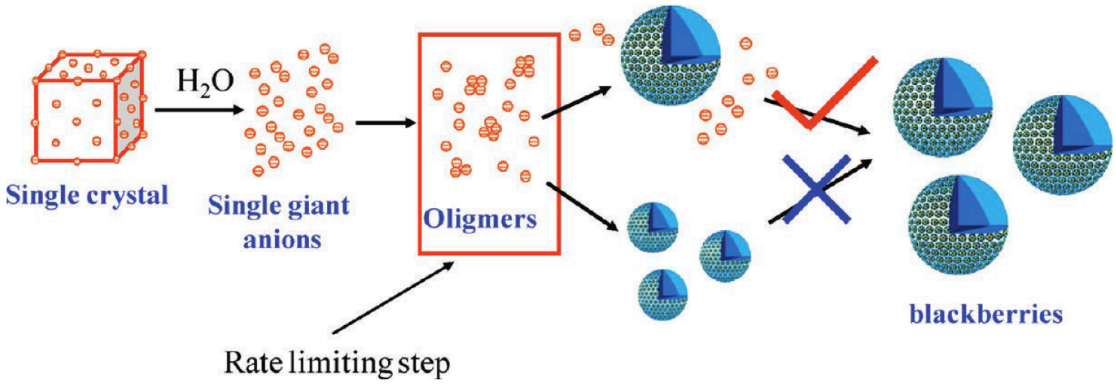

Figure 2.5-12. Possible mechanisms of $\{Mo_{72}Fe_{30}\}$ blackberry formation in dilute aqueous solution. The upper mechanism has been proven to be correct based on SLS and DLS results, while the bottom mechanism can be ruled out. Reprinted with permission from ref. 104. Copyright 2006 American Chemical Society.

Since we considered the transition of macroions to oligomers as the rate-determining step, the slowness of the blackberry formation was attributed to the high energy barrier for this process. (*105, 106*) By using the Arrhenius equation $\ln(k)=-E_a/RT+\ln A$ (with k, A, E_a, R, and T being the reaction rate, the frequency factor, the activation energy, the universal gas constant, and the temperature, respectively.), the activation energy can be estimated by studying the temperature dependence of k. Time-resolved SLS studies were used to determine the initial reaction rates in $\{Mo_{72}Fe_{30}\}$ aqueous solutions at different temperatures. The calculated activation energy of the oligmer formation was indeed very high as ~115±8 kJ/mol (Figure 2.5-13).

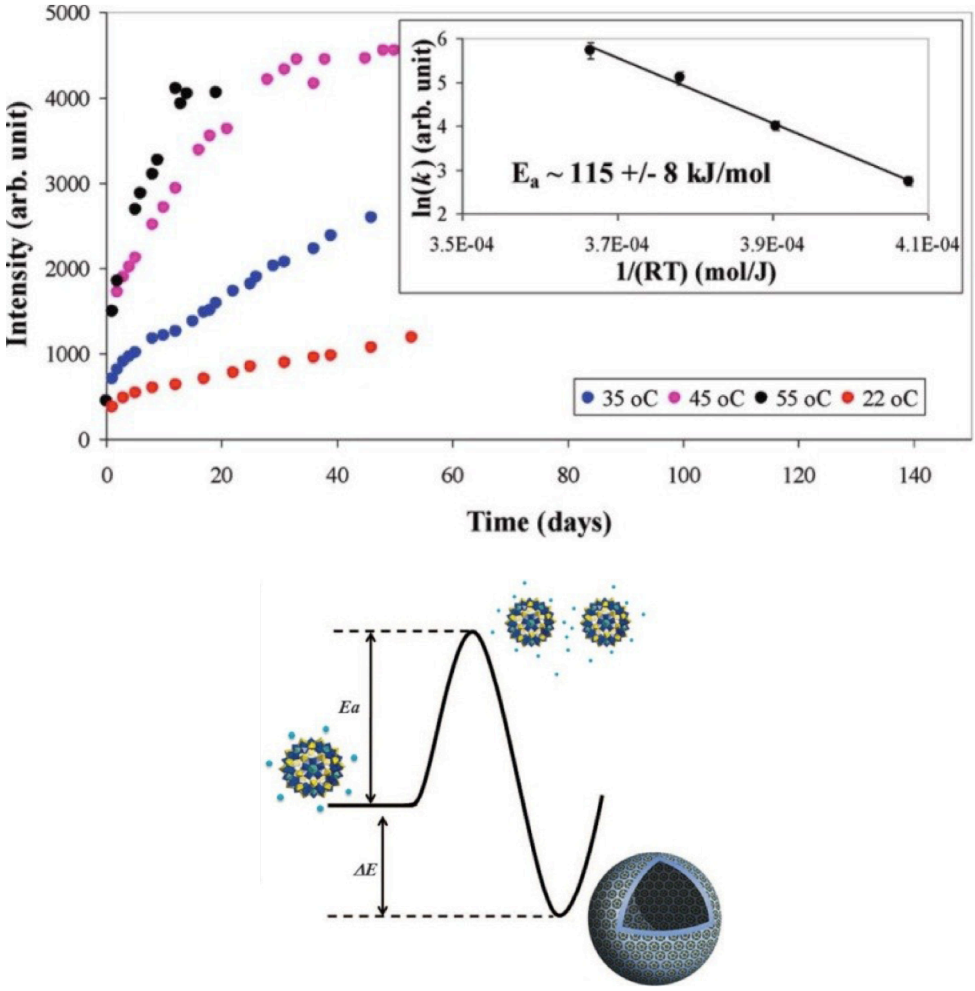

Figure 2.5-13. Top: Increment of the scattered intensity (I) from 0.5 $mgmL^{-1}$ $\{Mo_{72}Fe_{30}\}/H_2O$ solutions at different temperatures (22, 35, 45, and 55 ˚C) with time indicates the progress of blackberry formation. (Inset) Calculation of the activation energy (Ea) for the blackberry formation. Reprinted with permission from ref. 105. Copyright 2005 American Chemical Society. Bottom: Thermodynamic demonstration of the blackberry formation. Reprinted with permission from ref. 106. Copyright 2011 AAAS.

2.5.7.2 Lag phase during the blackberry formation and its similarity to the virus capsid formation

In aqueous solution of $\{Mo_{72}Fe_{30}\}$ with no or tiny amount of extra salts (e.g. NaCl, NaBr, NaI, and Na_2SO_4 at concentrations of 0.017 mol/L), the time-resolved SLS studies showed that there is a short lag period at the beginning (see Figures 4, 8, and 10 in ref 100). This lag phase becomes significant when the extra salt

concentration is higher (Figure 2.5-14). (*107*) The initial scattered intensity from the $\{Mo_{72}Fe_{30}\}$ (with concentrated NaCl) solution was very low, suggesting that almost all the macroanions exist as discrete ions. After a lag period of 20 days, the intensity suddenly started to increase until it stabilized at a very high level after months. Overall, the whole kinetic curve is sigmoidal with an extended lag phase.

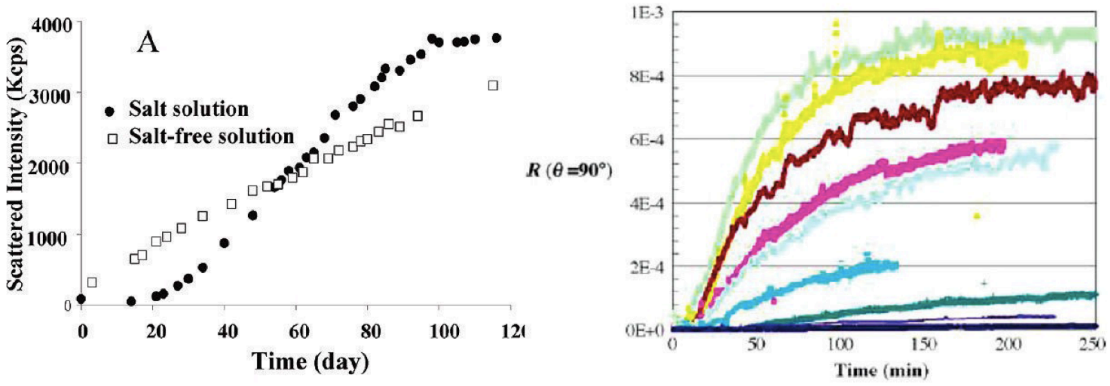

Figure 2.5-14. Left: Comparison of scattered intensity increment of two $\{Mo_{72}Fe_{30}\}$ samples along reaction time in 0.9 wt% NaCl and salt-free solutions Reprinted with permission from ref. 109. Copyright 2010 American Chemical Society. Right: Light scattering study of the assembly of HPV capsid proteins at various HPV concentrations. The lag time, reaction slope, and extent of assembly were dependent upon the initial protein concentration. Changes in scattered light were not observed until minutes later. Reprinted with permission from ref. 108. Copyright 2004 Elsevier.

The self-assembly process possessing a sigmoidal kinetic curve has also been reported in other systems such as virus capsid proteins (Figure 2.5-14, right), (*108-111*) ester hydrolysis, (*112, 113*) vesicle formation, (*114*) and nanoparticle preparation. (*115*) Generally, the sigmoidal curve represents a two-step process: in the initial lag period, the "reaction" begins with the slow formation of oligomer nucleus (which is rate determining); once the amount of the nucleus has exceeded a critical value, oligomers or monomers can quickly assemble to larger structures until reaching the equilibrium. (*116*)

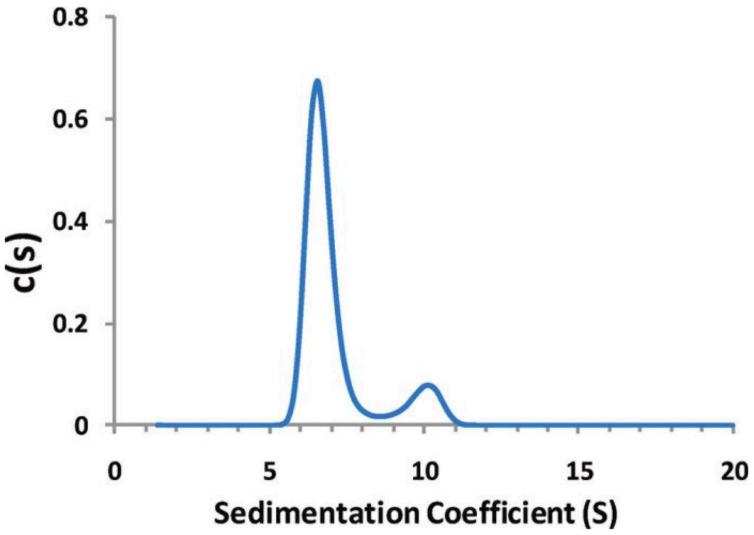

Figure 2.5-15. Continuous size distribution c(s) analysis of $\{Mo_{72}Fe_{30}\}$ solution versus sedimentation coefficient, s. Experiments were performed at a $\{Mo_{72}Fe_{30}\}$ concentration of 10 mg/mL in 170 mM NaCl solution at 20 °C. Reprinted with permission from ref. 107. Copyright 2010 American Chemical Society.

Sedimentation velocity (SV) experiments were performed on the 18th day after the sample solution was prepared (which is corresponding to the final stage of the lag period in the kinetic curve) to identify the oligomeric state during the lag period. In a typical SV experiment, the time-dependent changes in solution absorbance is recorded as a result of sedimentation boundary movement. The rate at which the sedimentation boundary moves is a measure of the sedimentation coefficient s and corresponding sedimentation coefficient distributions c(s) of the investigated species which can be fitted by Lamm equation. From the results of the $\{Mo_{72}Fe_{30}\}$ solution on the 18th day, two species were observed: the dominant one (56%) with s ~ 6.6 S and the other (10%) with s ~ 9.5 S (Figure 2.5-15). (*107*) The theoretical sedimentation coefficients for $\{Mo_{72}Fe_{30}\}$ monomers, dimmers, and trimers are 6.9 S, 11.0 S, and 14.5 S, respectively if assuming all the species are spherical; thus, the 6.6 S species corresponds to the $\{Mo_{72}Fe_{30}\}$ monomers, and the 9.5 S species is attributed to dimers (The lower value compared with the theoretical value is possibly due to the

fact that dimmers are not spherical.). The existence of macroionic dimers by SV measurements further confirmed our proposed mechanism of the blackberry formation.

In additional to the concentration of extra salts, the length of the lag period also depends on temperature, the valence of the cations or the anions, as well as the solvent content. (*107*) Importantly, blackberries demonstrated interesting similarities with virus capsids (mostly spherical, single-layered structures formed by the ordered assembly of capsid protein units which are also soluble macroanions) in both the assembly structures and formation processes. (*109-111*) For example, a sigmoidal kinetic curve in SLS studies was found for the in vitro assembly of human papillomavirus (HPV) from protein subunits to icosahedral HPV capsids (Figure 2.5-14, right). The lag period of the in vitro assembly depended on the protein concentration and the ionic strength. A theoretical nucleation-elongation model was applied for explaining the delay time in which the slow formation of dimers of protein subunits was suggested at the beginning of HPV assembly. (*108*) Similar results were also reported in the in vitro assembly process of hepatitis B virus capsids (*110, 117*) and cowpea chlorotic mottle virus capsids, (*118*) which also showed temperature and ionic strength dependence.

Both virus capsid proteins and POMs are nanoscale, soluble macroion, being able to self-assemble into single layered spherical structures, and they show similar sigmoidal curves in their kinetic assembly process; thus, it is reasonable to postulate that their might share similar self-assembly mechanism, as well as driving forces. Ideally and potentially, the POMs or other simple macroions might be useful as simple model systems for helping understand the more complicated biomacromolecular systems. Currently, the hydrophobic interaction is widely

believed as the dominant driving force for the virus capsid formation, while hydrophobic interaction does not play a role in the blackberry formation since POMs do not contain any hydrophobic moieties. Then one open question is: is it possible that the electrostatic interaction is underestimated in the virus shell formation?

2.6 Self-assemblies of covalently functionalized amphiphilic hybrid POMs

POMs, carrying many charges and a large amount of oxo ligands on their surfaces, are hydrophilic and soluble in aqueous solution; thus, many of them are not compatible with organic media. Chemically attaching organic components to POMs can not only tune their electric properties, but also improve their compatibility and processibility. (*10*) Moreover, the introduced hydrophobic organic ligands could renders the clusters amphiphilic features, leading to hydrophobic interaction participating in their self-assembly behavior in water/air and water/oil interface, polar and nonpolar solvents. (*119-129*) The self-assembly of amphiphilic hybrid POMs is more complicated than pure macroions and common amphiphilic surfactants, since both solvophobic interaction, the interaction between charged macroions, as well as the counterion effect, molecule topology, and solvent polarity, need be taken into consideration. (*122*) The current research on all the effects will be summarized in the following sections.

2.6.1 Surfactants with POMs as polar head groups

Conventinal surfactants usually have one polar head group covalently linked with one or several hydrophobic tails. Packing parameter P, a definition of a

surfactant's geometrical parameters, is always used to predict the morphology of assemblies formed by surfactants in polar or nonpolar solvents, by taking into account the volume of the hydrophobic chain, the cross sectional area of the hydrophilic core, and the length of the hydrophobic chain. (*122*) The surfactant type POM-organic amphiphiles with POMs as polar heads have higher negative charge and much larger sizes and show their unique features in the self-assembly process. (*121*)

Table 2.6-1. Formulas and molecular structures of the hybrid surfactants previously studied in our group.

Abbreviation	Hybrid surfactants formula	Molecular structure
S1	$(TBA)_3[MnMo_6O_{18}\{(OCH_2)_3CNHCO(CH_2)_4CH_3\}_2]$	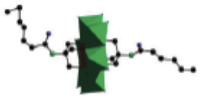
S2	$(TBA)_3[MnMo_6O_{18}\{(OCH_2)_3CNHCO(CH_2)_{14}CH_3\}_2]$	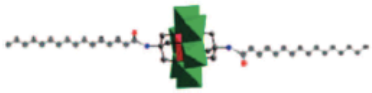
S3	$(TBA)_2[V_6O_{13}\{(OCH_2)_3CCH_2OOC(CH_2)_{16}CH_3\}_2]$	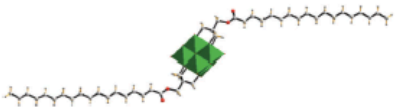
S4	$(TBA)_2[V_6O_{13}\{(OCH_2)_3CNHOC(CH_2)_3C_{16}H_9\}\{(OCH_2)_3CNH_2\}]$	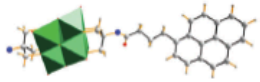
S5	$(TBA)_2[V_6O_{13}\{(OCH_2)_3CNHOC(CH_2)_3C_{16}H_9\}_2]$	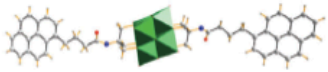
S6	$((TBA)_5H[P_2V_3W_{15}O_{59}(OCH_2)_3CNHCOC_{15}H_{31}]$	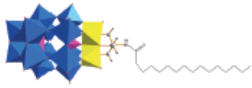
S7	$TBA_{10}H_2[\{P_2V_3W_{15}O_{59}(OCH_2)_3CNHCO\}_2]$	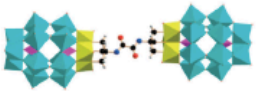

Table 2-3 lists all POM-organic hybrids we have investigated. The surfactants S1, S2, S3 and S6 show amphiphilic properties by self-assembling into vesicle structures in proper polar solvents (Figure 2.6-1). (*128-130*) Comparing with lipid surfactant which possesses the same double alkyl chains as S2, the POM-organic hybrids formed much bigger vesicles in aqueous solution, which is due to the larger

polar heads (POMs) affecting the packing of the whole surfactants. Moreover, the vesicle formation process of the POM-organic surfactants is much slower than the common surfactants, which takes up to two months for reaching equilibrium. The possible reason can be that the two hydrophobic tails on both side of Anderson cluster need to bend into the solvent-phobic layer, resulting a high bending energy. Moreover, two hybrids S1 and S2 were able to form reverse vesicles in nonpolar solvents (acetonitrile/toluene mixed solvents) (*129*) with the sizes of the assemblies continuously increasing when lowering solvent polarity (Figure. 2.6-2), which is due to the increasing solvophobic interaction. (*128, 130*)

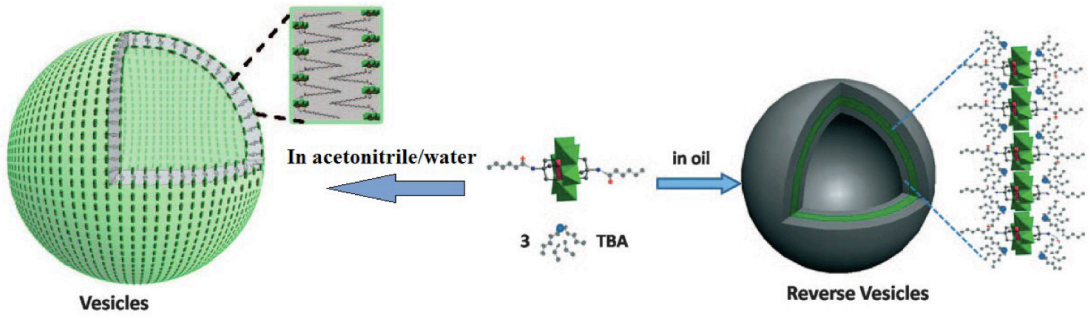

Figure 2.6-1. The formation of vesicles and reverse vesicles structures in polar and nonpolar solvent, respectively. Adapted with permission from ref. 128 and 129. Copyright 2008 American Chemical Society and 2010 Wiley-VCH.

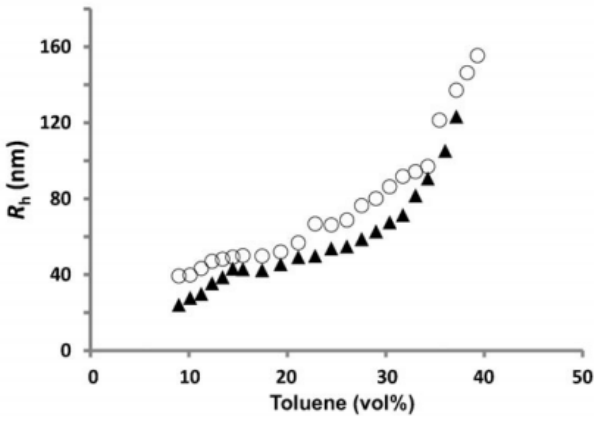

Figure 2.6-2. Change of R_h of Mn-Anderson-C_{16} (triangle) and Mn-Anderson-C_6 (circle) in MeCN solution with a concentration of 0.1 mgmL^{-1} as a function of titrated toluene contents. Reprinted with permission from ref. 129. Copyright 2010 Wiley-VCH.

The self-assembly of POM-organic hybrid was also found to be influenced by solvent polarity. For example, the vesicle sizes of both S3 and S6 decreased linearly with the inverse of the dielectric constant of the solvent, indicating a charge regulated process. S3 demonstrated a much more negative slope than S6, which might be attributed to the different degree of counterion dissociation of hybrids' polar heads. The counterion disassociation is controlled by factors such as static charge interaction, solvent polarity and solvation of ions. Possessing the same type of counterions, Dawson-type POM (in S6 with 6 charges) is more negative charged than hexavanadate (in S3 with 2 charges), leading to stronger attraction to TBA counterions in the former case. (*130, 131*) Therefore, the dissociation of TBA, as well as the effective charge on the S3 increases more significantly when the solvent polarity increases, which finally results in a more negative slope. (*130, 131*)

Counterions are also able to tune the size of vesicles formed by S6. The vesicle size decreased gradually with adding more $ZnCl_2$, while the vesicle size remained unchanged at first upon addition of NaI, and then gradually became bigger when the concentration of NaI exceeds 0.03 mg/mL. The size dependence on $ZnCl_2$ may be related to the coordination of Zn^{2+} ions to the terminal or bridging oxo ligands on the surface of the Dawson clusters, which forces the exposure of the polar domains to the solvent environment, and consequently increases the curvature of the vesicles. On the other hand, upon the addition of NaI, the sodium ions were proved to replace the original TBA counterions, and reduced the repulsion between the polar head groups by shielding the net charge of the POMs. As a result, the curvature of vesicles decreased and size became bigger. Other salts such as $CuCl_2$, TBAI or DTMABr didn't obviously affect the vesicle size because those cations were not able to replace the original cations surrounding the polar Dawson clusters. However, TBAI and

DTMABr were found to cause the disassembly of the vesicles since the accumulation of those hydrophobic cations around the polar heads would weaken the amphiphilic nature of the hybrids.

The hybrids can sometimes response to the pH of the solvent when the POM head groups reversibly release and associate protons with their surface oxo ligands and the net charge of POMs changes. Consequently, their assembly sizes varies with the aqueous solution pH since the repulsion between the POMs on the surface of vesicles can be tuned. (*121, 130*)

2.6.2 Molecular bola of organic-POM hybrids

Table 2.6-2. Five dumbbell-shaped inorganic-organic hybrid molecules

Molecular Formulae of Hybrids	Polar head to polar head length	Molecular Structure
$TBA_{10}H_2[(P_2V_3W_{15}O_{59}(OCH_2)_3CNHCO)_2]$ **(1)**	4.03 nm	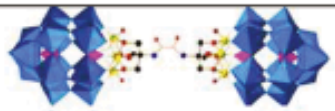
$TBA_{10}H_2[(P_2V_3W_{15}O_{59}(OCH_2)_3CNHCO)_2CH_2]$ **(2)**	4.12 nm	
$TBA_{10}H_2[(P_2V_3W_{15}O_{59}(OCH_2)_3CNHCOCH_2)_2]$ **(3)**	4.25 nm	
$TBA_{10}H_2[(P_2V_3W_{15}O_{59}(OCH_2)_3CNHCOC_5H_3N)_2]$ **(4)**	4.72 nm	
$TBA_{10}H_2[(P_2V_3W_{15}O_{59}(OCH_2)_3CCH_2)_2O]$ **(5)**	3.35 nm	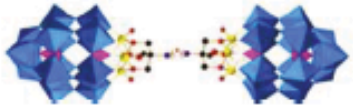

[a] The inorganic parts are Wells–Dawson-type clusters connected by five different bis(TRIS) ligands: L^1–L^5. The second column shows approximate lengths of each hybrid. (blue ○) tungsten, (yellow ○) vanadium, (purple ○) phosphorous, (red ○) oxygen, (●) carbon, and (blue ○) nitrogen. For clarity, hydrogen is not shown.

Here bola-amphiphiles are referred to a class of molecules with a hydrophobic skeleton and two hydrophilic end groups. The development of synthetic method rendered us to obtain molecular bolas with Lindqvist and Dawson type POMs as the hydrophilic end groups (Table 2-4). (*124, 125*) In our research, five dumbbell-shaped POM-organic amphiphiles were studied and compared with POM-based surfactants due to the extraordinarily large polar head groups and relatively small hydrophobic domains in the former case. The bola-amphiphiles were observed to form vesicle structures with POMs on the outside surface while the organic linkers stayed inside the shell (Figure 2.6-3). The sizes of the vesicles showed a increasing trend when the polarities of the solvents were lowered, (*124, 125*) which was the opposite trend with that of POM-organic hybrid surfactants. The bulky and hydrophobic counterions TBA were speculated to get involved in forming the hydrophobic domains (*123*) because of the electrostatic interation with the POMs and spatial obstruction. The vesicle formation was found to be an entropy-driven process, and the entropy term TΔS was much larger than that for the conventional surfactants, such as the inonic Gemini surfactants. The high entropy may be attributed to the TBA ions which will destroy the hydrogen bonds of well-organized water molecules around the alkyl tails when they are involved in the vesicle formation. In addition, the length of the organic linker seems to be related to the TΔS, since more hydrogen bonds need to be broken, and the entropy gain tends to be more negative for a longer linker. The water/air interfacial behavior of these bola hybrids was investigated by the Langmuir-Blodgett technique (Figure 2.6-4). Hybrids with alkyl chain linkers cannot form a compact monolayer at the interface, while hybrids with bipyridine and ether linkers showed the formation of an interfacial compact monolayer. We believed that the hydrophibicity of the organic linkers play a dominant roles in the monolayer formation.

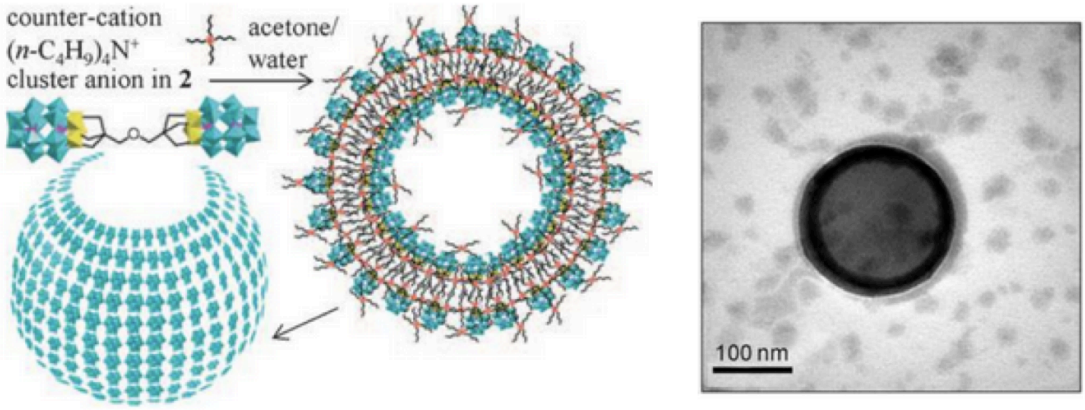

Figure 2.6-3. Left: Molecular structures of Dawson-type POMs-based bola-amphiphiles and its self-assembly into vesicle structures. Right: TEM image showing a hollow vesicle structure of the self-assembly. Reprinted with permission from ref. 124. Copyright 2009 Wiley-VCH.

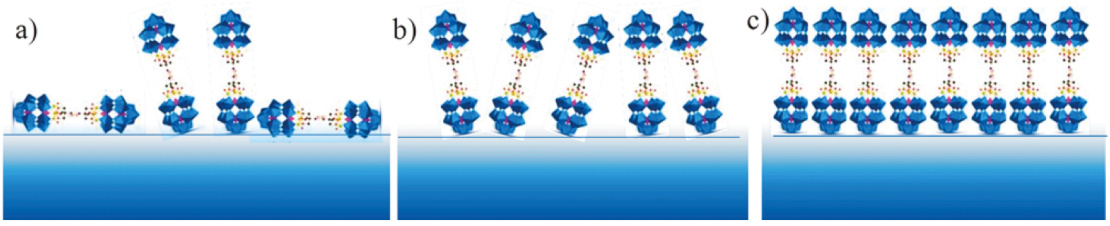

Figure 2.6-4. Monolayer formation for the dumbbell-shaped hybrid surfactants at the water/vapor interface: a) liquid expansion (LE)/G phase, b) LE phase, and c) liquid condensed (LC) phase. Reprinted with permission from ref. 123. Copyright 2010 American Chemical Society.

2.7 Conlusion and outlook

The past decades has witnessed the significant advancement of the research on the synthesis and application of POMs-based materials. The solution study of those large polyoxoanions fills the gap between simple ions and colloids, and they serve as ideal models for helping understand polyelectrolytes and biomacromolecules. The unique self-assembly process of macroions and smart recognition behavior reveal the prossible mechanism for the self-assembly of bio-macroanions such as virus capsid proteins. Our further research will expand the fields from POMs to other macroionic

systems including fully organic systems. Meanwhile, the currently investigated amphiphilic POM-based hybrids possess a small portion of organic parts. In the future, we will create various hybrid materials, e.g. polymer-tethered molecular nanoparticles, with a lot of potential applications.

CHAPTER III

EXPERIMENTAL

3.1 Laser light scattering

When the particles interact with the light that strikes them and deflect some of that light from its original direction, we think this light as being "scattered". The intensity of scattered light depends on several parameters such as the wavelength of the incident light, the size and shape of the scattering particles, the optical properties of the scatterers, the angle of observation, etc. Generally, laser light scattering (LLS) can be classified as static and dynamic light scattering based on how the intensity is measured. In static light scattering (SLS), the time-average total intensity is measured as a function of scattering angle; while in dynamic light scattering (DLS), the fluctuation of the intensity is measured and is represented through the intensity autocorrelation function.

3.1.1 The theory of Rayleigh scattering

The Rayleigh scattering is applicable when the scattering centers are much smaller than the wavelength of the radiation. In other words, the size and shape of the scatterer is negligible. The scattering by single molecule can written as, (*132, 133*)

$$\frac{i_s}{I_{0,u}} = \frac{2\pi^2 M}{r^2 \lambda_0^4 N_A \rho}(n-1)^2(1+\cos^2\phi_x) \tag{3.1}$$

in which i_s is the intensity of light scattered per unit volume measured at r and ϕ_x, I_0 is the intensity of the unpolarized incident light, M is the molecular weight, n is the refractive index, ρ is the density, λ_0 is the wavelength in vacuum.

Furthermore, in solution, the molecular motion results in small fluctuations in density at the molecular level. Thus we need develop the Rayleigh equation depending on the square of fluctuation in polarizability α and concentration c.

$$\frac{i}{I_0} = \frac{\pi^2 \overline{(\delta\alpha)}}{2\varepsilon_0^2 r^2 \lambda^4}(1+\cos^2\phi_x) \tag{3.2}$$

$$\frac{i}{I_0} = \frac{2\pi^2 [n(dn/dc)]^2 k_B T c}{r^2 \lambda^4 (\partial \pi_{osm}/\partial c)_0}(1+\cos^2\phi_x) \tag{3.3}$$

where π_{osm} is the equilibrium osmotic pressure of a solution and equals to $RT(c/M+Bc^2)$. Thus,

$$\frac{i}{I_0} = \frac{2\pi^2 [n(dn/dc)]^2 c}{N_A r^2 \lambda^4 (1/M + 2Bc)}(1+\cos^2\phi_x) \tag{3.4}$$

It can be written as

$$\frac{Kc}{R_\theta} = \frac{1}{M} + 2A_2c \tag{3.5}$$

with define $K=2\pi^2n^2(dn/dc)^2/(N_A\lambda^4)$ as a constant and $R_\theta=ir^2/[I_0(1+\cos^2\theta)]$ as Rayleigh ratio which is a measure of the relative scattering capability of different species.

3.1.2 The theory of Debye scattering

When the particles are large and their size cannot be negligible, different regions of the same particle will behave as scattering centers, consequently there will be interference between waves of scattered light. Therefore, the Rayleigh ratio must be modified by multiplying by a correction factor P(θ) as follows, (*132, 133*)

$$\frac{Kc}{R_\theta} = \frac{1}{P(\theta)}(\frac{1}{M} + 2A_2c) \tag{3.6}$$

With interference, the scattered intensity measured at a point C i_C, equals to,

$$i_C \propto [2\cos(\frac{\pi\Delta x}{\lambda})]^2 \left|E_0\right|^2 \tag{3.7}$$

in which Δx is the distance between the pair of scattering centers, E_0 is the original electric field. Without interference,

$$i_s \propto 2^2 \left|E_0\right|^2 \tag{3.8}$$

Thus, we obtain P(θ) as follows,

$$P(\theta) = \frac{i_C}{i_s} = \cos^2(\frac{\pi \Delta x}{\lambda}) = 1 + \frac{\sin[(4\pi r / \lambda)\sin(\theta / 2)]}{(4\pi r / \lambda)\sin(\theta / 2)} \tag{3.9}$$

Defining scattering factor q=4π/λ×sin(θ/2), then Equation 3.9 can be simplified as ,

$$\frac{i_C}{i_s} = 1 + \frac{\sin(qr)}{qr} \tag{3.10}$$

If we expand this result to a particle that consists of N scattering centers, then the form factor P(θ) can be written as,

$$P(\theta) = \frac{i_C}{i_s} = \frac{1}{N^2} \sum_i \sum_j \frac{\sin(qr_{ij})}{qr_{ij}} \tag{3.11}$$

$$\approx 1 - \frac{q^2}{6N^2} \sum_i \sum_j r_{ij}^2$$

Therefore,

$$\frac{Kc}{R_\theta} = (\frac{1}{M} + 2A_2 c)(1 + \frac{16\pi^2 R_g^2}{3\lambda^2} \sin^2 \frac{\theta}{2}) \tag{3.12}$$

3.1.3 Static light scattering

Static light scattering is applied to study the angular dependence of the scattered light intensity. (*132, 133*) (Figure 3.1-1) Measurement of the scattering intensity at different angles can tell us the root mean square radius, also called the radius of gyration R_g. The second virial coefficient A_2 can be calculated by measuring the scattering intensity for the species at various concentrations. A typical Zimm plot can be made by measuring a series of solutions with different concentrations, and extrapolating data to zero scattering angle and zero concentration, which can tell the weight average molecular weight M_w of the species. Zimm plot is not very broadly used when dealing with complex solution systems because the calculation requires accurate particle concentration.

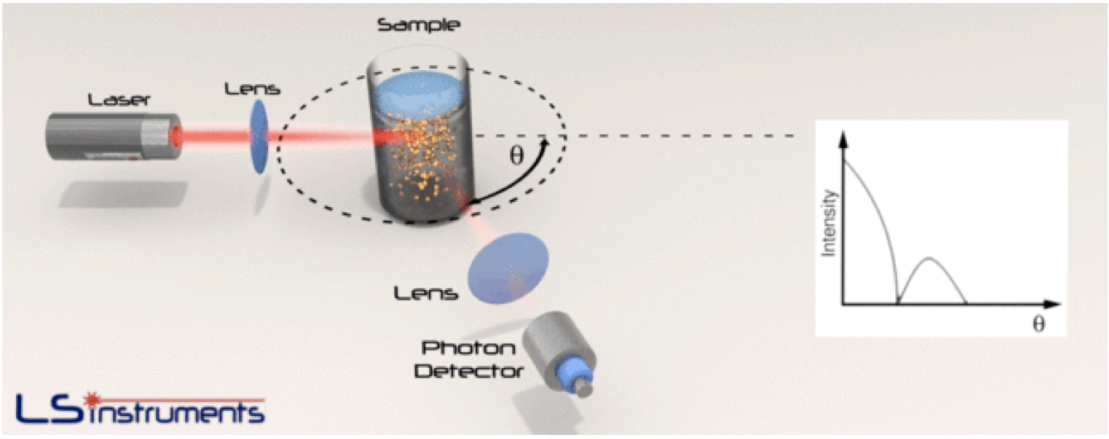

Figure 3.1-1. A typical static light scattering measurement.

3.1.4 Dynamic light scattering

Generally, the scattered intensity not only depends on the detection angel θ, but also the time t since the scattering centers are in constant random motion due to

their kinetic energy. The dynamic of the molecules directly determine the fluctuation of the intensity with time, as well as the rate at which these fluctuations decay to the equilibrium. The time dependence of intensity, monitored by DLS, is represented by the autocorrelation function, (*132, 133*)

$$\langle I(t)I(t+\tau)\rangle = \lim_{t_n\to\infty}\frac{1}{t_n}\int_0^{t_n} I(t)I(t+\tau)dt \tag{3.13}$$

in which τ is the decay time. The autocorrelation function has its highest value at τ=0. When τ is large, I(t) and I(t+τ) are uncorrelated. The ratio of the autocorrelation function to its asymptotic value $\langle I(t)\rangle^2$ can be written as,

$$\frac{\langle I(t)I(t+\tau)\rangle}{\langle I(t)\rangle^2} = g^{(2)}(\tau) = 1+\xi[g^{(1)}(\tau)]^2 \tag{3.14}$$

an equation known as the Siegert relation, in which ξ is an instrumental constant.

DLS instruments using digital correlators can calculate the intensity autocorrelation function automatically and generate the results in terms of the first order correlation function $g^{(1)}(\tau)$. Different mathematical approaches can be employed to analyze the correlation data. For monodispersed systems, $g^{(1)}(\tau)$ can be treated as a single exponential decay,

$$g^{(1)}(\tau) = \exp(-\Gamma\tau) \tag{3.15}$$

where Γ is the decay rate. For heterodispersed or polydispersed systems, the correlation function is a sum of the exponential decays corresponding to each of the species in solution,

$$g^{(1)}(\tau) = \int G(\Gamma)\exp(-\Gamma\tau)d\Gamma \tag{3.16}$$

The decay rate is related to translational diffusion coefficient D with scattering vector $q=4\pi n_0/\lambda\sin(\theta/2)$,

$$\Gamma = q^2 D \tag{3.17}$$

By using the Stokes-Einstein equation, the hydrodynamic radius R_h of the particle and the size distribution can be obtained.

$$D = \frac{k_B T}{6\pi\eta R_h} \tag{3.18}$$

3.1.5 Laser light scattering experimental procedure

Static Light Scattering:

A commercial Brookhaven Instrument LLS spectrometer equipped with a solid-state laser operating at 532 nm was used for both SLS and DLS measurements. SLS experiments were performed at scattering angles between 40° and 120° at 2° intervals. The Rayleigh−Gans−Debye equation (*133*) can be used to obtain the weight-average molar mass (M_w) and the radius of gyration (R_g) of the assemblies.

Dynamic Light Scattering:

DLS measures the intensity−intensity time correlation function by means of a BI-9000AT multichannel digital correlator. The field correlation function $|g^{(1)}(\tau)|$ was analyzed by the CONTIN method (*134*) to yield the distribution of the characteristic line width Γ from $|g^{(1)}(\tau)|=\int G(\Gamma)e^{-\Gamma\tau}d\Gamma$. The normalized distribution function of the characteristic line width G(Γ) can be used to determine the apparent translational diffusion coefficient, $D_{app}=\Gamma/q^2$. The hydrodynamic radius R_h is related to D via the Stokes−Einstein equation, $R_h=kT/6\pi\eta D$, where k is the Boltzmann constant and η is the viscosity of the solvent at temperature T. DLS measurements lead to the particle-size distribution in solution from a plot of ΓG(Γ) versus R_h. The R_h of the particles is obtained by extrapolating $R_{h,app}$ to zero scattering angle.

3.2 Zeta-potential analysis

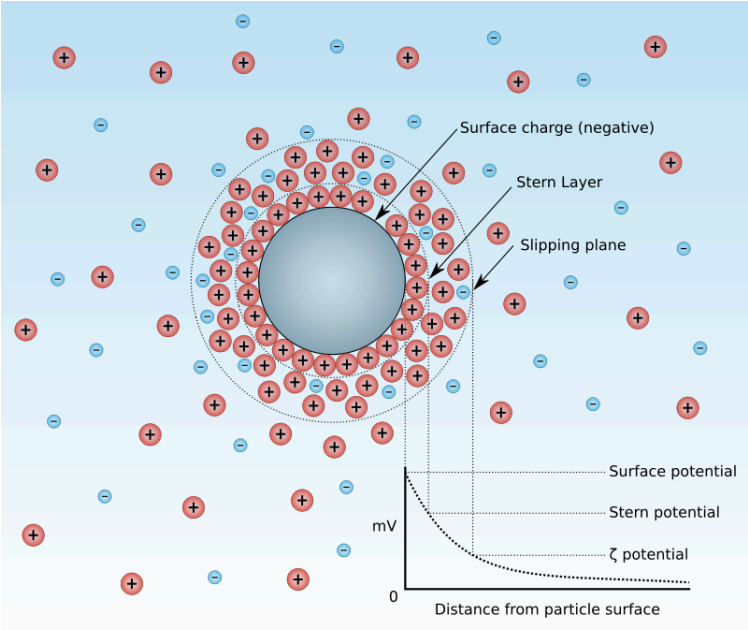

Figure 3.2-1. Stern layer, slipping plane and zeta potential representation in a charged spheical particle.

The Zeta potential ζ is the electric potential in the interfacial double layer at the location of the slipping plane (Figure 3.2-1). It is caused by the net electrical charge consisting of the charges from the central particle and the surrounding ions within the region of slipping plane. The Zeta potential is a key indicator of the stability of colloidal dispersions and its magnitude is related to the degree of electrostatic repulsion between adjacent, like-charge particles. The Zeta potential is not directly measurable but can be calculated from an experimentally determined electrophoretic mobility based on theoretical models. (*135*)

3.2.1 The Mobility measurement and Doppler effect

Since the early 1970s, laser light scattering have been utilized to measure electrophoresis. The moving particles under observation can cause the Doppler shift of the scattered light, which indicates the particle movement. (*136*)

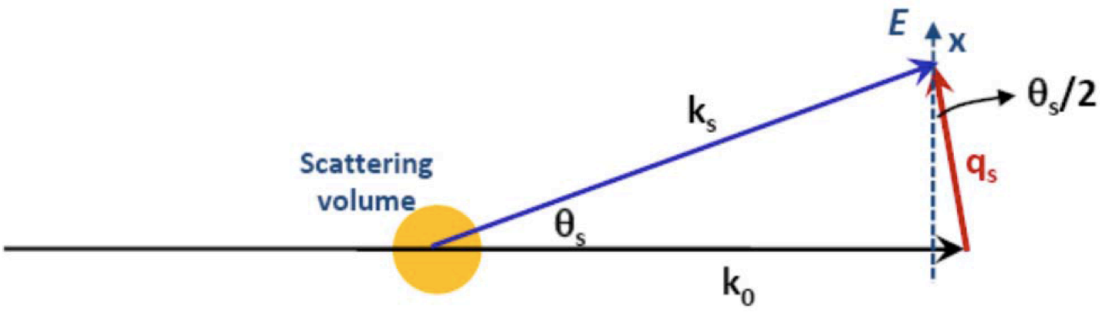

Figure 3.2-2. Phase diagram for light scattering. The applied electric field E along the x-axis drives electrophoresis.

As shown in Figure 3.2-2, the incident light is scattered by a particle to a new direction with a scattering angle θ. The scattering vector q is defined as the difference between the wave vectors of the scattered and incident light ($q=k_s-k_0$). An external

electric field E along the x-axis results in electrophoresis of charged particles in the x direction with a velocity v=μE (μ is electrophoretic mobility). The optical phase ϕ of the scattered light depends on the positions of the scattering particles. Taking electrophoretic movement into consideration, the optical phase difference between time 0 and Δt is,

$$\Delta\phi = \vec{q} \bullet \vec{v} \Delta t \tag{3.19}$$

The Doppler shift can be written as,

$$\omega = d\phi / dt = \mu \cdot 2\pi n \cdot \sin(\theta) E / \lambda \tag{3.20}$$

In general, the movement of particles can be collective (due to fluid flow, electrophoresis, etc.) and diffusional (due to Brownian motions). The diffusional component can average to zero over time, and the collective component can be revealed if enough measurements are able to average away the diffusional component. The electrophoretic mobility μ can be obtained during experiments by measuring the average optical phase shift per unit time dϕ/dt.

3.2.2 Parameters derived from the mobility

Several important molecular parameters such as Zeta potential and effective charge can be derived from μ based on appropriate models and/or theories.

Smoluchowski's equation is applied to deduce Zeta potential in the limiting case where the molecular hydrodynamic radius R_h is much larger than the Debye

length κ^{-1}. It can be written as, (*135*)

$$\zeta = \frac{\eta\mu}{\varepsilon_o\varepsilon_r} \tag{3.21}$$

where η is the sample viscosity. Hückel's equation is applicable in the other limiting case where the molecular hydrodynamic radius R_h is much smaller than the Debye length κ^{-1}, and it can be written as,

$$\zeta = \frac{3\eta\mu}{2\varepsilon_o\varepsilon_r} \tag{3.22}$$

Henry's equation is the most general of the three formalisms. It includes both the Smoluchowski's and Hückel's equations as its limiting cases. To utilize Henry's equation, researchers need to know the ionic strength I of their sample solution.

$$\zeta = \frac{3\eta\mu}{2\varepsilon_o\varepsilon_r f(\kappa R_h)} \tag{3.23}$$

where $f(\kappa R_h)$ is Henry's function.

The effective charge of particles under observation can be deduced from mobility if the hydrodynamic radius R_h is known according to the equation shown below, where Z is the valence of the detected species.

$$Ze = 6\pi\eta R_h\mu\frac{1+\kappa R_h}{f(\kappa R_h)} \tag{3.24}$$

3.2.3 Zeta potential analysis experimental procedure

Zeta potential analysis measurements were performed on a Malvern Instruments *Inc*. Zeta Potential Analyzer equipped with a red laser operating at 633 nm wavelength and has an accuracy of ± 2% for filtrated samples. The sample chamber was kept at 25 ± 0.1 °C, and all sample solutions were loaded 30 min prior to measurements in order to achieve thermal equilibrium with the chamber.

3.3 Transmission Electron Microscopy (TEM)

The bright-field TEM was operated in a JEOL-1230 electron microscope with an accelerating voltage of 120 kV, and the images were taken by a digital CCD camera and processed with the accessory digital imaging system. Samples for the TEM analysis were prepared by dropping 10 uL of the solution samples onto the carbon film coated copper grids. The excess solution was wicked away by a piece of filter paper and samples were then allowed to dry under ambient conditions.

3.4 Conductivity analysis

Conductivity analysis measurements were performed on a VWR traceable conductivity meter and have an accuracy of .5% for filtrated samples. The measurements were conducted at room temperature and repeated three times.

3.5 Size Exclusion Chromatography (SEC)

SEC analyses were performed using a TOSOH HLC-8320 gel permeation chromatograph (GPC) equipped with refractive index (RI) detector. SEC used two separation columns of SuperAW3000 and SuperAW-H (TSK-GEL, Tosoh). *N*,*N*-Dimethylformamide (DMF) (with 0.01 M LiBr) was used as the eluent with a flow rate of 0.8 mL/min at 50 °C. The molecular mass was calculated from universal calibration based on poly(methyl methacrylate) standards.

3.6 Nuclear Magnetic Resonance (NMR) Spectroscopy

The ^{1}H and ^{31}P NMR spectra of the products were obtained in D_2O (99.8% D, Sigma-Aldrich) or acetonitrile-d_3 (99.9 % D, Sigma-Aldrich) using a Varian NMRS 500 spectrometer equipped with an auto-sampling robot at 30 $^{\circ}C$. The following abbreviations were used to explain the multiplicities: s = singlet, d = doublet, t = triplet, br = broad singlet, m = multiplet. Data analysis was done by ACD/NMR Processor Software. The ^{1}H NMR spectra were referenced to the residual proton impurities in D_2O δ 4.80 ppm or in CD_3CN at 1.95 ppm.

3.7 Fourier-transform Infrared (FTIR) Spectroscopy

FTIR spectra were recorded on a Shimadzu MIRacle 10 ATR-FTIR spectrometer from 600 to 4000 cm^{-1}. Resolution was 4 cm^{-1} and scan numbers were 128. Data analysis was done by Win-IP Pro Software.

3.8 Matrix-assisted Laser Desorption/Ionization Time-of-Flight (MALDI-TOF) Mass Spectroscopy

MALDI-TOF mass spectra were recorded on a Bruker Ultraflex III TOF/TOF mass spectrometer (Bruker Daltonics) equipped with a Nd:YAG laser emitting at 355 nm. The matrix compound used here was trans-2-[3-(4-tert-butylphenyl)-2-methyl-2-propenylidene]malononitrile (DCTB, 99%, Aldrich) and was dissolved in $CHCl_3$ at a concentration of 20.0 mg/mL. When necessary, sodium trifluoroacetate (NaTFA) was used as the cationizing agent and was prepared as a MeOH/$CHCl_3$ (v/v = 1/3) solution at a concentration of 10.0 mg/mL. The matrix and cationizing agent solutions were mixed in the ratio of 10/1 (v/v). The sample was prepared by depositing 0.5 μL of matrix and salt mixture on the wells of a 384-well ground-steel plate, allowing the spots to dry, depositing 0.5 μL of each sample on a spot of dry matrix, and adding another 0.5 μL of matrix and salt mixture on top of the dry sample. Mass spectra were measured in the reflection mode, and the mass scale was calibrated externally with a PMMA or PS standard at the molecular weight region under consideration. Data analyses were conducted with the Bruker's flexAnalysis software.

CHAPTER IV

SELF-ASSEMBLY OF SUBNANOMETER-SCALED POLYHEDRAL OLIGOMERIC SILSESQUIOXANE (POSS) MACROIONS IN DILUTE SOLUTION

Portions of this work have been published previously as

Jing Zhou, Panchao Yin, Lang Hu, Fadi Haso, and Tianbo Liu

Eur. J. Inorg. Chem. 2014, 4593–4599

4.1 Outline

Both positively and negatively charged polyhedral oligomeric silsesquioxane (POSS) electrolytes were observed to self-assemble into blackberry-type supramolecular structures in water/acetone mixed solvents, driven by the counterion-mediated attraction. (Figure 4.1-1) Laser light-scattering studies reveal that the sizes of the blackberry structures increase with increasing acetone content, which suggests a charge-regulated process. Studies on two oppositely charged POSS macroions with identical charges and similar sizes show the discrepancy between positively and negatively charged POSS macroions, which is related to counterions, ionic domains of macroions, and the water-bridged hydrogen bonding between monomers. These POSS ions further decrease the lower size limit of macroions that can self-assemble in polar solvents reported to date. The new phenomena were observed in the self-assembly process of POSS macroions relative to other macroion systems.

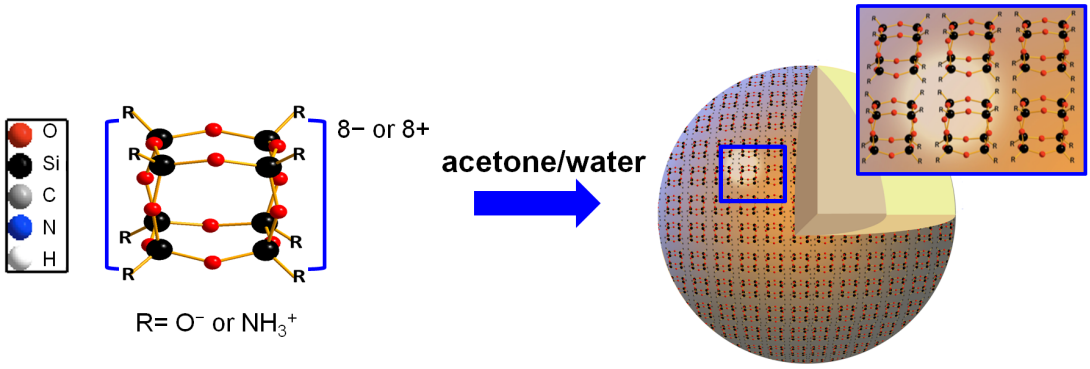

Figure 4.1-1. Two oppositely charged polyhedral oligometric silsesquioxane (POSS) macroions with identical charge and similar sizes can self-assemble into blackberry-type supramolecular structures in dilute solution. This transition from simple macroions to assemblies can be regulated by the solvent polarity.

4.2 Introduction

Sub-nanometer-scaled polyhedral oligomeric silsesquioxanes (POSS) are structurally well-defined, cage-shaped silica molecular clusters which have many attractive advantages due to the features such as nontoxic, biocompatible, chemically inert and mechanically stable. (*27, 137-139*) Octa-silsesquioxane ($R_8Si_8O_{12}$, T_8) is a typical POSS molecule with a roughly spherical shape (0.87 nm maximum diameter) and eight corner groups which can be chemically modified to achieve desired solubility and functionality. (*27, 140*) The low dielectric constant (*k*) of POSS materials makes them good thin film insulators. (*141*) Moreover, their three dimensionality, high symmetry, and size make them promising building blocks for nanocomposties. (*22, 142-147*) Recently, various synthesis protocols have been developed to modify POSS molecules and integrating them into various architectures such as POSS-containing hybrid polymers, with applications in electronics, LED, catalysis, as well as superhydrophobic and antimicrobial coatings. (*46*) The self-assembly of amphiphilic POSS-organic hybrids driven by non-covalent interactions

(hydrophobic interactions, metal coordination, hydrogen bonding, *etc*.) has been studied extensively in the past decades. (*35-39, 148, 149*)

An interesting but obviously ignored question is that how the ionic POSS molecules themselves behave in solution. In aqueous solution, the POSS molecules can stay as large, soluble cations or anions, depending on their surface modification. Such large ions, sitting between simple ions (point charges and valid for the Debye-Hückel Theory) and colloidal suspensions, have their unique solution behavior mostly related to the macroion-counterion interaction. (*101, 150*) Understanding the solution behaviors of macroions is of great significance in polymer, biology, and many other fields of science, since polyelectrolytes and biomacromolecules are all complex macroions. (*151-155*) Our previous studies on the unique self-assembly of macroions were mostly based on polyoxometalate (POM) anions (*5, 8, 68, 156, 157*) and metal-organic cationic nanocages (*14, 158*) in aqueous solution driven by counterion mediated attraction and hydrogen bonding (*77, 101, 150, 159*) The source for counterion association and mediated attraction (*85*) is significantly determined by the charge density of macroions which is reported to locate within the range of 0.05-2.0/nm^2 for 2-4 nm-sized POM anions, as well as their size disparity with the small counterions. (*150*) The counterions (even monovalent ions) around the POM macroions with suitable charge density can generate attraction among macroions, resulting in the formation of hollow, spherical, single-layered blackberry-type structures. (*78, 80, 96, 101*) Currently, the smallest polyoxoanions that were proved to be able to self-assemble are $\{(Ta(O_2)_4)Cs_4K_{12}(UO_2(O_2)_{1.5})_{28}\}$ ($CsKU_{28}$) and $\{(Ta(O_2)_4)Rb_4Na_{12}(UO_2(O_2)_{1.5})_{28}\}$ ($RbNaU_{28}$) clusters with the diameter being 1.77 nm and the charge density being 3.15/nm^2. (*160-163*) The lower critical size limit of macroions that tend to attract with each other and form blackberry structures is still

unclear and needs to be further clarified. Thus, it's highly necessary to explore solution behaviors of macroionic candidates with smaller size.

Ionic POSSs are ideal models for macroions. Their sizes are smaller than those POMs we have studied, which will provide a valuable opportunity for us to explore the unknown boundary between simple ions and macroions. In this paper, the self-assembly of POSS macroions in polar solvents which have the smallest size (~0.87 nm in diameter) and highest charge density (>4/nm^2) compared with previously studied macroions was reported. This is also the first chance that of oppositely charged macroions with similar structure, size, and charge density can be simultaneously studied and compared.

4.3 Experimental Section

Materials and Methods:

PSS hydrate-Octakis(tetramethylammonium) substituted and OctaAmmonium POSS were purchased from Sigma-Aldrich and Hybrid Plastics, respectively. For a typical procedure, the POSS sample was dissolved in deionized (DI) water with an initial concentration of 1.0 mg/mL. The obtained solutions were filtered with 200-nm pore size hydrophilic PTFE membrane filters and put into dust-free light scattering sample vials. Acetone was filtered and added into the aqueous solution.

All the characterization methods have been included in the Chapter III.

4.4 Results and discussions

All of the experimental results are included in this section. A detail discussion is provided our clarify our observations.

4.4.1 Polyhedral oligomeric silsesquioxane (POSS) macroions

The POSS has a cage-like structure that is formed by covalently connecting $RSiO_{3/2}$ units at regular intervals via Si-O-Si bonds. (*140*) Most POSS clusters are hydrophobic in nature, but recently a large family of electrolytic POSS molecular clusters with NH_3^+, O^- *etc*. as peripheral groups were also synthesized. (*140*) These hydrophilic POSS macroions have well-defined molecular structures, uniform shapes, and negligible intra-molecular charge interactions. Figure 4.4-1 shows the chemical structures of the electrolytic POSSs used in our study. The counterions for 1a and 1b macroions are tetramethylammonium (TMA) and chlorine ions, respectively.

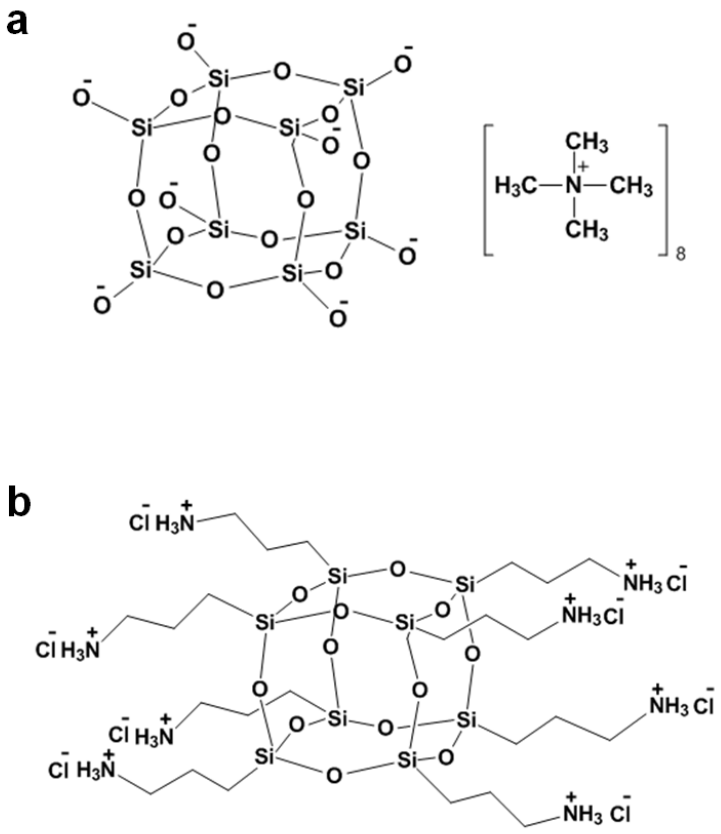

Figure 4.4-1. Chemical structures of POSS macroions: (a) negatively charged POSS with tetramethylammonium (TMA) counterions; (b) positively charged POSS with chlorine counterions.

POSS 1a and 1b are quite soluble in water at 1.0 mg/mL, and form clear, stable, homogeneous solutions. In pure water each POSS macroion carries up to eight charges after releasing the eight counterions (TMA or Cl^-) into solution if not considering any counterion assocaition. Very low scattered intensity for pure aqueous solutions was collected by the SLS, indicating that POSS molecules exist as discrete anions or cations. The fully dissolved solutions were filtered into dust free vials and used as stock solutions for further treatments. Laser light scattering (LLS) was used to monitor these solutions for the formation of any large assemblies.

4.4.2 The assembly of POSS and controlling the blackberry size

Due to their high surface charge density, the two POSS electrolytes 1a and 1b do not self-assemble into large supramolecular structures in water. It is known that the transition of single ions to blackberries, as well as tuning the sizes of blackberries, can be achieved by adjusting the parameters such as the macroionic charger density, solvent polarity, or adding extra salts. (*101, 150, 159, 164*) In the current case, different amounts of acetone were added into POSS aqueous solutions to make 1.0 mg/mL solutions, and sample preparation conditions were the same for the POSS 1a and 1b. As a result of the lower polarity of water/acetone mixed solvents, more counterions are expected to be associated with the discrete POSS macroions and decrease their charge density, which promotes the possible counterion-mediated attraction and the formation of supramolecular blackberry structures.

From SLS studies, a significant increase of the total scattered intensity after acetone was introduced into POSS aqueous solutions was observed. Since the POSS macroions are quite soluble in such water/acetone mixed solvents (solutions remain

clear, homogeneous and stable, up to 90 vol% acetone), the growth of the scattered intensity is not due to the aggregation of insoluble species but the self-assembly of discrete macroions. Some typical CONTIN analysis from the DLS study show that the large assemblies have formed in solutions with a new peak appeared (R_h around tens to over 100 nm, Figure 4.4-2) with a narrow size distribution. The R_h value does not show significant angular dependence.

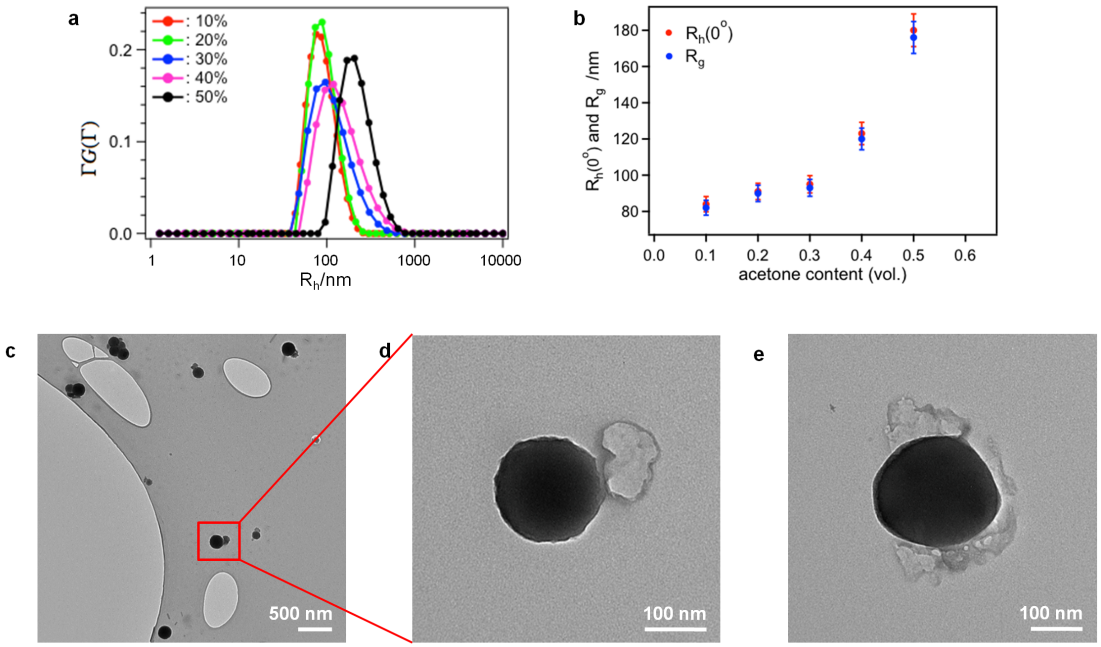

Figure 4.4-2. (a) CONTIN analysis of DLS studies on POSS 1a in water/acetone mixed solvents with 10, 20, 30, 40, and 50 vol.-% of acetone, respectively. (b) Average $R_{h,0}$ (R_h extrapolated to 0° scattering angle) and R_g of the blackberries formed by POSS 1a in different water/acetone mixed solutions, measured by DLS and SLS, respectively. (c) TEM image of the assemblies of POSS 1a in the mixed solvent with 20 vol.-% acetone. (d) Magnified image of (c). (e) TEM image of the assembly of POSS 1a in the mixed solvent with 40 vol.-% acetone.

For POSS 1a, the self-assembly with tunable sizes can be achieved by adjusting the volume fraction of acetone in the water-acetone mixed solvents in the range from 10 to 50 vol% acetone, which shows a raising trend with increasing acetone amount (Figure 4.4-2), from R_h = 80 nm to 180 nm when the acetone content

increases from 10 to 50 vol%. As the volume fraction of acetone was over 60%, no self-assembly of 1a was observed, indicating that the macroions have been significantly neutralized by the associated counterions due to the lower solvent polarity. For individual solution of 1a with different amount of acetone, the ratio of $R_h/R_g \approx 1.0$ is always obtained for the large assemblies (Figure 4.4-2), suggesting their hollow, spherical structures, which is also confirmed by TEM results (Figures 4.4-2). Unlike regular bilayer vesicles formed via hydrophobic interactions, (*121, 128, 130*) the assembly of POSS 1a should be driven by counterion-mediated attraction. In the former case a more polar solvent should promote the vesicle formation, while in our system no assembly was observed in pure water. On the other hand, 1a is fully hydrophilic in polar solutions and its assembly size increases with decreasing solvent polarity, which is the same as other macroionic systems. Therefore, 1a should form blackberry-type structures, as shown schematically in Figure 4.4-3.

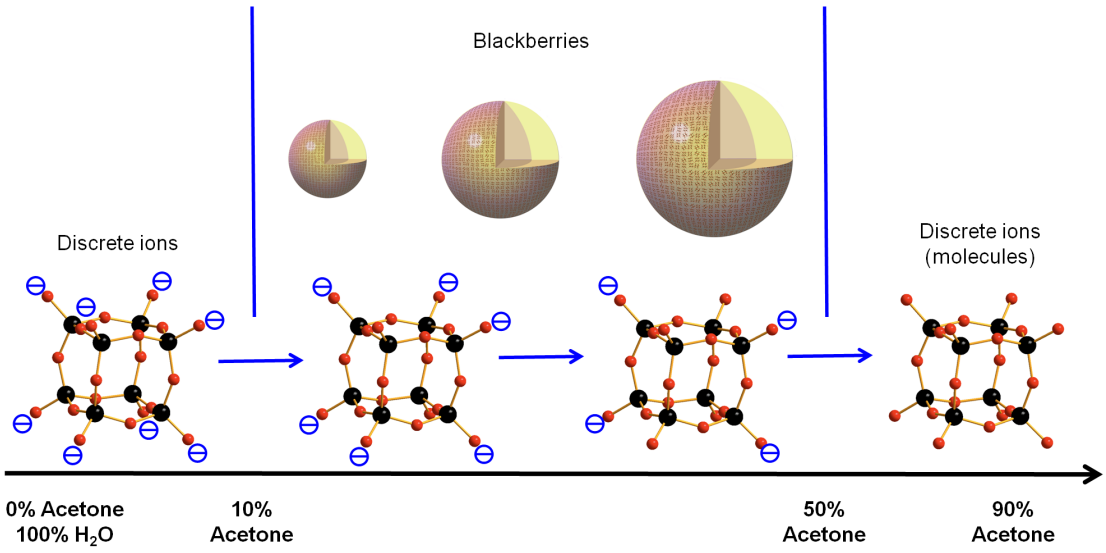

Figure 4.4-3. Transition from discrete macroions (molecules) to blackberries, then to discrete macroions owing to the change of solvent content for 1.0 mgmL^{-1} POSS 1a in water/acetone mixed solvents.

It is known that the size of the macroionic (including POMs and metal-organic nanocages) assemblies has a clear trend with the inverse of dielectric constant (1/ε) when the self-assembly process is charge-regulated. (*99*) To clarify the driving force of the self-assembly of POSS macroions, the average assembly sizes (in R_h) of 1a is plotted as a function of 1/ε.

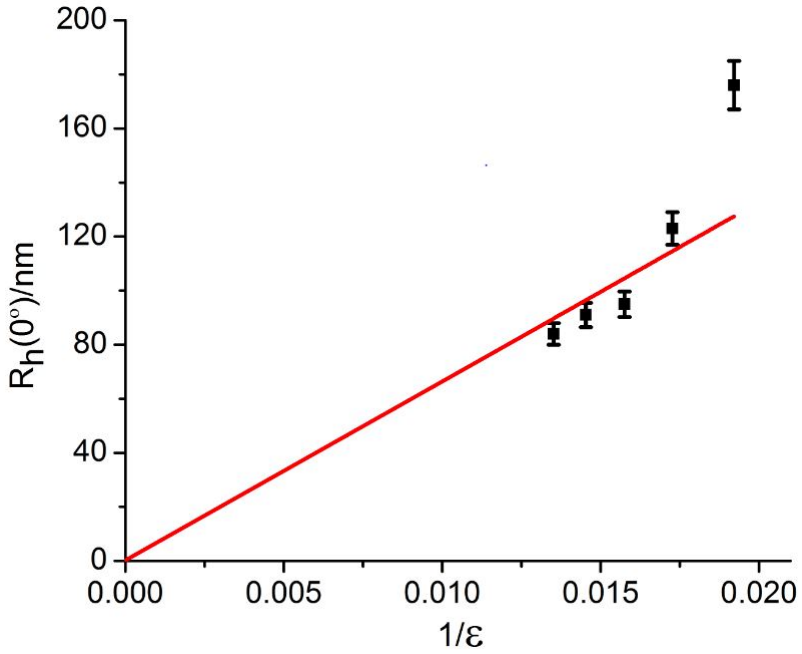

Figure 4.4-4. Plot of the average blackberry radius (in R_h) versus the inversed dielectric constant (1/ε) of various POSS 1a macroions in water/acetone mixed solvents. A linear relationship roughly follows for these systems.

Figure 4.4-4 shows a roughly linear relationship between the vesicle's average R_h value and the 1/ε, confirming that the self-assembly is charge-regulated. (The possible reason for the deviation of the data point with 50% acetone could be that the charge on macroions is low with such high acetone content, which leads to weak like-charge attraction, and consequently a possible different mechanism of self-assembly.) The Zeta potential for 1a blackberries (in 20 vol% acetone/water solvent) is~-60 mV, which is equivalent to ~529 effective charges on each blackberry according to

equations shown below (*165*), suggesting that that over 99% of the counterions are closely associated with the blackberries due to their large sizes.

$$Ze=6\pi\eta R_h\mu(1+\kappa R_h)/f(\kappa R_h) \quad (4.1)$$

$$\zeta=3\eta\mu/(2\varepsilon_0\varepsilon_r f(\kappa R_h)) \quad (4.2)$$

where Z is the valence of the macromolecules (the effective charge), e is the elementary charge,η is the sample viscosity, R_h is the hydrodynamic radius, μ is the electrophoretic mobility, κ is the Debye-Hückel parameter, and $f(\kappa R_h)$ is Henry's function. ζ is the Zeta potential, ε_0 is the permittivity of free space, and ε_r is the solvent dielectric constant.

Positively charged POSS 1b behaves qualitatively similar with POSS 1a. Its self-assembly occurs in the water-acetone mixed solvents with 10-50% vol% of acetone, according to the SLS measurements. For example, based on DLS, SLS and TEM measurements, 1b can form hollow spherical structures (R_h~R_g=160±8 nm) in water-acetone mixed solvent with 20 vol% acetone (Figure 4.4-5). However, the scattered intensities (*I*) from SLS measurements from such solutions are much lower than those assembly solutions of POSS 1a. The scattered intensity is mainly determined by the assembly concentration (C) and size (in R_h) with the relationships of $I \propto C \cdot R_h^2$ for hollow, spherical objects. The low *I* for positively charged POSS macroions indicates that the amount of 1b assemblies is much fewer than the POSS 1a in the same solvent. That is, the equilibrium between single macroions and large assemblies favors the former for the POSS 1b. This is interesting since in our earlier

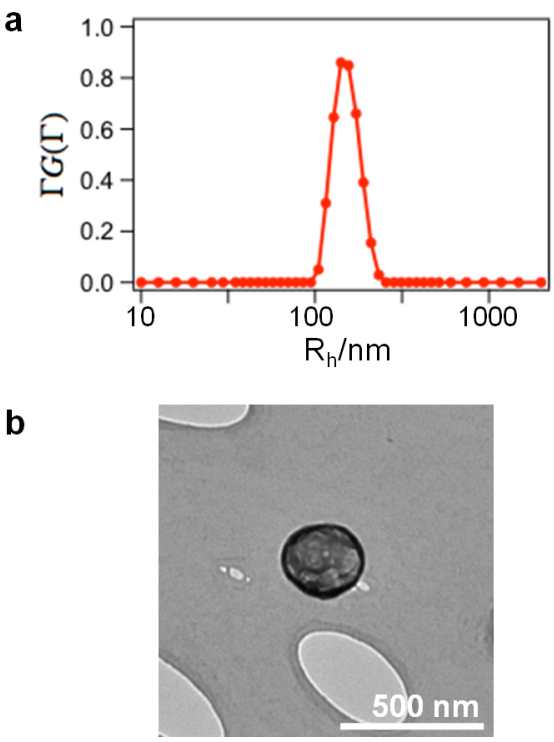

Figure 4.4-5. (a) DLS results of the assemblies of POSS 1b in water/acetone mixed solvents with 20 vol.-% acetone at a 45° scattering angle. (b) TEM image of the assembly of POSS 1b in the mixed solvent with 20 vol.-% acetone.

work we noticed similar phenomenon in other types of macroanions such as metal-organic cages. (*159*)

A difference between POSS 1b and POSS 1a (also POMs) needs to be considered: 1a is fully hydrophilic while 1b contains hydrophobic CH_2 groups and hydrophilic ionic domains on the periphery. (Similarly, metal-organic nanocages also have hydrophobic ligands. (*159*)) However, hydrophobic interaction can't be the dominant driving force for the self-assembly of 1b because there is no supramolecular formation in pure water but self-assembly occurs in less polar solvents. POSS 1b macrocations should behave similarly to macroanionic POMs and nanocages in solution, and form blackberry structures driven by counterion-mediated attraction.

4.4.3 Comparing the assemblies of two oppositely charged POSS macroions

Based on our knowledge, it's the first time that we can compare the assembly behavior of oppositely charged macroions with almost identical sizes and charge densities experimentally. Here we choose POSS macroions as ideal model systems since POSS electrolytes with O^- and NH_3^+ as terminal groups have the identical charge and similar size (The size of 1b should be slightly larger than 1a due to its alkyl chains). The solutions were prepared under the same condition and the experimental results showed certain different solution behaviors between oppositely charged macroions. POSS 1a responds immediately to the decrease of the solvent polarity and formed the blackberry structures, while for POSS 1b it takes longer time for the self-assembly and the amount of final assemblies are obviously fewer.

One of our explanations for the discrepancy is the counterion effect in the two systems. It is suggested from our previous work that less hydrated monovalent cations tend to have stronger affinities with the macroions than the more hydrated ones. (*166-168*) Such stronger binding of the macroions via the bridging cations leads to the formation of spherical shells with smaller curvature, i.e., larger blackberries. In the solution of 1a, the counterions are bulky, amphiphilic TMAs. Thus, we expect the less hydrated TMA ions have stronger affinities to the macroions, which promotes the vesicle formation. Compared with 1a system, the counterion Cl^- in 1b system may have weaker affinities for the macroions and makes the assembly more difficult.

In additional to the counterions' role in the attraction among POSS macroions, the nature of the ionic domains of macroions should also be taken into consideration. Hawker *et al*. pointed out that ionic group character determines the ionic association-driven hydrogel formation, (*169*) by studying the ABA triblock copolyelectrolytes

functionalized with ionic groups. Polyelectrolyete solutions with opposite charges were mixed together for coacervate crosslinking and the formation of a network structure. They found mixing solutions bearing weaker ionic groups (i.e. ammonium and carboxylate ions) produced viscous fluid, while mixing of the strongest ionic groups, sulfonate and guanidinium ions, formed the most stable, mechanically resilient gels. The results revealed the effect of polymer ionic strength on ionic association-driven crosslinking process. In our study, 1b POSSs with ammonium groups may contribute to the difficulty of macroionic self-assembly because of the nature of the ionic groups. This hypothesis will be further checked by our future study of POSS macroions with different functionalized ionic groups.

Moreover, previous study proved the existence of water-bridged hydrogen bonding as auxiliary driving force for the blackberry formation to strengthen the interaction between macroions. (*170*) Wipff *et al*. conducted detailed theoretical simulations on the changes in free energy as a function of the inter-POM macroions distance, and demonstrated the importance of stabilizing bridging water molecules by comparing the Keggin anion (PW^{3-}) to its spherical analogues (S^{3-}) and to Keggin cations (PW^{3+}). (*171*) The results showed that the specific water-bridged hydrogen bonds in the dimer of Keggin anions were much stronger than the non-specific ones in the dimer of S^{3-}. However, water could not afford bridging H-bonds with the cationic dimer; instead, it solvated the contact region of this dimer via its O_{H2O} oxygen atoms. The difference of water-bridged hydrogen bonding in positive and negative charged macroions' systems can also be used to explain the discrepancy of self-assemblies of our two POSS systems.

In the same solvent, such as 20 vol% water/acetone mixture, the blackberries of 1b with R_h=160±8 nm are considerably larger than that of 1a with R_h=90±4 nm.

This discrepancy could be partially due to the size difference between the two macroions – 1b has larger size therefore lower charge density, resulting in larger blackberries. Another important factor is the total solution ionic strength. Extra HCl was added into POSS 1b system during the synthesis, which might lead to the existence of extra salts with 1b sample. The excessive Cl^- ions can lead to stronger screening effect on the 1b macroions, and consequently reduce the repulsion between discrete macroions, resulting in larger blackberries. (*105*) It should be noticed that extra Cl^- will decrease the tendency of blackberry formation as well, because the extra salts can stabilize the single macroions, which explains why the self-assembly of 1b is more difficult. (*105*)

Overall, this is the first study on the assembly of the oppositely charged, similar macroions in solution, providing direct comparison between the macrocations and macroanions.

4.4.4 Comparing the assembly of POSS with POMs and nanocages

It's interesting to compare the assembly process of POSS macroions with POMs and metal-organic nanocages. It should be noticed that POSS electrolytes enable us to further explore the size and charge density limit of macroions that can self-assemble in dilute solution, and new phenomena have been observed in this process.

According to the relation obtained earlier in $\{Mo_{132}\}$ blackberries, (*99*) the slope of the linear regression in Figure 4 can be used to estimate the cohesive bond energy u, revealing the magnitude of the attractive forces among the macroions on the blackberry shell:

$$R \approx -48\lambda_b u/\zeta^2 \quad (4.3)$$

$$\lambda_b = e^2/4\pi\varepsilon_o\varepsilon_r k_B T \approx 56/\varepsilon_r \quad (4.4)$$

where ζ is the Zeta potential, λ_b is the Bjerrum length, ε_o is the vacuum permittivity, ε_r is the relative dielectric constant of the medium, e is the electron charge, k_B is the Boltzmann constant and T is the absolute temperature.

Taking a solution of POSS 1a with 20 vol. % acetone as an example, with ζ=-59.7 mV, u~-12.7 k_BT. This value is more negative than larger $\{Mo_{72}Fe_{30}\}$, $\{Mo_{132}\}$ and metal-organic nanocage macroions (*65, 67*). The POSS 1a's higher bond energy indicates stronger attraction between macroions and better stability of vesicular structures, which could be due to their high charge density.

Another difference comes from the vesicle formation process. The scattered intensity of each POSS solution reached equilibrium within one day, while POM and nanocage solutions showed slow increment of the scattered intensities, taking days to weeks to reach equilibrium in dilute solutions. (*107, 159, 172*) It indicates that the POSS macroions experience a faster self-assembly process. In our previous study, we proposed the slow association of unimers into oligomers as the rate-determining step of blackberry formation. (*104, 105*) This slow process were attributed to the energy barrier for the transition for single macroions to dimers/oligomers, and eventually determine the kinetic properties of the self-assembly. (*105*) Basing the self-assembly process on this mechanism, we suggest the strong charge attraction, which is revealed by the high u value, in POSS systems favors macroions overcoming the energy barrier and fasten the blackberry formation.

4.5 Conclusions

The negatively and positively charged POSS macroions (POSS 1a and 1b, respectively) are observed to form blackberry-type structures in the water/acetone mixed solvents. The size of POSS 1a assemblies increases with increasing the acetone content, which confirms the charge-regulated assembly mechanism. POSS 1b can self-assemble in polar solvents, forming fewer supramolecular structures compared to POSS 1a. The discrepancy of solution behaviors of the oppositely charged macroions can be related to different counterions, different ionic domains of macroions, the ionic strength in solution, and the water-bridged hydrogen bonding between macroions. The current work expands our exploration of macroionic behavior to a totally new area, with the model POSS macroions representing so far the smallest macroions which demonstrate strong inter-macroionic attraction and the consequent self-assembly in polar solvents.

4.6 Acknowledgements

T. Liu acknowledges the support from the National Science Foundation (CHE1332446) and The University of Akron.

CHAPTER V

SPONTANEOUS SELF-ASSEMBLY OF γ-CYCLODEXTRINS IN DILUTE SOLUTIONS WITH TUNABLE SIZES AND THERMODYNAMIC STABILITY

Portions of this work have been published previously as

Jing Zhou, Panchao Yin, Yunyi Gao, Lang Hu, and Tianbo Liu

Chem. Eur. J. 2015, 21, 9563 – 9568

5.1 Outline

The solution behavior of phosphate-functionalized γ-cyclodextrin macroanions with eight charges on the rim in dilute solution was explored. The hydrophilic macroions in mixed solvents show strong attraction between each other mediated by the counterions, and consequently self-assemble into blackberry-type hollow spherical structures (Figure 5.1-1). Time-resolved LLS measurements at high temperature ruled out the possibility of hydrogen bonding as the main driving force in the self-assembly and indicated the good thermodynamic stability of assemblies regulated by the charge. The transition from single macroions to blackberries can be tuned by adjusting the solvent content of organic solvent. The sizes of blackberries vary with the charge density of γ-cyclodextrin by adjusting pH. It's the first report that pure cyclodextrins can generate supramolecular structures by themselves in dilute solution. The unique solution behavior of macroions provides a new opportunity to assemble cyclodextrin into functional materials and devices.

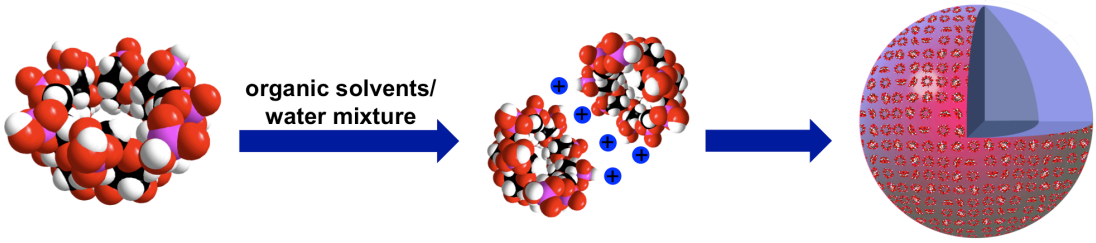

Figure 5.1-1. Charged cyclodextrins can self-assemble into blackberry-type supramolecular structures in dilute solution. This transition from simple macroions to assemblies can be regulated by the solvent polarity.

5.2 Introduction

Cyclodextrins (CDs) are a class of cyclic oligosaccharides consisting of six, seven or eight glucose entities, which are called α-, β-, or γ-CDs. CDs show a toroidal shape with the diameter of the primary hydroxyl rim narrower than that of the secondary hydroxyl rim. (*42, 44, 45, 173*) Due to the abundant OH groups, the external surface of CD toroid is highly hydrophilic, while the internal cavity is relatively hydrophobic, which enables CDs to host various guests. (*46, 47*) In virtue of its water-solubility, biocompatibility, and strong ability of incorporating guest molecules, CD has applications in areas such as food, pharmaceutical, drug delivery, chemical industries and etc. (*41, 43*) The inclusion complexation between CDs and guests, as well as its impacts on the assembly of these systems, has been extensively investigated. (*46, 48*) Previous works demonstrated that CDs crucially participate in the self-assembly of amphiphilic systems (either as a modulator or as a building block), as well as realize the reversibility and stimuli-responsiveness of assemblies and materials particularly hydrogels that use inclusion complexes as crosslinks. (*49-51*) Furthermore, the involvement of CDs in macromolecular assemblies provided many other applications such as controlling solution properties, DNA decompaction

and protein reconstruction. (*51*) Recently, it was found that CDs and CDs/surfactants complexes could self-assemble in the aqueous solution driven by CD-CD H-bonds, instead of hydrophobic interactions in amphiphilic systems. (*52, 55-57*)

However, it is still unknown in dilute solutions, to our knowledge, how the pure, hydrophilic CDs themselves behave. It seems that such hydrophilic CDs are naturally believed to exist as single molecules in water and in other polar solvents, and act as ideal "hosts" for interacting with "guests". Driven by curiosity, we want to examine the detailed behavior of the highly soluble ionic CDs in polar solvents; especially, to check if such CDs form any spontaneous self-assembled structures in dilute solutions.

Our motivation is based upon our recent progress on studying inorganic macroionic solutions. Such macroions, have sizes between simple ions (point charges valid for the Debye-Hückel Theory) and colloidal suspensions (usually described by the DLVO Theory). (*101, 150*) Previous studies of macroions (include polyoxometalate (POM) anions, metal-organic cationic nanocages, polyhedral oligomeric silsesquioxane (POSS) ions and fullerene anions) demonstrated unique solution behavior by self-assembling into ordered, single layer, hollow, spherical "blackberry" structures, which is driven by counterion-mediated attraction and hydrogen bonding. (*77, 102, 104, 107, 159, 174*) By properly adjusting the parameters such as the macroionic charge density, solvent polarity, or adding extra electrolytes, the transition between single macroions and blackberries, as well as tunable blackberries sizes, can be achieved. (*101, 150*) These precisely charge-controlled self-assemblies are very useful to interpret the variability and diversity in biological systems. (*107*)

It would be interesting to see if the organic CDs, which are also macroions based on their size and charge, demonstrate similar solution behavior. The difference between the CDs and the previously studied macroions are also obvious – especially the strong tendency of hydrogen bonding formation for the CDs. The role of hydrogen bonding therefore becomes an interesting topic for the current study.

5.3 Experimental section

Materials and Methods:

γ-Cyclodextrin phosphate sodium salt was purchased from Sigma-Aldrich. For a typical procedure, the γ–CD-P sample was dissolved in deionized (DI) water with an initial concentration of 1.25 mg/mL. The obtained solutions were filtered with 200-nm pore size hydrophilic PTFE membrane filters and put into dust-free light scattering sample vials. Acetone, isopropanol and HFIP were filtered and added into the aqueous solution, respectively.

5.4 Results and discussions

All of the experimental results are included in this section. A detail discussion is provided our clarify our observations.

5.4.1 γ–Cyclodextrin Phosphate Sodium (γ–CD-P)

CD has a cuplike structure formed by α-1,4-linked D-glucopyranosides. (*42, 173*) Many CD derivatives were obtained by a wide variety of synthetic methods. (*58-*

60) Ionic CDs (*61*) such as phosphate, sulfate and carboxylate sodium salts are readily commercialized and can be treated as ideal models of macroions for studying the charge-related solution behaviors. Figure 5.4-1 shows the chemical structures of γ–CD-P used in our study with sodium being counterions.

In deionized water, the PH of γ–CD-P solution (0.25 mg/mL) is 8.47 and the measured conductivity is 53.7 μs/cm. The calculated number of sodium ions per γ–CD-P molecule that contribute to the total conductivity is very close to 8 (the calculation is shown in the supporting information), indicating that all the counterions are released in pure water and each CD has 8 charges. If we regard a γ–CD-P molecule as a toroid, the charge density of for each molecule is 1.050 per nm^2.

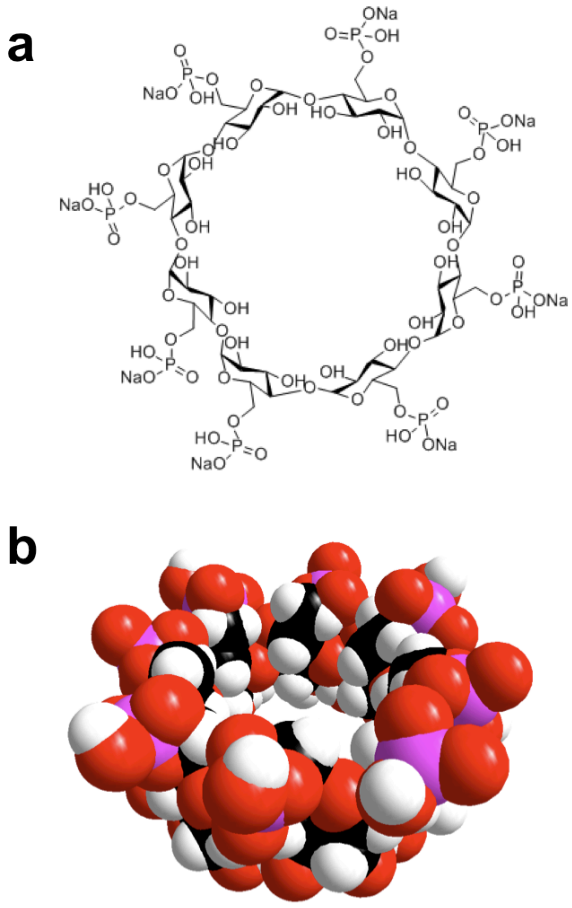

Figure 5.4-1. a) Chemical structure and b) space-filling model of the g-CD-P macroion. Color code of spheres: black, C; red, O; white, H; pink, P.

5.4.2 The Assembly of γ–CD-P in Water/acetone Mixed Solvents

γ–CD-P is quite soluble in water at 1.25 mg/mL, and forms clear, stable and homogeneous solution. Very low scattered intensity for pure aqueous solutions was collected by means of static light scattering (SLS) technique, indicating that γ–CD-P molecules exist as discrete single anions. The fully dissolved solutions were filtered into dust free vials and used as stock solutions for further treatments. In the current case, different amounts of acetone were added into γ–CD-P aqueous solutions to make the final solution concentration as 0.125 mg/mL. Laser light scattering (LLS) was used to monitor these solutions for the formation of any large assemblies.

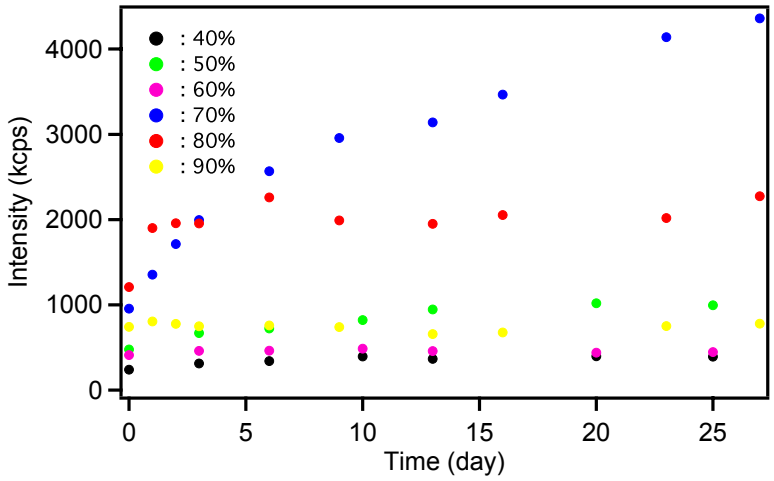

Figure 5.4-2. Time-resolved SLS monitoring results of 0.125 mg/mL γ-CD-P solutions in water/acetone mixed solvents with 40, 50, 60, 70, 80 and 90 vol.-% of acetone. The experiments were done in LLS with green laser (532 nm) with calibration intensity as 88 kcps (the scattered intensity of benzene at 90˚).

During SLS studies, a significant, continuous increase in the total scattered intensity was observed for those γ–CD-P water/acetone mixed solutions with acetone volume fraction more than 0.4 (Figure 5.4-2). Since the γ–CD-P macroions are quite soluble in such water/acetone mixed solvents (solutions remain clear, homogeneous,

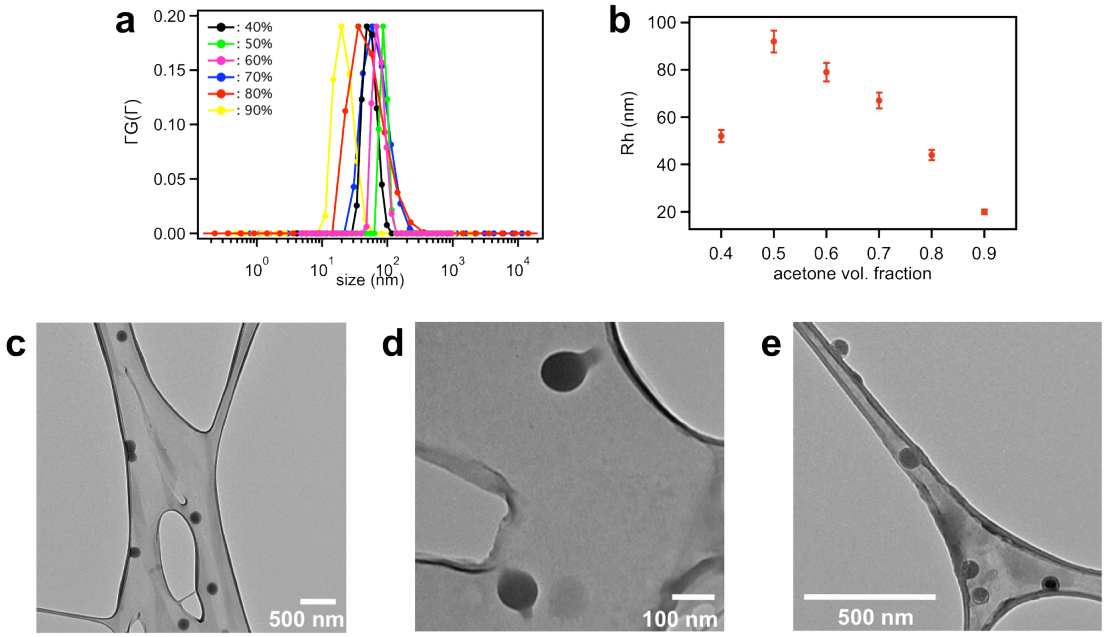

Figure 5.4-3. a) CONTIN analysis of DLS studies on γ-CD-P in water/acetone mixed solvents with 40, 50, 60, 70, 80, and 90 vol.% of acetone. b) Average R_h of the blackberries formed by γ -CD-P in different water/acetone mixed solutions, measured by DLS. c–e) TEM image of the assemblies of γ -CD-P in the mixed solvents with 50, 70, and 90 vol.% acetone, respectively.

and stable, up to 95 vol.-% acetone), the growth of the scattered intensity is not due to the aggregation of insoluble species but the self-assembly of discrete macroions, because the final assemblies are still stable and soluble in solution and their final sizes do not continue to grow with time. Typical CONTIN analyses of the dynamic light scattering (DLS) results shown in Figure 5.4-3a indicate that peaks appear around tens to 100 nm in Figure 5.4-3a which correspond to the hydrodynamic radius (R_h) of those assemblies. The R_h of the sample with 40 vol.-% acetone is 52±3 nm and increases to 92±5 nm when the acetone content increases to 50 vol.-%. As the volume fraction of acetone was over 60%, the sizes of assemblies show a decreasing trend with adding more acetone into the solution (shown in Figure 5.4-3b). For individual solution of γ–CD-P with different amounts of acetone, the R_h value for the large assemblies does not show angular dependence and the ratio of $R_h/R_g \approx 1.0$ is always

obtained, suggesting their hollow, spherical structures, which is also confirmed by TEM results (Figure 5.4-3c–e). The solution behavior of γ–CD-P was further studied in isopropanol/water and hexafluoro-2-propanol (HFIP)/water mixed solvents, and we found γ–CD-P could also self-assemble into hollow, spherical structures in all of these solutions. To our knowledge, no example has been demonstrated to form hollow spherical structures by CDs themselves. Thus, this work might provide a new and facile strategy to generate assemblies of CDs and their derivatives, as well as properly tune the sizes of assemblies.

5.4.3 The Mechanism of Self-assembly

Different from regular double-layered vesicles formed by CD-based amphiphiles, (*175*) the possibility that the γ–CD-P assembly is driven by hydrophobic interactions can be ruled out, because in the current system no assembly was observed in pure water; while for bilayer vesicles, a more polar solvent should promote the self-assembly since the hydrophobic interaction is dominant.

Recently, hydrogen bonding was reported as the driving force for the formation of bilayer vesicles in the dilute solution of CD-surfactant inclusion complexes, (*56, 57*) which implies us the possible existing of H-bonds in our system. The morphology of the self-assembly of CD-surfactant inclusion complexes is concentration and temperature dependent, demonstrating a transition from vesicles to microtubes at a lower temperature and a higher concentration. However, in our study of γ–CD-P, the formation of vesicle-like structures is concentration independent, as well as the assembly size (Figure 5.4-4).

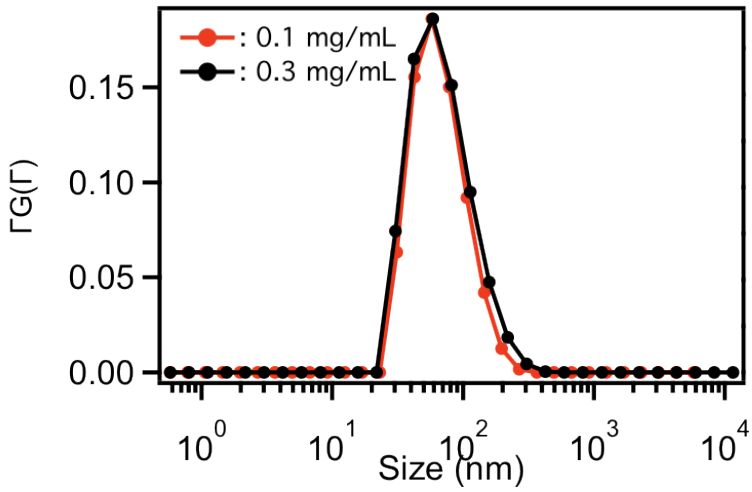

Figure 5.4-4. CONTIN analysis of DLS studies on γ-CD-P in water/acetone mixed solvents with 70 vol.-% of acetone at total concentration of 0.1 and 0.3 mg/mL, respectively.

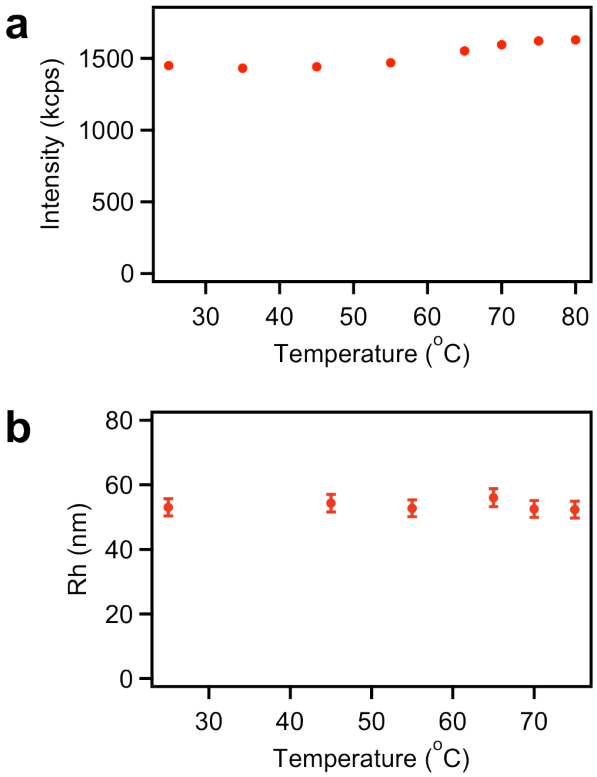

Figure 5.4-5. a) SLS monitoring intensities of 0.125 $mgmL^{-1}$ γ-CD-P solutions in water/isopropanol mixed solvents with 70 vol.% of isopropanol at various temperatures. b) The Rh of blackberries measured at corresponding temperatures. The experiments were done in LLS with green laser (532 nm) with calibration intensity as 38 kcps (the scattered intensity of benzene at 90°).

Time-resolved LLS was applied to monitor the solutions of γ–CD-P at different temperatures, which could provide information on the stability of the assemblies and check whether hydrogen bonding is the major driving force. SLS measurements on 0.125 mg/mL γ–CD-P in water/isopropanol mixed solvent with 70 vol.-% isopropanol indicates that the scattered intensity at 90° scattering angle doesn't change much as the temperature increases gradually from room temperature to 75 °C (Figure 5.4-5a). DLS studies of the same solution indicate that the R_h value of the assemblies does not change noticeably during the heating process (Figure 5.4-5b). It suggests that the number of the assemblies in solution remain almost the same at various temperatures. Same phenomenon was observed when studying γ–CD-P in water/acetone mixed solvent with 75 vol.-% acetone (Figure 5.4-6). Moreover, the assembly sizes measured at different scattering angles show no angular dependence, which means that there is no morphology change caused by temperature. The constant size and number of the assemblies indicates that the spherical structures are very stable at high temperatures and rules out that the main driving force for the assembly is hydrogen bonding.

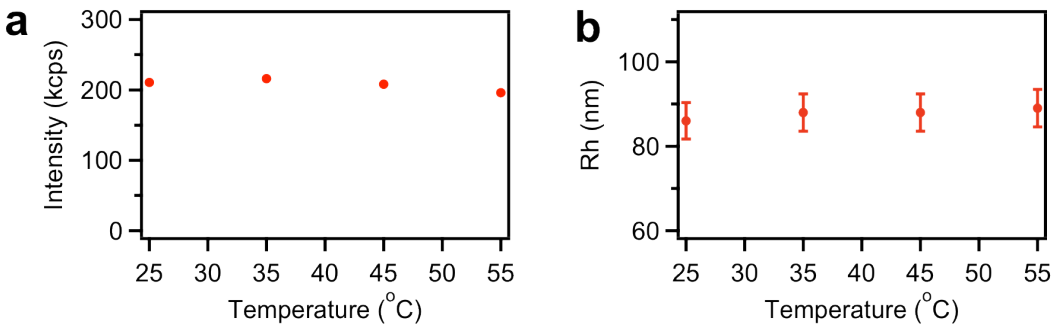

Figure 5.4-6. a) SLS monitoring intensities of 0.125 mg/mL γ-CD-P solutions in water/acetone mixed solvents with 75 vol.-% of acetone at various temperatures. b) The Rh of blackberries measured at corresponding temperatures. The experiments were done in LLS with red laser (637 nm) with calibration intensity as 10 kcps (the scattered intensity of benzene at 90˚).

Counterion-mediated like-charge attraction is believed to be the main driving force of γ–CD-P assembly. It's reasonable that γ–CD-P molecules exist as discrete macroions in pure water because each molecule has high charge density (carries 8 charge), leading to strong electrostatic repulsion between each other. Mixing organic solvent with the original water solution can lower the solvent polarity and promote closer counterions association with macroions, which in turn generates strong counterion-mediated attraction and forms blackberry structures. The control experiment was done by mixing different amounts of acetone with water solutions of native (non-charged) γ–CD. Very low scattered intensities for all solutions with 30 to 90 vol.-% were collected by means of static light scattering (SLS), thus indicating that γ–CD exist as discrete molecules and implying the important role of charges on the self-assembly of γ–CD-P anions. This observation supports our conclusion that counterion-mediated attraction is the main driving force for blackberry formation.

5.4.4 The Size Trends of Blackberries

In our previous studies the blackberry sizes become larger in solvents with lower polarity, and with adding excessive amount of organic solvent the blackberries dissociate back into single macroions due to the strong counterion condensation, which makes the effective charge of macroions very low. (*176*) It is worthy to note that in this study, the sizes of blackberries first increase with increasing acetone content, but then decrease after the acetone is more than 60 vol.-% (Figure 4). It's the first time we clearly observe such complicated trends in one macroionic system, suggesting the influence of specific interactions other than the counterion-mediated attraction on the blackberry sizes.

CDs always show strong tendency to form H-bonds in the aqueous solution because of abundant hydroxyl groups dangling on the rim of the molecule. The functionalized ionic domains of CDs such as phosphate groups in γ–CD-P are also possible to form strong H-bonds. Previous studies indicated that the H-bonds of CDs in the aqueous solution are critical to determine the size of their assemblies. (*56*) Although we don't consider hydrogen bonding as the main driving force for γ–CD-P's self-assembly, we expect both counterion-mediated attraction and H-bonds will contribute to the attractive force and play roles on the size of blackberry structures. As we know, with lowering the solvent polarity counterion-mediated attraction become stronger, favoring larger blackberries, while H-bonds is weaker, leading to smaller blackberries, and thus the balance between them determine the obtained size trends in different mixed solvents system. In water/acetone mixed solvents with acetone contents between 40 and 60 vol.%, the counterion-mediated attraction is dominant to induce the blackberry formation. As a result we see larger blackberries with more acetone – common for a charge-regulated assembly process. Further lowering the solvent polarity, the decrease of H-bonds is eminent, leading to a weaker total attractive force and consequently smaller blackberry sizes. The results demonstrate the key role of the solvent polarity on determining the balance between counterion-mediated attraction and H-bonds. Higher solvent polarity favors the dominance of counterion-mediated attraction, while the lower solvent polarity shifts the balance to H-bonds.

To clarify the new phenomenon, we compare the solution behaviors of γ–CD-P in different mixed solvents including acetone/water, isopropanol/water and HFIP/water. A significant continuous increase in the total scattered intensity was monitored by LLS for γ–CD-P water/isopropanol and water/HFIP mixed solvents

with 70, 80 and 90 vol.-% volume fraction of organic solvent respectively (Figure 5.4-7a and b). Interestingly, the sizes of blackberries decrease with adding more isopropanol, while they show the opposite trend with adding more HFIP (Figure 5.4-7 c and d), which is also confirmed by TEM results (Figures 5.4-8).

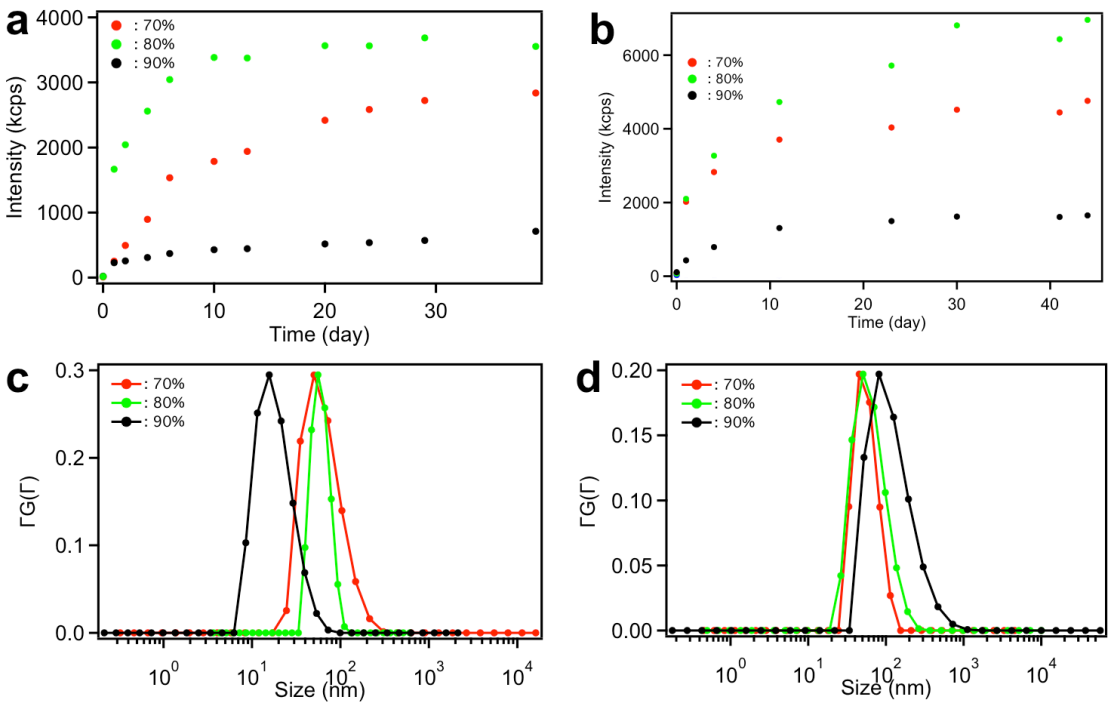

Figure 5.4-7. a, b) Time-resolved SLS monitoring results of 0.125 mgmL^{-1} γ-CD-P solutions in water/isopropanol and water/HFIP mixed solvents with 70, 80, and 90 vol.% of isopropanol and HFIP. c, d) CONTIN analysis of DLS studies on γ-CD-P in water/isopropanol and water/HFIP mixed solvents, respectively. The experiments were done in LLS with green laser (532 nm) with calibration intensity of 88 kcps (the scattered intensity of benzene at 90°).

In different mixed solvent systems, we did observe the effect of H-bonds on changing the assembly sizes, which make ionic CDs interesting and special among other macroions. Comparing the solvent polarity of the three types of organic solvent used in our study, the polarity of HFIP is the highest, followed by acetone, and isopropanol is the least polar. Smaller blackberry sizes were observed in acetone (or isopropanol)-richer system when the solvents effectively weakened the H-bonds and

the total attractive force. As HFIP is a more polar solvent, with adding the same amount of HFIP as acetone to the aqueous solution, the ε of the medium is higher for the former case and favors the dominance of counterion-mediated attraction and larger blackberry sizes.

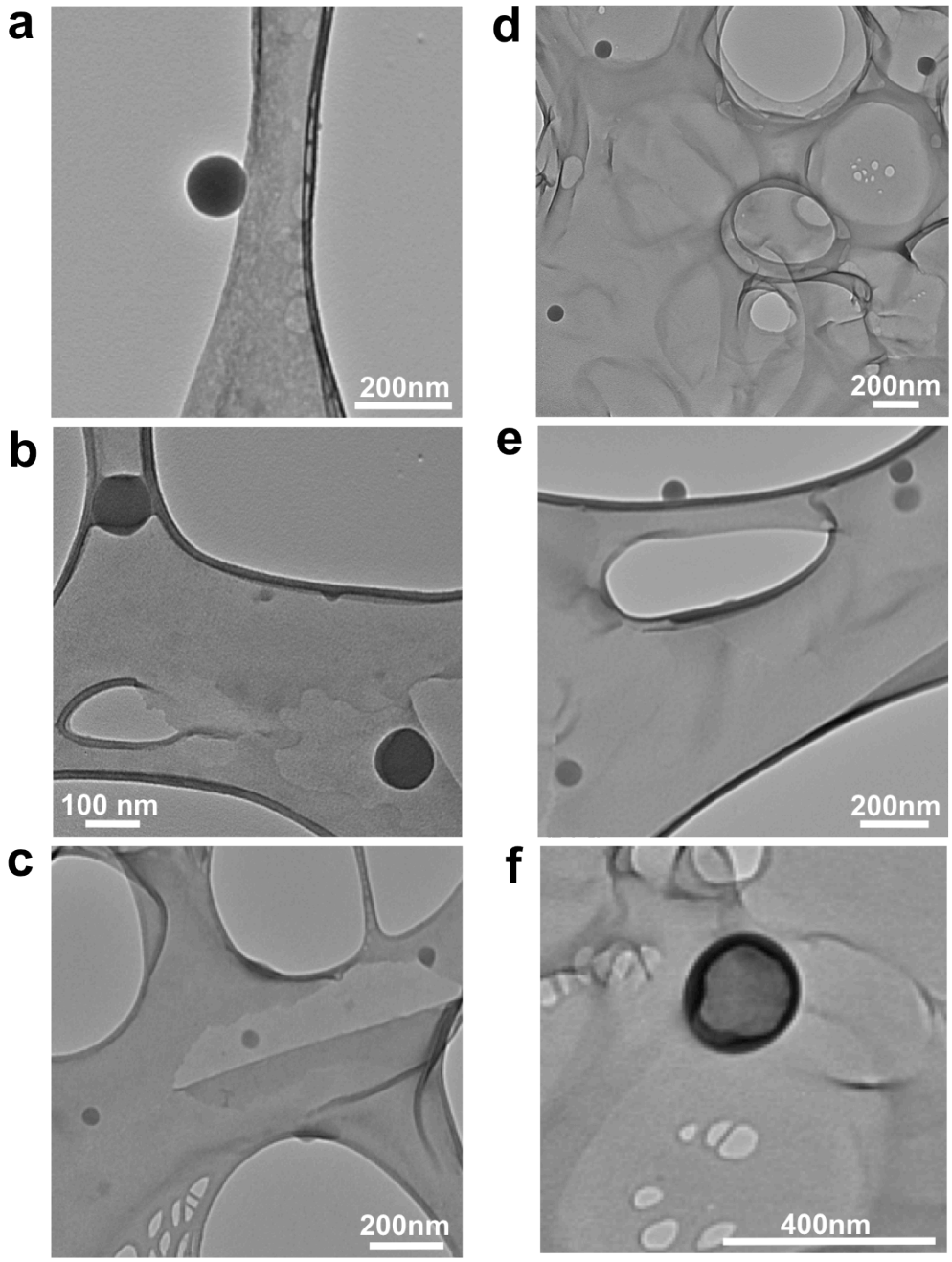

Figure 5.4-8. a–c) TEM image of the assemblies of γ-CD-P in the water/isopropanol mixed solvents with 70, 80, and 90 vol.% isopropanol, respectively. d–f) TEM image of the assemblies of γ-CD-P in the water/HFIP mixed solvents with 70, 80, and 90 vol.% HFIP, respectively.

Comparing γ–CD-P with macroions such as $\{Mo_{132}\}$ and ionic POSS, they all can self-assemble in mixed solvents, but only γ–CD-P can form blackberries with either increasing or decreasing trend of size as increasing the acetone amount. (*102, 176*) The difference may be related to the charge density of macroions among which γ–CD-P has the lowest charge density (1.050 per nm^2). It's worthy to notice that γ–CD-P possesses the anisotropic charge distribution (one side of the toroid is charged) which make it distinctive out of other macroions. The special feature could also be the possible reason for the transition from larger to smaller blackberries. This hypothesis will be further checked by our future study of macroions with anisotropic charge distribution.

5.4.5 Accurately Tuning the Sizes of Blackberries

It is known that the source for counterion association and mediated attraction is significantly determined by the charge density of macroions, which in turn tunes the sizes of blackberries. Besides changing the solvent content, there are several approaches to adjust macroionic charge density. For "weak acid" type POMs, the charge density is supposed to be varied by continuously tuning the solution pH. (*150*) Adding extra salts or surfactants to the solutions of macroions can also affect on the assembly sizes.

We decreased the pH of γ–CD-P water solution to around 4 by adding HCl and mixed the stock solution with different amounts of acetone. γ–CD-P, as a weak acid salt type macroion, can be more protonated (less charged) in lower pH solution. Consistently, the sizes of blackberries in acidic solutions are larger than those in

native γ–CD-P solutions (Figure 5.4-9), which further confirms that the self-assembly of γ–CD-P is charge regulated.

Considering the host-guest inclusion complexation nature of CD molecules, we can introduce guest molecules into γ–CD-P macroionic system in future study for various potential applications.

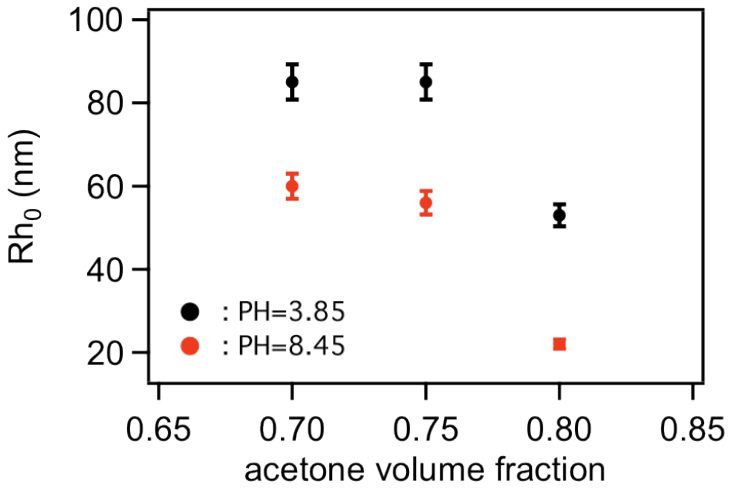

Figure 5.4-9. Average R_h of the blackberries formed by γ-CD-P in different water/acetone mixed solutions and different pHs of original γ-CD-P water solutions, measured by DLS.

5.5 Conclusions

In summary, a hydrophilic γ–CD-P with 8 phosphate groups located on the rim shows the unique solution behavior by self-assembling into blackberry-type hollow spherical structures in mixed solvents. It's the first time to observe the cyclodextrin itself generates supramolecular structures in dilute solution. Different from previous amphiphilic cyclodextrin systems, the major driving force is neither hydrophobic interaction nor hydrogen bonding, but, the counterion-mediated attraction. The vesicular structures are very stable at high temperature. The transition

from single macroions to blackberries can be achieved by properly decreasing the solvent polarity. Further lowering the medium dielectric constant, smaller blackberries was observed. We can also tune the sizes of assemblies by adjusting the charge density of macroions. Our protocol provides a new way to assemble cyclodextrin derivatives into ordered vesicular structures with good thermodynamic stability and size tunability.

5.6 Acknowledgement

TL acknowledges support from the National Science Foundation (CHE1305756) and The University of Akron.

CHAPTER VI

TEMPERATURE- AND SALT- RESPONSIVE POLYOXOMETALATE-POLY(N-ISOPROPYLACRYLAMIDE) HYBRID MACROMOLECULES IN AQUEOUS SOLUTION

Portions of this work have been published previously as

Jing Zhou, Panchao Yin, Xinyue Chen, Lang Hu, and Tianbo Liu

Chem. Comm. 2015, 51, 15982-15985

6.1 Outline

Polyoxometalates (POMs) as polar head groups were covalently functionalized with Poly (N-isopropylacrylamide) (PNIPAM) tails. The macromolecular hybrid demonstrates the solution behavior of hydrophilic macroions by self-assembling into blackberry structures at room temperature. It behaves like the amphiphilic surfactant by forming vesicular structure when the temperature is above the phase transition of PNIPAM. The reversible self-assembly is also salt sensitive and the salt-induced smaller vesicular formation is a result of counterion-association.

6.2 Introduction

To sustain life and maintain biological functions, living systems are able to adapt themselves to the changing environments from the molecular to

macroscopic level. (*177, 178*) Inspired by the nature, scientists have been designing and fabricating "smart" materials that can respond to physical and chemical external stimuli. (*179, 180*) Recently, stimuli-responsive formation of self-assembly has been developing rapidly from thin films to nanoparticles for various applications in catalysis, sensors, drug delivery capsules, and et al. (*181-185*) The typical responsive nanoparticles can be realized by utilizing amphiphilic systems, among which molecular shape amphiphiles, (*186, 187*) especially polymer-tethered molecular nanoparticles (MNPs), are appealing for self-assembling into diverse nanostructural materials. (*11, 188, 189*) Different from small molecular surfactants and amphiphilic diblock copolymers, those hybrids consisting rigid MNPs as polar head groups and hydrophobic polymer chains as tails can be treated as "giant surfactants" and demonstrate unique features in solution. (*189*)

Poly (N-isopropylacrylamide) (PNIPAM) is a thermo-responsive polymer which exhibits lower critical solution temperature (LCST) phase transition from hydrophilic random coiled conformation to hydrophobic collapsed globular conformation at ~32 °C in water. (*190-192*) Since the LCST of PNIPAM is near the temperature of human body, it has been recognized as a good model to predict the stability and solution behaviors of biomacromolecules under various environmental conditions. (*193-196*) Moreover, thermo-responsive polymers play a crucial role in applications such as tissue engineering, drug delivery and materials with switchable hydrophilic and hydrophobic properties. (*197-199*)

Polyoxometalates (POMs) are a group of metal-oxide clusters of early transition and actinide metals which have well-defined shapes and charges and vast

applications in catalysis, medicine, and materials science. (*4, 5, 200, 201*) More importantly, those molecular clusters such as POMs, polyhedral oligomeric silsesquioxane (POSS) and fullerene (C_{60}) attracted increasing attentions because they can provide precisely defined and tunable nanosized structural scaffolds. (*202*) The development of synthetic methods enabled us to tether POM clusters with organic ligands via covalent modifications. (*8, 9, 203-205*) Various POM hybrids have been reported to demonstrate amphiphilic features by self-assemble into various supramolecular structures in selective solvents while maintaining the unique properties of POM groups. (*128, 130, 150*) Specific hybrids have been designed to respond to external stimuli, such as pH, metal ions and UV radiation. (*206-209*)

Herein, we report the design, synthesis and self-assembly of a novel type of POM-polymer hybrid, namely, mono-vacant Keggin-type clusters (As the major types of POMs, Keggin, Lindqvist, Dawson, and Anderson type POMs have been synthesized and characterization several decades ago, they are still hot topics in catalysis and organic-inorganic hybrid materials. Keggin type POMs, first reported by Keggin in 1933 with formula $[XO_4M_{12}O_{36}]^{n-}$, have overall T_d symmetry and are based on a central XO_4 tetrahedron surrounded by twelve MO_6 octahedron arranged in four groups of three edge-shared octahedron, M_3O_{13}. (*210*)) were chemically linked with PNIPAM oligomeric chains.

6.3 Experimental section

This section includes materials used in my study, sample preparation procedures, and synthesis protocol and characterization results.

6.3.1 Materials and sample preparation

Sodium phosphotungstate (Sigma-Aldrich), poly(N-isopropylacrylamide) triethoxysilane terminated (PNIPAM, Sigma-Aldrich), sodium carbonate (Na_2CO_3, Sigma-Aldrich), potassium chloride (KCl, Sigma-Aldrich), hydrochloric acid (HCl, Fisher Scientific), tetrabutylammonium chloride (TBA, Sigma-Aldrich) and acetonitrile (Sigma-Aldrich) were all used as received.

For a typical light scattering measurement, the sample was dissolved in deionized (DI) water. The obtained solutions were filtered with 200 nm pore-size hydrophilic polytetrafluoroethylene (PTFE) membrane filters and put into dust-free light-scattering sample vials. Salt solution was also filtered and added to the aqueous solution.

6.3.2 Synthesis of POM-PNIPAM hybrid

The synthesis protocol includes two steps. The first step is to synthesize the 1-vacant Keggin precursor, and the second step is to chemically link polymer to the precursor.

6.3.2.1 Synthesis of $K_7[PW_{11}O_{39}]$ 1-vacant Keggin

The precursor $K_7[PW_{11}O_{39}]$ 1-vacant Keggin was systhesized according to previous literature.(*211*)

^{31}P NMR (500 MHz, D_2O): δ =-10.56 ppm.

6.3.2.2 Synthesis of POM-PNIPAM hybrid

To a suspension of $K_7[PW_{11}O_{39}]$ (1 eq.) in acetonitrile was added tetrabutylammonium chloride (TBA, 7.5 eq.). Then consecutively, poly(N-isopropylacrylamide) (2.2 eq.) and a 1M HCl solution (4.4 eq.) were added dropwise. After stirring overnight at room temperature, the solution was filtered and the solvent was evaporated. The solid residue was washed with DI water and dried in vacuum.

FTIR (cm^{-1}): 3615, 3543, 2975, 2944, 1645, 1539, 1445, 1376, 1109 (Si-O-Si), 967(W=O, as), 874($W-O_a-W$, as), 827($W-O_b-W$, as)

^{31}P NMR (500 MHz, Acetonitril-d_3): δ=-13.00 ppm.

^{1}H NMR (CD_3CN): δ= 3.96 (br, 1H, PNIPAM), 3.14 (t, 1H, TBA), 1.49-1.81(m&br, 2H in PNIPAM, 1H in TBA), 1.41 (m, 1H, TBA), 1.15 (s, 6H, PNIPAM), 1.01 (t, 1.5H, TBA).

MALDI-TOF (Acetonitrile): Take the example of 38 repeat units for calculation.

Calculated $[M \cdot H^+_4]^+$ 7231.8 Da, found 7232.2 Da.

6.4 Results and discussions

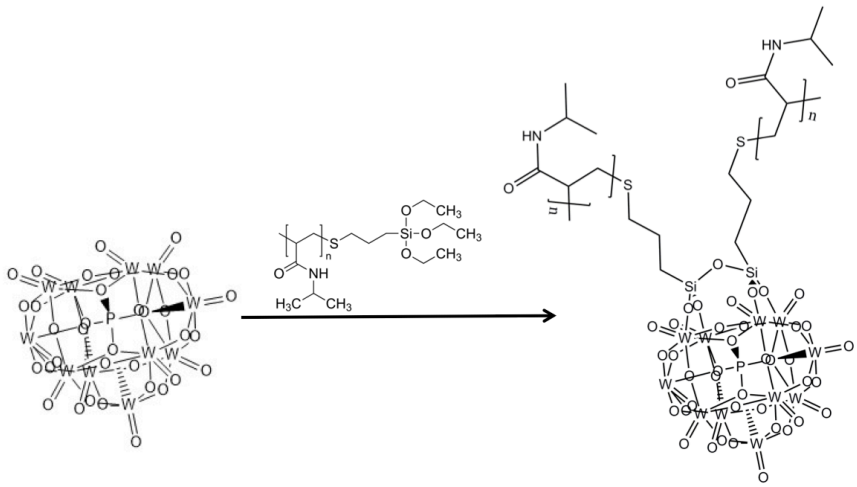

Figure 6.4-1. Synthetic scheme employed for synthesizing the temperature-responsive POM-PNIPAM hybrid.

Using a typical protocol of POMs' functionalization, two silane-terminated oligomeric PNIPAM (M_w~2,000, $RSi(OEt)_3$) chains were tethered to each mono-vacant Keggin cluster ($K_7PW_{11}O_{39}$), under acidic condition (Figure 6.4-1). By following previously reported method, (*120*) the reaction is conducted in acetonitrile into which tetrabutylammonium (TBA) bromide was used to solubilize Keggin clusters and consecutively added PNIPAM and hydrochloride acid dropwise. After the reaction, the solvent was evaporated, and the residue was washed with water to remove extra TBA-Br and dried in vacuum. The hybrid (K2P-TBA) structure was characterized by SEC, ^{31}P and ^{1}H-NMR, FTIR, and MALDI-TOF Mass Spectroscopy. In SEC measurements, the retention time of the hybrid obviously decreased and showed a narrower distribution, suggesting the success of POM functionalization, which is confirmed by the change of chemical shift in ^{31}P-NMR (Figure 6.4-2 and 6.4-3).

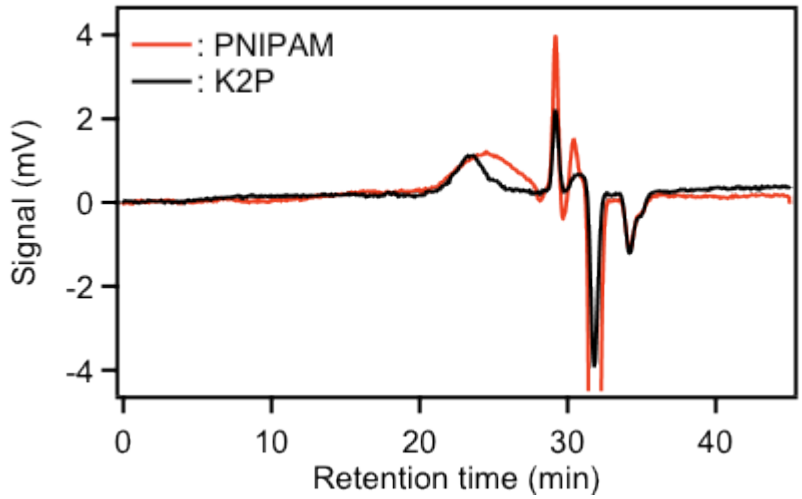

Figure 6.4-2. The SEC measurements of the pure PNIPAM and the K2P hybrid

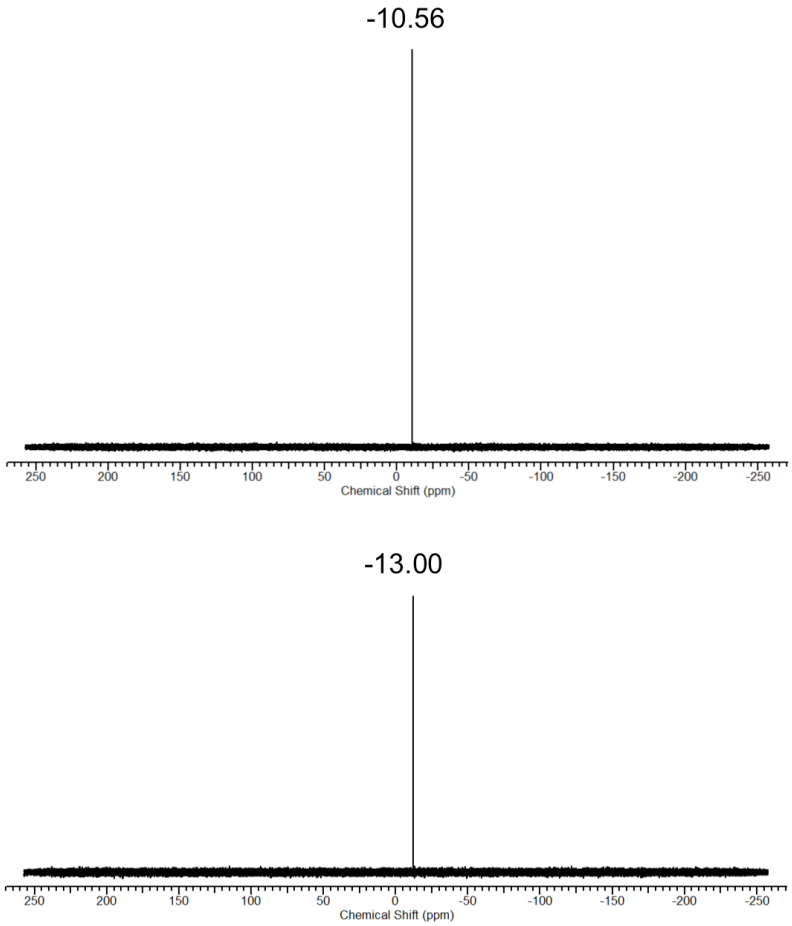

Figure 6.4-3. ^{31}P NMRs of 1-vacant Keggin and POM-PNIPAM hybrid.

The hybrid with different conterions such as K^+ ions can be achieved by dialyzing the K2P-TBA solution against salt solution such as KCl. The resulting solution was then dialyzed against deionized water to get rid of the extra ions. Very low scattered intensity for K2P-K solution at room temperature was collected by SLS, indicating that the K2P hybrid existed as discrete molecules (Figure 6.4-4). Time-resolved LLS was applied to monitor the aqueous solution of K2P at different temperatures, which could provide information on the thermo-responsiveness of this hybrid. With increasing the temperature to above 39 °C, a significant increase of intensity was observed and large assemblies began to form in solution. The scattered intensity as well

as the R_h (R_h is the hydrodynamic radius measured by dynamic light scattering (DLS)) were keeping going up when further increasing the temperature (Figure 6.4-4). The ratio of $R_h/R_g \approx 1.0$ (R_g is the radius of gyration of the assemblies measured by static light scattering (SLS)) was obtained for those assemblies, suggesting their hollow, spherical structures. The temperature induced self-assembly should be related to the thermo-response of PNIPAM chains which switched from hydrophilic to hydrophobic state. Consequently, the hybrid owning a charged polar head and two hydrophobic tails behaved similarly with common amphiphiles (*212*) by forming bilayer vesicles.

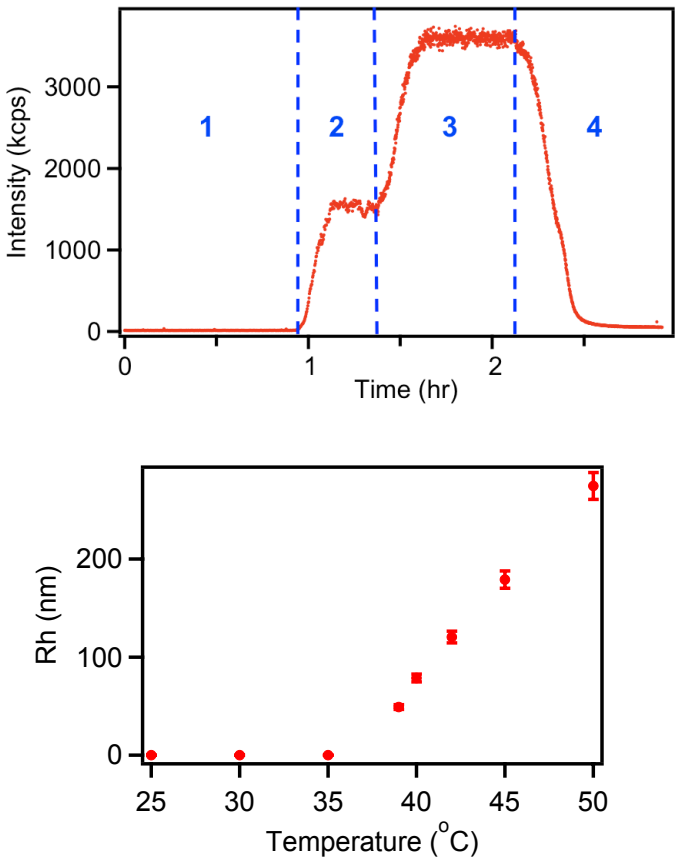

Figure 6.4-3. Top: Time-resolved SLS monitoring results of K2P (with K^+ ions as counterions) solution during varying the temperature which is divided into 4 regions (Regions: 1. Starting from room temperature RT, gradually increasing T to 35°C; 2. T is increase to 40°C; 3. T is increased to 45 °C; 4. T is decreased to 35 °C.). Bottom: Average R_h of the spherical structures formed by K2P-K as a function of temperature, measured by DLS.

POM clusters, as well as other macroions, have been reported for their unique solution behaviors by self-assembling into single-layer, hollow, spherical "blackberry" structures via counterion-mediated attraction. (*77, 101, 150*) Counterions are important in macroionic solutions and the binding affinity between macroions and counterions varies with the hydration size of counterions. (*96*) We expect different solution behaviors for the current hybrid systems with different counterions. The K2P-TBA solution was prepared for comparing with K2P-K solution. Although PNIPAM is hydrophilic in water at room temperature and the Keggin polar head is charged, with 3 TBA as counterions, interestingly the fully hydrophilic hybrids can self-assemble into vesicular structure in aqueous solution. A typical CONTIN analysis of the dynamic light scattering (DLS) results of the K2P-TBA solution (0.2 mg/mL) indicated that the R_h of the assemblies is 40±2 nm with no angular dependence.

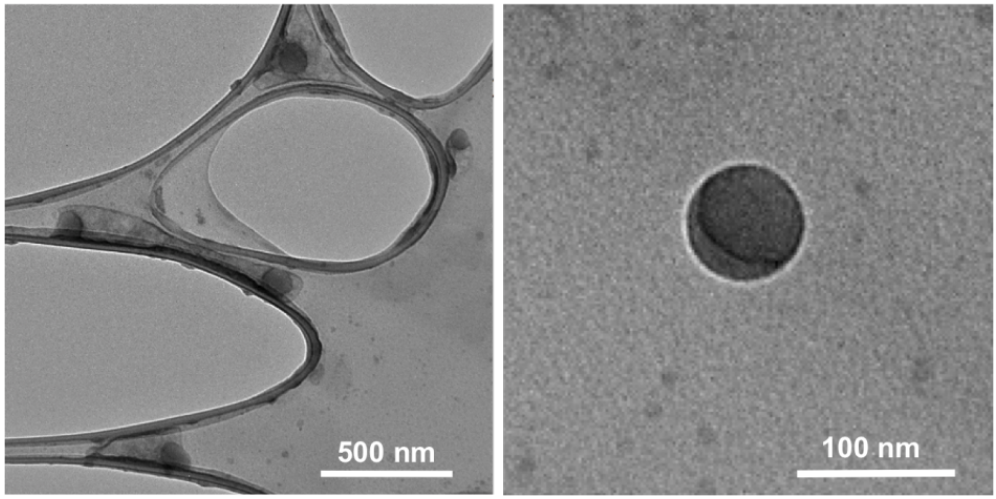

Figure 6.4-4. TEM images of the assemblies formed in 0.2 mg/mL K2P water solution at room temperature.

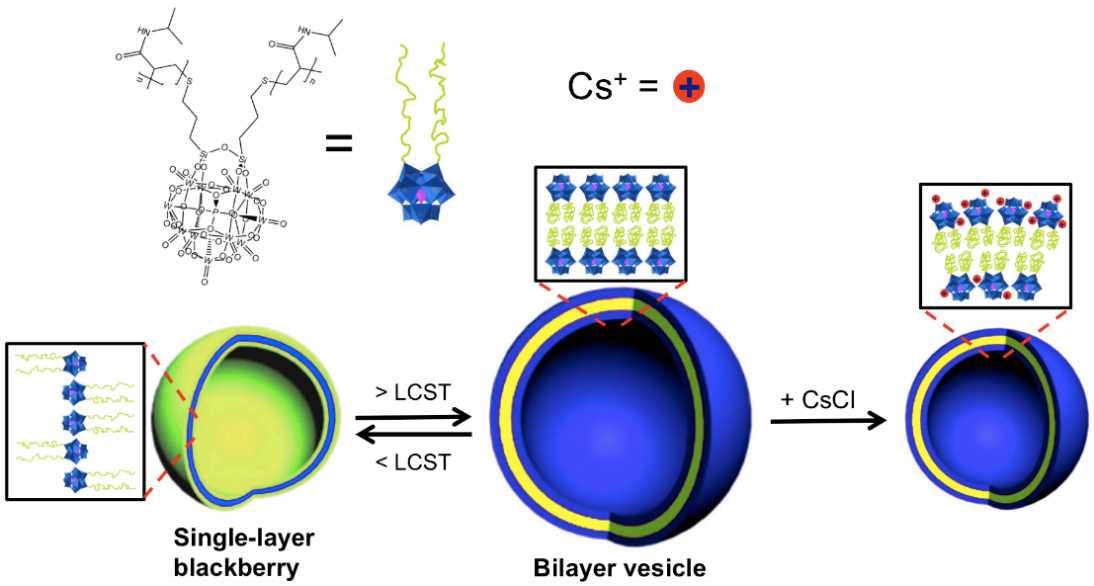

Figure 6.4-5. Graphical representation of the reversible transition from single-layer blackberry structures to bilayer vesicles with changing the solution temperature, and of the salt induced decrease of the vesicular size.

The ratio of $R_h/R_g \approx 1.0$ was obtained for those assemblies, suggesting their hollow, spherical structures, which is also confirmed by TEM measurements (Figures 6.4-5). The conductivity and Zeta potential measurements were performed and we obtained the values 29.4 μS/cm and -27.5 mV, respectively, confirming that the vesicles were charged in water and indicating their hydrophilicity. Similar with previous reports, in our study the Keggin heads can be treated as macroions, and TBA counterions associate with Keggins, consequently inducing the attraction between macroions and their self-assembly into blackberry type structures (Figure 6.4-6). This observation suggests that TBA^+ ions have stronger association with macroions than K^+ ions in pure water, causing the blackberry formation in the former case but not in the latter case. The effective charges on each blackberry can be estimated based on Equations (1) and (2), (*135*) which is equivalent to approximately 73, thereby

suggesting that most of TBA counterions are closely associated with blackberries.

$$Ze=6\pi\eta R_h\mu(1+\kappa R_h)/f(\kappa R_h) \quad (1)$$

$$\zeta=3\eta\mu/[2\varepsilon_0\varepsilon_r f(\kappa R_h)] \quad (2)$$

in which Z is the valence of the macromolecules (the effective charge), e is the elementary charge, η is the sample viscosity, R_h is the hydrodynamic radius, μ is the electrophoretic mobility, κ is the Debye–Hückel parameter, and $f(\kappa R_h)$ is Henry's function; ζ is the zeta potential, ε_0 is the permittivity of free space, and ε_r is the solvent dielectric constant. Since PNIPAM chains are hydrophilic and do not have special interaction with the Keggins; they should be dangling around the blackberry surface.

With increasing the temperature stepwise from room temperature to 40 °C, the scattered intensity of K2P-TBA solution increases gradually but slightly (Figure 6.4-7a). The R_h of assemblies remains almost the same in this temperature range (Figures 6.4-7c). From 40 to 41 °C, a significant increase of intensity was observed and it reached the plateau within 30 minutes. The scattered intensity as well as the R_h were keeping going up when further increasing the temperature (Figures 6.4-7b and c). The major changes happened at higher temperatures is due to the change of PNIPAM chains and the transition from blackberry structures to bilayer vesicles was proposed (Figure 6.4-6). Since the phase transition of PNIPAM is a reversible process, the reversibility of the self-assembly of the K2P-TBA hybrid can be expected,

which was confirmed by our observation of the scattered intensity returning to the original level of the same temperature (Figure 6.4-7a).

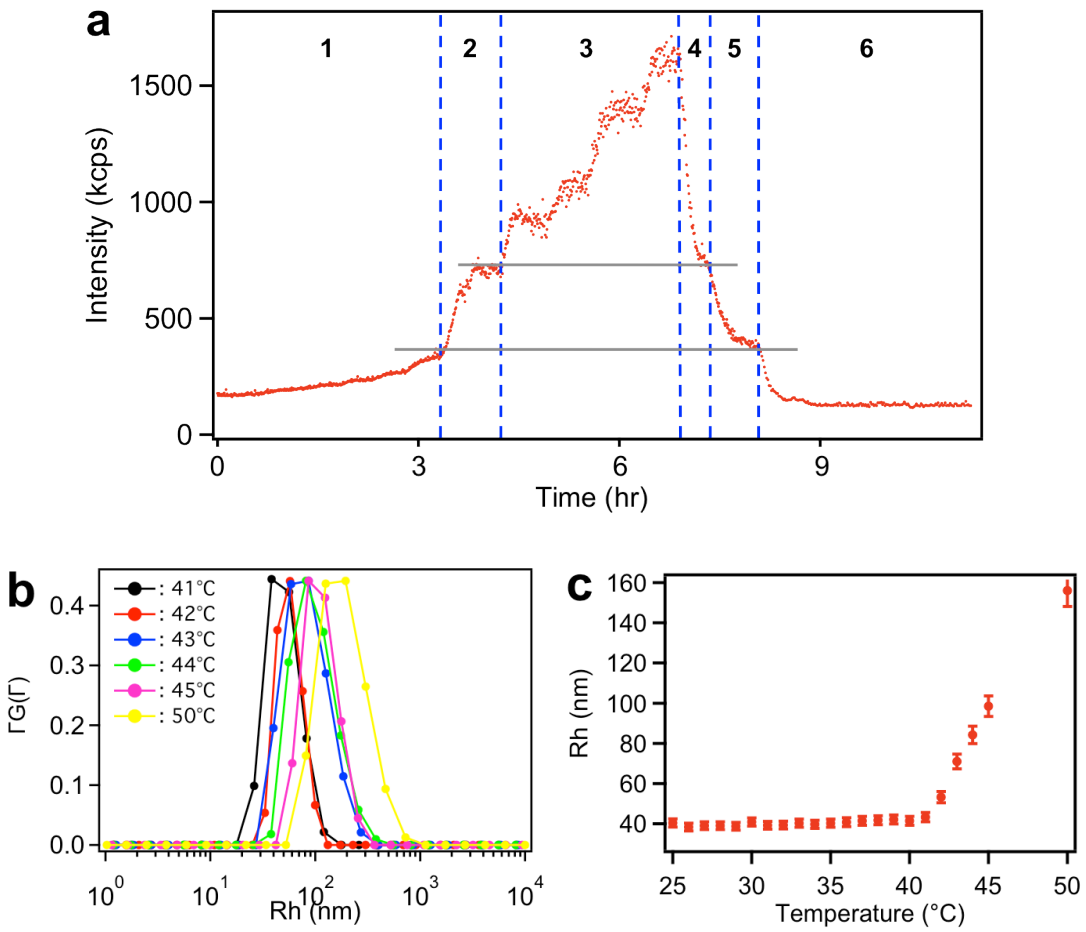

Figure 6.4-6. (a) Time-resolved SLS monitoring results of 0.2 mg/mL K2P solution during varying the temperature which is divided into 6 regions (Regions: 1. Starting from room temperature RT, gradually increasing T to 40 °C; 2. T is increase to 41 °C; 3. T is increased to 45 °C stepwise 1 °C by 1 °C; 4. T is decreased to 41 °C; 5. T is decreased to 40 °C; 6. Cooling down to RT.). (b) CONTIN analysis of DLS studies on K2P in aqueous solution at various temperatures. (C) Average R_h of the spherical structures formed by K2P as a function of temperature, measured by DLS.

Extra salts, such as NaCl, RbCl, CsCl and $CaCl_2$, were added into K2P-TBA solutions for studying the ionic effects on the temperature-sensitive self-assembly of K2P. Comparing the sizes of bilayer-vesicles formed in solutions with different extra salts at 45 °C, we found that the sizes of assemblies with extra CsCl and $CaCl_2$ are

Table 6.4-1. R_h values of vesicles formed at 45 °C in solutions without and with adding different salts.

	No Salt	Rb^+	Cs^+	Ca^{2+}
R_h (nm)	100±5	104±5	52±3	61±3

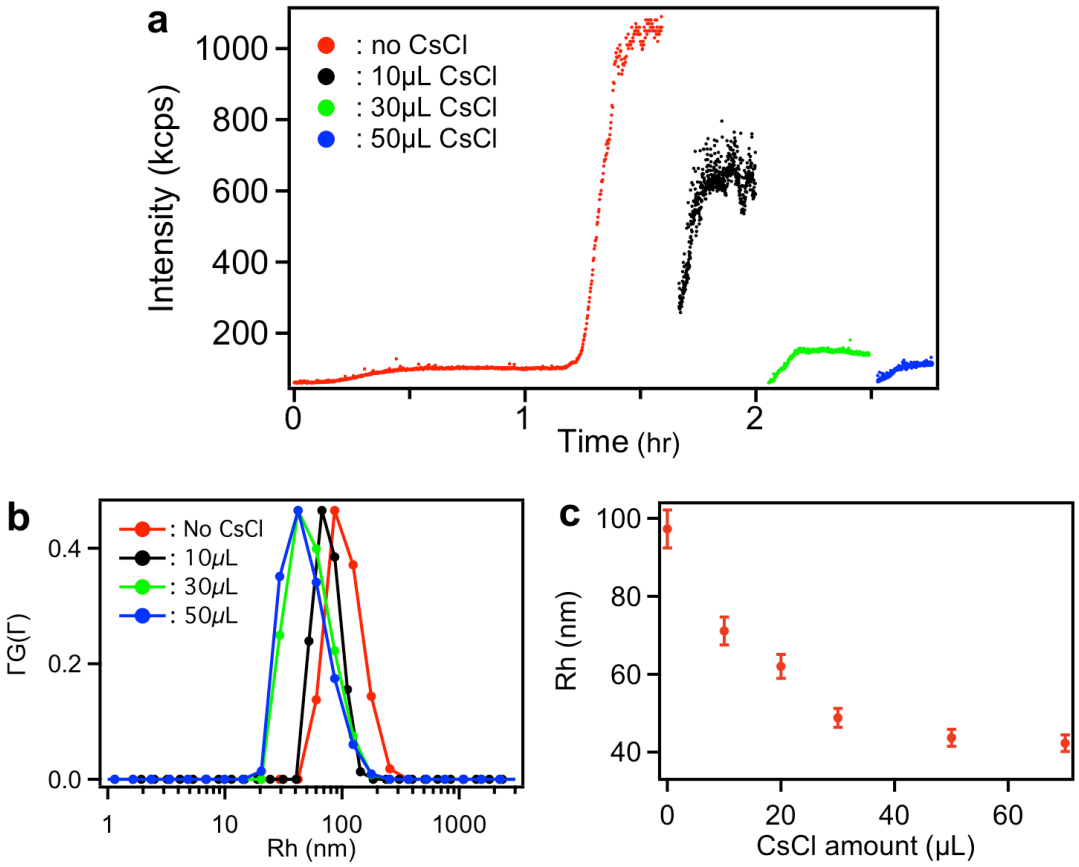

Figure 6.4-7. (a) Time-resolved SLS monitoring results of 0.2 mg/mL K2P solution under 45 °C during adding CsCl. (b) CONTIN analysis of DLS studies on K2P in aqueous solution with different amount of CsCl. (C) Average R_h of the spherical structures formed by K2P as a function of CsCl concentration, measured by the DLS.

much smaller than that without adding any salt (Table 6-1). To confirm this, in-situ experiment by adding CsCl stepwise to pre-heated K2P solution was performed. 10 μL CsCl solution (8.3 mM) was added into K2P solution (1 mL, 0.2 mg/mL) after the scattered intensity stabilized at 45 °C, and a significant decrease of intensity from LLS (Figure 6.4-8a) was observed. The intensity of the solution after adding extra salt

didn't reach the equilibrium immediately, but gradually increased and stabilized at certain level, because the temperature of the solution varied during the salt addition. By adding more CsCl to the solution, the scattered intensity further decreased, as well as the R_h of vesicles (Figure 6.4-8b and c), demonstrating the salt-responsiveness of the self-assembly of K2P hybrid (Figure 6.4-6).

It's well known that the phase transition of PNIPAM is influenced by the presence of salts, and the effect of alkali metal cations on lowering LCST correlates well to the position of corresponding ions in the classic Hoffmeister series. (*213*) However, the salt effect on PNIPAM isn't considered as the main reason for the vesicle shrink in our study since the concentration of salt we used is too low to affect the LCST of polymer. Moreover, control experiments of adding the same amount of salt to pure PNIPAM solution indicated no effects on the polymer's phase transition (Table 6-2). We expect that the salt-responsiveness is relative to the couterion association with Keggin, leading to bigger surface area of the polar head and consequently bigger curvature of vesicles (Figure 6.4-6). The hypothesis can also explain why cations with smaller hydration sizes such as Cs^+ and Ca^{2+} can effectively tune the assembly size, but not the ones with larger hydration size such as Rb^+, as cations in the former case demonstrate higher affinity to macroions.

Table 6.4-2. Temperatures of triggering aggregation and aggregate sizes formed at 39 °C in PNIPAM solutions without and with adding different salts.

	No Salt	Na^+	Cs^+
Temperature (°C)	38	39	38
R_h (nm)	125±6	122±6	122±6

6.5 Conclusions

In summary, a novel type of POM-PNIPAM macromolecular hybrid (K2P), possessing a rigid polar Keggin head group and two temperature-sensitive PNIPAM tails, was designed and synthesized. The obtained hybrid behaves like regular hydrophilic macroions in the aqueous solution at RT by showing the formation of blackberry structures via counterion-mediated attraction. At elevated temperatures, the K2P form amphiphilic bilayer vesicles in virtue of the phase transition of PNIPAM. The vesicle size can be tuned by introducing extra salt into the solution because of the consequent counterion-association with Keggin macroions.

CHAPTER VII

SUMMARY

In this dissertation, the self-assembly of two types of macroions in dilution solution, driven by counterion mediated attraction, were discussed. The study of polyhedral oligomeric silsesquioxane expands our exploration of macroionic behavior to a totally new area, with the model POSS macroions representing the smallest macroions to date. In the study of cyclodextrin, it is the first time that the generation of supramolecular structures from fully organic macroions has been observed in dilute solution. These precisely charge-controlled self-assemblies are very useful for interpreting the variability and diversity in biological systems.

For mimicking living systems, which are able to adapt themselves to the changing environment from molecular to macroscopic lever, a novel type of POM-PNIPAM macromolecular hybrid, was designed and synthesized. The obtained hybrid behaves like regular hydrophilic macroions in the aqueous solution at RT by showing the formation of blackberry structures via counterion-mediated attraction. At elevated temperatures, the K2P form amphiphilic bilayer vesicles in virtue of the phase transition of PNIPAM. The vesicle size can be tuned by introducing extra salt into the solution because of the consequent counterion-association with Keggin macroions.

BIBLIOGRAPHY

1. P. Debye, E. Hückel, De la théorie des électrolytes. i. abaissement du point de congélation et phénomènes associés. *Physikalische Zeitschrift* **24**, 185 (1923).

2. B. Derjaguin, Theory of the stability of strongly charged lyophobic sols and the adhesion of strongly charged particles in solutions of electrolytes. *Acta Physicochim. USSR* **14**, 633 (1941).

3. E. J. W. Verwey, J. T. G. Overbeek, J. T. G. Overbeek, *Theory of the stability of lyophobic colloids*. (Courier Corporation, 1999).

4. J. T. Rhule, C. L. Hill, D. A. Judd, R. F. Schinazi, Polyoxometalates in Medicine. *Chem. Rev.* **98**, 327 (1998).

5. D.-L. Long, E. Burkholder, L. Cronin, Polyoxometalate clusters, nanostructures and materials: from self assembly to designer materials and devices. *Chem. Soc. Rev.* **36**, 105 (2007).

6. P. Yin, D. Li, T. Liu, Counterion Interaction and Association in Metal-Oxide Cluster Macroanionic Solutions and the Consequent Self-Assembly. *Israel Journal of Chemistry* **51**, 191 (2011).

7. A. Müller, S. Roy, En route from the mystery of molybdenum blue via related manipulatable building blocks to aspects of materials science. *Coord. Chem. Rev.* **245**, 153 (2003).

8. A. Proust, R. Thouvenot, P. Gouzerh, Functionalization of polyoxometalates: towards advanced applications in catalysis and materials science. *Chem. Commun.*, 1837 (2008).

9. D.-L. Long, R. Tsunashima, L. Cronin, Polyoxometalates: Building Blocks for Functional Nanoscale Systems. *Angew. Chem. Int. Edit.* **49**, 1736 (2010).

10. A. Dolbecq, E. Dumas, C. d. R. Mayer, P. Mialane, Hybrid organic− inorganic polyoxometalate compounds: from structural diversity to applications. *Chem. Rev.* **110**, 6009 (2010).

11. X. Yu *et al.*, Giant surfactants provide a versatile platform for sub-10-nm nanostructure engineering. *Proc. Natl. Acad. Soc.* **110**, 10078 (2013).

12. N. Branda, R. Wyler, J. Rebek, Encapsulation of methane and other small molecules in a self-assembling superstructure. *Science* **263**, 1267 (1994).

13. E. Coronado, C. J. Gomez-Garcia, Polyoxometalate-based molecular materials. *Chem. Rev.* **98**, 273 (1998).

14. M. Fujita *et al.*, Self-assembly of ten molecules into nanometre-sized organic host frameworks. *Nature* **378**, 469 (1995).

15. C. Hartmann-Thompson, in *Applications of Polyhedral Oligomeric Silsesquioxanes*. (Springer, 2011), pp. 247-325.

16. H. J. Kang, F. Coulibaly, F. Clow, T. Proft, E. N. Baker, Stabilizing isopeptide bonds revealed in gram-positive bacterial pilus structure. *Science* **318**, 1625 (2007).

17. H. J. Kang, N. G. Paterson, A. H. Gaspar, H. Ton-That, E. N. Baker, The Corynebacterium diphtheriae shaft pilin SpaA is built of tandem Ig-like modules with stabilizing isopeptide and disulfide bonds. *Proc. Natl. Acad. Soc.* **106**, 16967 (2009).

18. D. E. Katsoulis, A survey of applications of polyoxometalates. *Chem. Rev.* **98**, 359 (1998).

19. M. Tominaga, K. Suzuki, T. Murase, M. Fujita, 24-Fold endohedral functionalization of a self-assembled M12L24 coordination nanoball. *J. Am. Chem. Soc.* **127**, 11950 (2005).

20. D. Whitford, *Proteins: structure and function*. (John Wiley & Sons, 2013).

21. F. Carniato *et al.*, Synthesis and characterisation of metal isobutylsilsesquioxanes and their role as inorganic–organic nanoadditives for enhancing polymer thermal stability. *Eur. J. Inorg. Chem.* **2007**, 585 (2007).

22. S.-W. Kuo, F.-C. Chang, POSS related polymer nanocomposites. *Prog. Polym. Sci.* **36**, 1649 (2011).

23. M. Asuncion, R. Laine, Fluoride Rearrangement Reactions of Polyphenyl-and Polyvinylsilsesquioxanes as a Facile Route to Mixed Functional Phenyl, Vinyl T10 and T12 Silsesquioxanes. *J. Am. Chem. Soc.* **132**, 3723 (2010).

24. M. Z. Asuncion, M. Ronchi, H. Abu-Seir, R. M. Laine, Synthesis, functionalization and properties of incompletely condensed “half cube” silsesquioxanes as a potential route to nanoscale Janus particles. *C. R. Chim.* **13**, 270 (2010).

25. F. Feher, K. Wyndham, R. Baldwin, J. Ziller, J. Lichtenhan, Methods for effecting monofunctionalization of (CH 2 [double bond, length half m-dash] CH) 8 Si 8 O 12. *Chem. Commun.*, 1289 (1999).

26. Y. Li *et al.*, Tuning "thiol-ene" reactions toward controlled symmetry breaking in polyhedral oligomeric silsesquioxanes. *Chem. Sci.* **5**, 1046 (2014).

27. W. Zhang, A. H. E. Müller, Architecture, self-assembly and properties of well-defined hybrid polymers based on polyhedral oligomeric silsequioxane (POSS). *Prog. Polym. Sci.* **38**, 1121 (2013).

28. K. L. Chan, P. Sonar, A. Sellinger, Cubic silsesquioxanes for use in solution processable organic light emitting diodes (OLED). *J. Mater. Chem.* **19**, 9103 (2009).

29. S. Fabritz *et al.*, From pico to nano: biofunctionalization of cube-octameric silsesquioxanes by peptides and miniproteins. *Org. Biomol. Chem.* **10**, 6287 (2012).

30. G. Li, L. Wang, H. Ni, C. Pittman, Jr., Polyhedral Oligomeric Silsesquioxane (POSS) Polymers and Copolymers: A Review. *J. Inorg. Organomet. P.* **11**, 123 (2001).

31. P. Majumdar *et al.*, Antimicrobial activity of polysiloxane coatings containing quaternary ammonium-functionalized polyhedral oligomeric silsesquioxane. *J. Coat. Technol. Res.* **7**, 455 (2010).

32. K. Tanaka, Y. Chujo, Advanced functional materials based on polyhedral oligomeric silsesquioxane (POSS). *J. Mater. Chem.* **22**, 1733 (2012).

33. A. Tuteja *et al.*, Designing Superoleophobic Surfaces. *Science* **318**, 1618 (December 7, 2007, 2007).

34. Y. Zhang, Z. Ye, Homogeneous polyhedral oligomeric silsesquioxane (POSS)-supported Pd-diimine complex and synthesis of polyethylenes end-tethered with a POSS nanoparticleviaethylene "living" polymerization. *Chem. Commun.*, 1178 (2008).

35. L. Chen *et al.*, A metal-sensitive organic–inorganic hybrid surfactant: POSS-capped dipicolinic acid-functionalized poly(ethylene glycol) amphiphile. *React. Funct. Polym* **73**, 1022 (2013).

36. X. Kuang *et al.*, Assembly of a metal–organic framework by sextuple intercatenation of discrete adamantane-like cages. *Nature chemistry* **2**, 461 (2010).

37. C.-M. Leu, G. M. Reddy, K.-H. Wei, C.-F. Shu, Synthesis and Dielectric Properties of Polyimide-Chain-End Tethered Polyhedral Oligomeric Silsesquioxane Nanocomposites. *Chem. Mater.* **15**, 2261 (2003).

38. M. E. Pérez-Ojeda *et al.*, Controlled Click-Assembly of Well-Defined Hetero-Bifunctional Cubic Silsesquioxanes and Their Application in Targeted Bioimaging. *Chem.-Eur. J.* **19**, 6630 (2013).

39. Z. Wang *et al.*, Giant gemini surfactants based on polystyrene-hydrophilic polyhedral oligomeric silsesquioxane shape amphiphiles: sequential "click" chemistry and solution self-assembly. *Chem. Sci.* **4**, 1345 (2013).

40. W. Zhang, B. Fang, A. Walther, A. H. E. Müller, Synthesis via RAFT Polymerization of Tadpole-Shaped Organic/Inorganic Hybrid Poly(acrylic acid) Containing Polyhedral Oligomeric Silsesquioxane (POSS) and Their Self-assembly in Water. *Macromolecules* **42**, 2563 (2009).

41. M. E. Davis, M. E. Brewster, Cyclodextrin-based pharmaceutics: past, present and future. *Nat Rev Drug Discov* **3**, 1023 (2004).

42. E. M. M. Del Valle, Cyclodextrins and their uses: a review. *Process Biochem.* **39**, 1033 (2004).

43. K. Uekama, F. Hirayama, T. Irie, Cyclodextrin drug carrier systems. *Chem. Rev.* **98**, 2045 (1998).

44. K. A. Connors, The stability of cyclodextrin complexes in solution. *Chem. Rev.* **97**, 1325 (1997).

45. G. Wenz, B.-H. Han, A. Müller, Cyclodextrin rotaxanes and polyrotaxanes. *Chem. Rev.* **106**, 782 (2006).

46. G. Chen, M. Jiang, Cyclodextrin-based inclusion complexation bridging supramolecular chemistry and macromolecular self-assembly. *Chem. Soc. Rev.* **40**, 2254 (2011).

47. W. Saenger, Cyclodextrin Inclusion Compounds in Research and Industry. *Angew. Chem. Int. Edit.* **19**, 344 (1980).

48. Y. Chen, Y. Liu, Cyclodextrin-based bioactive supramolecular assemblies. *Chem. Soc. Rev.* **39**, 495 (2010).

49. W. Deng, D. H. Thompson, pH and cation-responsive supramolecular gels formed by cyclodextrin amines in DMSO. *Soft Matter* **6**, 1884 (2010).

50. L. Jiang, Y. Yan, M. Drechsler, J. Huang, Enzyme-triggered model self-assembly in surfactant-cyclodextrin systems. *Chem. Commun.* **48**, 7347 (2012).

51. L. Jiang, Y. Yan, J. Huang, Versatility of cyclodextrins in self-assembly systems of amphiphiles. *Adv. Colloid Interface Sci.* **169**, 13 (2011).

52. L. Jiang *et al.*, Helical Colloidal Sphere Structures through Thermo-Reversible Co-Assembly with Molecular Microtubes. *Angew. Chem. Int. Edit.* **52**, 3364 (2013).

53. L. Jiang *et al.*, "Annular Ring" microtubes formed by SDS@2[small beta]-CD complexes in aqueous solution. *Soft Matter* **6**, 1731 (2010).

54. L. Jiang, Y. Peng, Y. Yan, J. Huang, Aqueous self-assembly of SDS@2[small beta]-CD complexes: lamellae and vesicles. *Soft Matter* **7**, 1726 (2011).

55. Z. Wu, Y. Yan, J. Huang, Advanced Molecular Self-Assemblies Facilitated by Simple Molecules. *Langmuir* **30**, 14375 (2014).

56. C. Zhou, X. Cheng, Y. Yan, J. Wang, J. Huang, Reversible Transition between SDS@2β-CD Microtubes and Vesicles Triggered by Temperature. *Langmuir* **30**, 3381 (2014).

57. C. Zhou *et al.*, Self-Assembly of Nonionic Surfactant Tween 20@2β-CD Inclusion Complexes in Dilute Solution. *Langmuir* **29**, 13175 (2013).

58. F. Bellia *et al.*, Selectively functionalized cyclodextrins and their metal complexes. *Chem. Soc. Rev.* **38**, 2756 (2009).

59. S. Hanessian, A. Benalil, C. Laferriere, The Synthesis of Functionalized Cyclodextrins As Scaffolds and Templates for Molecular Diversity, Catalysis, and Inclusion Phenomena. *J. Org. Chem.* **60**, 4786 (1995).

60. D. Vizitiu, C. S. Walkinshaw, B. I. Gorin, G. R. J. Thatcher, Synthesis of Monofacially Functionalized Cyclodextrins Bearing Amino Pendent Groups. *J. Org. Chem.* **62**, 8760 (1997).

61. L. Szente, J. Szejtli, Highly soluble cyclodextrin derivatives: chemistry, properties, and trends in development. *Adv. Drug Deliv. Rev.* **36**, 17 (1999).

62. B. Botar, P. Kögerler, C. L. Hill, [{(Mo) Mo 5 O 21 (H 2 O) 3 (SO 4)} 12 (VO) 30 (H 2 O) 20] 36−: A molecular quantum spin icosidodecahedron. *Chem. Commun.*, 3138 (2005).

63. R. C. Howell *et al.*, A new type of heteropolyoxometalates formed from lacunary polyoxotungstate ions and europium or yttrium cations. *Angew. Chem. Int. Edit.* **40**, 4031 (2001).

64. S. S. Mal, U. Kortz, The Wheel-Shaped Cu20 Tungstophosphate [Cu20Cl (OH) 24 (H2O) 12 (P8W48O184)] 25− Ion. *Angew. Chem. Int. Edit.* **44**, 3777 (2005).

65. A. Mueller, Sarkar Sh., Koegerler P., Hauptfleisch B., Trautwein AX and Schuenemann V. *Angew. Chem. Int. Ed. Engl* **38**, 3238 (1999).

66. A. Müller *et al.*, Rapid and Simple Isolation of the Crystalline Molybdenum-Blue Compounds with Discrete and Linked Nanosized Ring-Shaped Anions: Na15 [Mo {126}{VI} Mo {28} VO462H14 (H2O) 70] 0.5 [Mo {124}{VI} Mo {28} VO457H14 (H2O) 68] 0.5· ca. 400 H2O and Na22 [Mo {118}{VI} Mo {28} VO442H14 (H2O) 58]· ca. 250 H2O. *Zeitschrift für anorganische und allgemeine Chemie* **625**, 1187 (1999).

67. A. Müller, E. Krickemeyer, H. Bögge, M. Schmidtmann, F. Peters, Organizational forms of matter: an inorganic super fullerene and keplerate based on molybdenum oxide. *Angew. Chem. Int. Edit.* **37**, 3359 (1998).

68. A. Müller, S. Roy, En route from the mystery of molybdenum blue via related manipulatable building blocks to aspects of materials science. *Coord. Chem. Rev.* **245**, 153 (2003).

69. A. M. Todea *et al.*, Extending the {(Mo) Mo5} 12M30 capsule Keplerate sequence: A {Cr30} cluster of s= 3/2 metal centers with a {Na (H2O) 12} encapsulate. *Angew. Chem.* **119**, 6218 (2007).

70. M. R. Wright, *An introduction to aqueous electrolyte solutions*. (John Wiley & Sons, 2007).

71. D. F. Evans, H. Wennerstrom, *Colloidal domain*. (Wiley-Vch, 1999).

72. N. Ise, I. Sogami, *Structure formation in solution: Ionic polymers and colloidal particles*. (Springer Science & Business Media, 2005).

73. A. Kose, M. Ozaki, K. Takano, Y. Kobayashi, S. Hachisu, Direct observation of ordered latex suspension by metallurgical microscope. *Journal of Colloid and Interface Science* **44**, 330 (1973).

74. W. I. Lee, J. M. Schurr, Dynamic light scattering studies of poly-L-lysine HBr in the presence of added salt. *Biopolymers* **13**, 903 (1974).

75. K. S. Schmitz, M. Lu, N. Singh, D. J. Ramsay, Comments on the "ordinary–extraordinary phase transition" of poly (lysine). *Biopolymers* **23**, 1637 (1984).

76. A. Müller *et al.*, [Mo154 (NO) 14O420 (OH) 28 (H2O) 70](25±5)−: A Water-Soluble Big Wheel with More than 700 Atoms and a Relative Molecular Mass of About 24000. *Angew. Chem. Int. Edit.* **34**, 2122 (1995).

77. T. Liu, E. Diemann, H. Li, A. W. Dress, A. Müller, Self-assembly in aqueous solution of wheel-shaped Mo154 oxide clusters into vesicles. *Nature* **426**, 59 (2003).

78. J. M. Pigga, M. L. Kistler, C. Y. Shew, M. R. Antonio, T. Liu, Counterion Distribution around Hydrophilic Molecular Macroanions: The Source of the Attractive Force in Self-Assembly. *Angew. Chem. Int. Edit.* **48**, 6538 (2009).

79. A. Müller *et al.*, Archimedean Synthesis and Magic Numbers: "Sizing" Giant Molybdenum-Oxide-Based Molecular Spheres of the Keplerate Type. *Angew. Chem. Int. Edit.* **38**, 3238 (1999).

80. M. L. Kistler, T. Liu, P. Gouzerh, A. M. Todea, A. Muller, Molybdenum-oxide based unique polyprotic nanoacids showing different deprotonations and related assembly processes in solution. *Dalton Trans.*, 5094 (2009).

81. A. Oleinikova *et al.*, Self-Association Based on Interfacial Structured Water Leads to {Mo154}≈ 1165 Super Clusters: A Dielectric Study. *ChemPhysChem* **8**, 646 (2007).

82. K. S. Schmitz, Macroion Clustering in Solutions and Suspensions: The Roles of Microions and Solvent†. *J. Phys. Chem. B* **113**, 2624 (2009).

83. W.-B. Zhang *et al.*, Molecular nanoparticles are unique elements for macromolecular science: From "nanoatoms" to giant molecules. *Macromolecules* **47**, 1221 (2014).

84. T. Liu *et al.*, Deprotonations and charges of well-defined {Mo72Fe30} nanoacids simply stepwise tuned by pH allow control/variation of related self-assembly processes. *J. Am. Chem. Soc.* **128**, 15914 (2006).

85. I. Sogami, N. Ise, On the electrostatic interaction in macroionic solutions. *J. Chem. Phys.* **81**, 6320 (1984).

86. R. Das *et al.*, Counterion distribution around DNA probed by solution X-ray scattering. *Phys. Rev. Lett.* **90**, 188103 (2003).

87. X. Qiu *et al.*, Inter-DNA attraction mediated by divalent counterions. *Phys. Rev. Lett.* **99**, 038104 (2007).

88. X. Qiu, K. Andresen, J. S. Lamb, L. W. Kwok, L. Pollack, Abrupt transition from a free, repulsive to a condensed, attractive DNA phase, induced by multivalent polyamine cations. *Phys. Rev. Lett.* **101**, 228101 (2008).

89. G. S. Manning, Limiting laws and counterion condensation in polyelectrolyte solutions I. Colligative properties. *J. Chem. Phys.* **51**, 924 (1969).

90. F. Oosawa, Interaction between parallel rodlike macroions. *Biopolymers* **6**, 1633 (1968).

91. M. T. Pope, *Heteropoly and isopoly oxometalates*. (Springer Verlag, 1983), vol. 8.

92. V. A. Grigoriev, D. Cheng, C. L. Hill, I. A. Weinstock, Role of alkali metal cation size in the energy and rate of electron transfer to solvent-separated 1: 1 [(M+)(acceptor)](M+= Li+, Na+, K+) ion pairs. *J. Am. Chem. Soc.* **123**, 5292 (2001).

93. V. A. Grigoriev, C. L. Hill, I. A. Weinstock, Role of Cation Size in the Energy of Electron Transfer to 1: 1 Polyoxometalate Ion Pairs {(M+)(X n+ VW11O40)}(8-n)-(M= Li, Na, K). *J. Am. Chem. Soc.* **122**, 3544 (2000).

94. F. Leroy, P. Miró, J. M. Poblet, C. Bo, J. Bonet Ávalos, Keggin polyoxoanions in aqueous solution: Ion pairing and its effect on dynamic properties by molecular dynamics simulations. *J. Phys. Chem. B* **112**, 8591 (2008).

95. J. M. Pigga, M. L. Kistler, C.-Y. Shew, M. R. Antonio, T. Liu, Counterion Distribution around Hydrophilic Molecular Macroanions: The Source of the Attractive Force in Self-Assembly. *Angew. Chem. Int. Edit.* **48**, 6538 (2009).

96. J. M. Pigga, J. A. Teprovich, R. A. Flowers, M. R. Antonio, T. Liu, Selective Monovalent Cation Association and Exchange around Keplerate Polyoxometalate Macroanions in Dilute Aqueous Solutions. *Langmuir* **26**, 9449 (2010).

97. A. M. Todea *et al.*, Porous Capsules {(M) M5} 12FeIII30 (M= MoVI, WVI): Sphere Surface Supramolecular Chemistry with 20 Ammonium Ions, Related Solution Properties, and Tuning of Magnetic Exchange Interactions. *Angew. Chem. Int. Edit.* **49**, 514 (2010).

98. M. L. Kistler, K. G. Patel, T. Liu, Accurately Tuning the Charge on Giant Polyoxometalate Type Keplerates through Stoichiometric Interaction with Cationic Surfactants. *Langmuir* **25**, 7328 (2009).

99. A. A. Verhoeff *et al.*, Charge Regulation as a Stabilization Mechanism for Shell-Like Assemblies of Polyoxometalates. *Phys. Rev. Lett.* **99**, 066104 (2007).

100. C. Schäffer *et al.*, Unprecedented and Differently Applicable Pentagonal Units in a Dynamic Library: A Keplerate of the Type {(W) W5} 12 {Mo2} 30. *Angew. Chem.* **121**, 155 (2009).

101. T. Liu, Hydrophilic Macroionic Solutions: What Happens When Soluble Ions Reach the Size of Nanometer Scale? *Langmuir* **26**, 9202 (2009).

102. J. Zhou, P. Yin, L. Hu, F. Haso, T. Liu, Self-Assembly of Subnanometer-Scaled Polyhedral Oligomeric Silsesquioxane (POSS) Macroions in Dilute Solution. *Eur. J. Inorg. Chem.* **2014**, 4593 (2014).

103. T. Liu, An unusually slow self-assembly of inorganic ions in dilute aqueous solution. *J. Am. Chem. Soc.* **125**, 312 (2003).

104. G. Liu, T. Liu, S. S. Mal, U. Kortz, Wheel-Shaped Polyoxotungstate [Cu20Cl(OH)24(H2O)12(P8W48O184)]25- Macroanions Form Supramolecular "Blackberry" Structure in Aqueous Solution. *J. Am. Chem. Soc.* **128**, 10103 (2006).

105. G. Liu, T. Liu, Thermodynamic Properties of the Unique Self-Assembly of {Mo72Fe30} Inorganic Macro-Ions in Salt-Free and Salt-Containing Aqueous Solutions. *Langmuir* **21**, 2713 (2005).

106. T. Liu *et al.*, Self-Recognition Among Different Polyprotic Macroions During Assembly Processes in Dilute Solution. *Science* **331**, 1590 (2011).

107. J. Zhang, D. Li, G. Liu, K. J. Glover, T. Liu, Lag Periods During the Self-Assembly of {Mo72Fe30} Macroions: Connection to the Virus Capsid Formation Process. *J. Am. Chem. Soc.* **131**, 15152 (2009).

108. G. L. Casini, D. Graham, D. Heine, R. L. Garcea, D. T. Wu, In vitro papillomavirus capsid assembly analyzed by light scattering. *Virology* **325**,

320 (2004).

109. P. Ceres, A. Zlotnick, Weak protein-protein interactions are sufficient to drive assembly of hepatitis B virus capsids. *Biochemistry* **41**, 11525 (2002).

110. P. E. Prevelige Jr, D. Thomas, J. King, Nucleation and growth phases in the polymerization of coat and scaffolding subunits into icosahedral procapsid shells. *Biophysical journal* **64**, 824 (1993).

111. A. Zlotnick, J. M. Johnson, P. W. Wingfield, S. J. Stahl, D. Endres, A Theoretical Model Successfully Identifies Features of Hepatitis B Virus Capsid Assembly. *Biochemistry* **38**, 14644 (1999).

112. P. A. Bachmann, P. L. Luisi, J. Lang, Autocatalytic self-replicating micelles as models for prebiotic structures. *Nature* **357**, 57 (1992).

113. P. V. Coveney, A. N. Emerton, B. M. Boghosian, Simulation of self-reproducing micelles using a lattice-gas automaton. *J. Am. Chem. Soc.* **118**, 10719 (1996).

114. A. Veronese, P. L. Luisi, An autocatalytic reaction leading to spontaneously assembled phosphatidyl nucleoside giant vesicles. *J. Am. Chem. Soc.* **120**, 2662 (1998).

115. Y. Song *et al.*, Controlled synthesis of 2-D and 3-D dendritic platinum nanostructures. *J. Am. Chem. Soc.* **126**, 635 (2004).

116. J. Hofrichter, P. D. Ross, W. A. Eaton, Kinetics and mechanism of deoxyhemoglobin S gelation: a new approach to understanding sickle cell disease. *Proc. Natl. Acad. Soc.* **71**, 4864 (1974).

117. A. Zlotnick, Are weak protein–protein interactions the general rule in capsid assembly? *Virology* **315**, 269 (2003).

118. A. Zlotnick, R. Aldrich, J. M. Johnson, P. Ceres, M. J. Young, Mechanism of capsid assembly for an icosahedral plant virus. *Virology* **277**, 450 (2000).

119. J. J. Giner-Casares, G. Brezesinski, H. Möhwald, S. Landsmann, S. Polarz, Polyoxometalate surfactants as unique molecules for interfacial self-assembly. *The Journal of Physical Chemistry Letters* **3**, 322 (2012).

120. S. Landsmann, C. Lizandara-Pueyo, S. Polarz, A New Class of Surfactants with Multinuclear, Inorganic Head Groups. *J. Am. Chem. Soc.* **132**, 5315 (2010).

121. D. Li *et al.*, Inorganic–Organic Hybrid Vesicles with Counterion- and pH-Controlled Fluorescent Properties. *J. Am. Chem. Soc.* **133**, 14010 (2011).

122. D. Li, P. Yin, T. Liu, Supramolecular architectures assembled from amphiphilic hybrid polyoxometalates. *Dalton Trans.* **41**, 2853 (2012).

123. M. F. Misdrahi *et al.*, Amphiphilic properties of dumbbell-shaped inorganic–organic–inorganic molecular hybrid materials in solution and at an interface. *Langmuir* **27**, 9193 (2011).

124. C. P. Pradeep *et al.*, Synthesis of Modular "Inorganic–Organic–Inorganic" Polyoxometalates and Their Assembly into Vesicles. *Angew. Chem. Int. Edit.* **48**, 8309 (2009).

125. F. Xiao *et al.*, Buildup of Amphiphilic Molecular Bola from Organic–Inorganic Hybrid Polyoxometalates and Their Vesicle-Like Supramolecular Assembly. *Chemistry-A European Journal* **17**, 12006 (2011).

126. P. Yin *et al.*, Controllable Self-Assembly of Organic–Inorganic Amphiphiles Containing Dawson Polyoxometalate Clusters. *Chem.-Eur. J.* **18**, 8157 (2012).

127. P. Yin *et al.*, A Double-Tailed Fluorescent Surfactant with a Hexavanadate Cluster as the Head Group. *Angew. Chem.* **123**, 2569 (2011).

128. J. Zhang, Y.-F. Song, L. Cronin, T. Liu, Self-Assembly of Organic−Inorganic Hybrid Amphiphilic Surfactants with Large Polyoxometalates as Polar Head Groups. *J. Am. Chem. Soc.* **130**, 14408 (2008).

129. J. Zhang, Y. F. Song, L. Cronin, T. Liu, Reverse-Vesicle Formation of Organic–Inorganic Polyoxometalate-Containing Hybrid Surfactants with Tunable Sizes. *Chemistry-A European Journal* **16**, 11320 (2010).

130. P. Yin *et al.*, A Double-Tailed Fluorescent Surfactant with a Hexavanadate Cluster as the Head Group. *Angew. Chem.* **123**, 2569 (2011).

131. P. Yin *et al.*, Controllable Self-Assembly of Organic–Inorganic Amphiphiles Containing Dawson Polyoxometalate Clusters. *Chemistry-A European Journal* **18**, 8157 (2012).

132. B. Chu, *Laser light scattering*. (Elsevier, 1974).

133. P. C. Hiemenz, R. Rajagopalan, *Principles of Colloid and Surface Chemistry, revised and expanded*. (CRC Press, 1997), vol. 14.

134. S. W. Provencher, CONTIN: A general purpose constrained regularization program for inverting noisy linear algebraic and integral equations. *Comput. Phys. Commun.* **27**, 229 (1982).

135. R. J. Hunter, *Zeta potential in colloid science: principles and applications*. (Academic press, 2013), vol. 2.

136. A. Eden, in *The Search for Christian Doppler*. (Springer, 1992), pp. 27-37.

137. R. H. Baney, M. Itoh, A. Sakakibara, T. Suzuki, Silsesquioxanes. *Chem. Rev.* **95**, 1409 (1995).

138. P. D. Lickiss, F. Rataboul, in *Advances in Organometallic Chemistry,* F. H. Anthony, J. F. Mark, Eds. (Academic Press, 2008), vol. Volume 57, pp. 1-116.

139. M. Voronkov, V. Lavrent'yev, in *Inorganic Ring Systems*. (Springer Berlin Heidelberg, 1982), vol. 102, pp. 199-236.

140. D. B. Cordes, P. D. Lickiss, F. Rataboul, Recent developments in the chemistry of cubic polyhedral oligosilsesquioxanes. *Chem. Rev.* **110**, 2081 (2010).

141. Y.-L. Liu, M.-H. Fangchiang, Polyhedral oligomeric silsesquioxane nanocomposites exhibiting ultra-low dielectric constants through POSS orientation into lamellar structures. *J. Mater. Chem.* **19**, 3643 (2009).

142. J. Choi, J. Harcup, A. F. Yee, Q. Zhu, R. M. Laine, Organic/Inorganic Hybrid Composites from Cubic Silsesquioxanes. *J. Am. Chem. Soc.* **123**, 11420 (2001).

143. R. Y. Kannan, H. J. Salacinski, P. E. Butler, A. M. Seifalian, Polyhedral Oligomeric Silsesquioxane Nanocomposites: The Next Generation Material for Biomedical Applications. *Acc. Chem. Res.* **38**, 879 (2005).

144. Y. Li *et al.*, Cascading One-Pot Synthesis of Single-Tailed and Asymmetric Multitailed Giant Surfactants. *ACS Macro Lett.* **2**, 1026 (2013).

145. J. D. Lichtenhan, Polyhedral oligomeric silsesquioxanes: building blocks for silsesquioxane-based polymers and hybrid materials. *Comment. Inorg. Chem.* **17**, 115 (1995).

146. S. H. Phillips, T. S. Haddad, S. J. Tomczak, Developments in nanoscience: polyhedral oligomeric silsesquioxane (POSS)-polymers. *Curr. Opin. Solid St. M.* **8**, 21 (2004).

147. F. Wang, X. Lu, C. He, Some recent developments of polyhedral oligomeric silsesquioxane (POSS)-based polymeric materials. *J. Mater. Chem.* **21**, 2775 (2011).

148. W. Zhang, B. Fang, A. Walther, A. H. Müller, Synthesis via RAFT polymerization of tadpole-shaped organic/inorganic hybrid poly (acrylic acid) containing polyhedral oligomeric silsesquioxane (POSS) and their self-assembly in water. *Macromolecules* **42**, 2563 (2009).

149. X. Yu *et al.*, Giant surfactants provide a versatile platform for sub-10-nm nanostructure engineering. *Proc. Natl. Acad. Soc.*, (2013).

150. P. Yin, D. Li, T. Liu, Solution behaviors and self-assembly of polyoxometalates as models of macroions and amphiphilic polyoxometalate-organic hybrids as novel surfactants. *Chem. Soc. Rev.* **41**, 7368 (2012).

151. A. J. Olson, Y. H. E. Hu, E. Keinan, Chemical mimicry of viral capsid self-

assembly. *Proc. Natl. Acad. Soc.* **104**, 20731 (2007).

152. B. Maier, J. O. Rädler, Conformation and Self-Diffusion of Single DNA Molecules Confined to Two Dimensions. *Phys. Rev. Lett.* **82**, 1911 (1999).

153. L. Wang, V. A. Bloomfield, Small-angle x-ray scattering of semidilute rodlike DNA solutions: polyelectrolyte behavior. *Macromolecules* **24**, 5791 (1991).

154. M. Sedlák, Generation of multimacroion domains in polyelectrolyte solutions by change of ionic strength or pH (macroion charge). *J. Chem. Phys.* **116**, 5256 (2002).

155. M. Sedlák, E. J. Amis, Concentration and molecular weight regime diagram of salt-free polyelectrolyte solutions as studied by light scattering. *J. Chem. Phys.* **96**, 826 (1992).

156. A. Müller, P. Kögerler, A. W. M. Dress, Giant metal-oxide-based spheres and their topology: from pentagonal building blocks to keplerates and unusual spin systems. *Coord. Chem. Rev.* **222**, 193 (2001).

157. C. L. Hill, Introduction: PolyoxometalatesMulticomponent Molecular Vehicles To Probe Fundamental Issues and Practical Problems. *Chem. Rev.* **98**, 1 (1998).

158. D. L. Caulder, K. N. Raymond, Supermolecules by Design. *Acc. Chem. Res.* **32**, 975 (1999).

159. D. Li, J. Zhang, K. Landskron, T. Liu, Spontaneous Self-Assembly of Metal−Organic Cationic Nanocages to Form Monodisperse Hollow Vesicles in Dilute Solutions. *J. Am. Chem. Soc.* **130**, 4226 (2008).

160. A. Gil *et al.*, A Journey inside the U28 Nanocapsule. *Chem.-Eur. J.* **18**, 8340 (2012).

161. M. Nyman, M. A. Rodriguez, T. M. Alam, The U28 Nanosphere: What's Inside? *Eur. J. Inorg. Chem.* **2011**, 2197 (2011).

162. D. Li, S. Simotwo, M. Nyman, T. Liu, Evolution of Actinyl Peroxide Clusters U28 in Dilute Electrolyte Solution: Exploring the Transition from Simple Ions to Macroionic Assemblies. *Chem.-Eur. J.* **20**, 1683 (2014).

163. P. C. Burns *et al.*, Actinyl Peroxide Nanospheres. *Angew. Chem. Int. Edit.* **44**, 2135 (2005).

164. P. Yin *et al.*, Self-Recognition of Structurally Identical, Rod-Shaped Macroions with Different Central Metal Atoms during Their Assembly Process. *J. Am. Chem. Soc.* **135**, 4529 (2013).

165. R. J. Hunter, *Zeta Potential in Colloid Science: Principles and Applications*. (Academic Press, 1988).

166. F. A. Cotton, G. Wilkinson, P. L. Gaus, R. Bryant, *Basic inorganic chemistry*. (Wiley New York, 1987).

167. F. W. Tavares, D. Bratko, H. W. Blanch, J. M. Prausnitz, Ion-Specific Effects in the Colloid−Colloid or Protein−Protein Potential of Mean Force: Role of Salt−Macroion van der Waals Interactions. *J. Phys. Chem. B* **108**, 9228 (2004).

168. K. H. Stern, E. S. Amis, Ionic Size. *Chem. Rev.* **59**, 1 (1959).

169. J. N. Hunt *et al.*, Tunable, High Modulus Hydrogels Driven by Ionic Coacervation. *Adv. Mater.* **23**, 2327 (2011).

170. A. Oleinikova *et al.*, Self-Association Based on Interfacial Structured Water Leads to {Mo154}≈1165 Super Clusters: A Dielectric Study. *ChemPhysChem* **8**, 646 (2007).

171. A. Chaumont, G. Wipff, Do Keggin anions repulse each other in solution? The effect of solvent, counterions and ion representation investigated by free energy (PMF) simulations. *C. R. Chim.* **15**, 107 (2012).

172. D. Li *et al.*, Viral-Capsid-Type Vesicle-Like Structures Assembled from M12L24 Metal–Organic Hybrid Nanocages. *Angew. Chem. Int. Edit.* **50**, 5182 (2011).

173. J. Szejtli, Introduction and general overview of cyclodextrin chemistry. *Chem. Rev.* **98**, 1743 (1998).

174. P. Yin *et al.*, Charge-Regulated Spontaneous, Reversible Self-Assembly of the Carboxylic Acid-Functionalized Hydrophilic Fullerene Macroanions in Dilute Solution. *Macromolecules* **48**, 725 (2015).

175. J. Zou, F. Tao, M. Jiang, Optical Switching of Self-Assembly and Disassembly of Noncovalently Connected Amphiphiles. *Langmuir* **23**, 12791 (2007).

176. M. L. Kistler, A. Bhatt, G. Liu, D. Casa, T. Liu, A Complete Macroion−"Blackberry" Assembly−Macroion Transition with Continuously Adjustable Assembly Sizes in {Mo132} Water/Acetone Systems. *J. Am. Chem. Soc.* **129**, 6453 (2007).

177. A. Nelson, Stimuli-responsive polymers: Engineering interactions. *Nat Mater* **7**, 523 (2008).

178. M. A. C. Stuart *et al.*, Emerging applications of stimuli-responsive polymer materials. *Nat Mater* **9**, 101 (2010).

179. E. G. Bellomo, M. D. Wyrsta, L. Pakstis, D. J. Pochan, T. J. Deming, Stimuli-responsive polypeptide vesicles by conformation-specific assembly. *Nat Mater* **3**, 244 (2004).

180. J. R. Capadona, K. Shanmuganathan, D. J. Tyler, S. J. Rowan, C. Weder, Stimuli-Responsive Polymer Nanocomposites Inspired by the Sea Cucumber Dermis. *Science* **319**, 1370 (2008).

181. M.-H. Li, P. Keller, Stimuli-responsive polymer vesicles. *Soft Matter* **5**, 927 (2009).

182. F. Liu, M. W. Urban, Recent advances and challenges in designing stimuli-responsive polymers. *Prog. Polym. Sci.* **35**, 3 (2010).

183. J. F. Mano, Stimuli-Responsive Polymeric Systems for Biomedical Applications. *Adv. Eng. Mater.* **10**, 515 (2008).

184. D. Roy, J. N. Cambre, B. S. Sumerlin, Future perspectives and recent advances in stimuli-responsive materials. *Prog. Polym. Sci.* **35**, 278 (2010).

185. X. Yan, F. Wang, B. Zheng, F. Huang, Stimuli-responsive supramolecular polymeric materials. *Chem. Soc. Rev.* **41**, 6042 (2012).

186. Zhang, M. A. Horsch, M. H. Lamm, S. C. Glotzer, Tethered Nano Building Blocks: Toward a Conceptual Framework for Nanoparticle Self-Assembly. *Nano Letters* **3**, 1341 (2003).

187. S. C. Glotzer, M. J. Solomon, Anisotropy of building blocks and their assembly into complex structures. *Nat Mater* **6**, 557 (2007).

188. X. Yu *et al.*, Giant Molecular Shape Amphiphiles Based on Polystyrene–Hydrophilic [60]Fullerene Conjugates: Click Synthesis, Solution Self-Assembly, and Phase Behavior. *J. Am. Chem. Soc.* **134**, 7780 (2012).

189. X. Yu *et al.*, A Giant Surfactant of Polystyrene−(Carboxylic Acid-Functionalized Polyhedral Oligomeric Silsesquioxane) Amphiphile with Highly Stretched Polystyrene Tails in Micellar Assemblies. *J. Am. Chem. Soc.* **132**, 16741 (2010).

190. S. Fujishige, K. Kubota, I. Ando, Phase transition of aqueous solutions of poly(N-isopropylacrylamide) and poly(N-isopropylmethacrylamide). *J. Phys. Chem.* **93**, 3311 (1989).

191. M. Heskins, J. E. Guillet, Solution Properties of Poly(N-isopropylacrylamide). *J. Macromol. Sci. Chem. A* **2**, 1441 (1968).

192. H. G. Schild, Poly(N-isopropylacrylamide): experiment, theory and application. *Prog. Polym. Sci.* **17**, 163 (1992).

193. M. J. Hey, J. M. Clough, D. J. Taylor, Ion effects on macromolecules in aqueous solution. *Nature* **262**, 807 (1976).

194. L. B. Sagle *et al.*, Investigating the Hydrogen-Bonding Model of Urea Denaturation. *J. Am. Chem. Soc.* **131**, 9304 (2009).

195. P. H. Von Hippel, T. Schleich, Ion effects on the solution structure of biological macromolecules. *Acc. Chem. Res.* **2**, 257 (1969).

196. Y. Zhang, P. S. Cremer, Interactions between macromolecules and ions: the Hofmeister series. *Curr. Opin. Chem. Biol.* **10**, 658 (2006).

197. C. d. l. H. Alarcon, S. Pennadam, C. Alexander, Stimuli responsive polymers for biomedical applications. *Chem. Soc. Rev.* **34**, 276 (2005).

198. C. Alexander, K. M. Shakesheff, Responsive polymers at the biology/materials science interface. *Adv. Mater.* **18**, 3321 (2006).

199. D. Schmaljohann, Thermo- and pH-responsive polymers in drug delivery. *Adv. Drug Deliv. Rev.* **58**, 1655 (2006).

200. H. N. Miras, J. Yan, D.-L. Long, L. Cronin, Engineering polyoxometalates with emergent properties. *Chem. Soc. Rev.* **41**, 7403 (2012).

201. M. Nyman, P. C. Burns, A comprehensive comparison of transition-metal and actinyl polyoxometalates. *Chem. Soc. Rev.* **41**, 7354 (2012).

202. W.-B. Zhang *et al.*, Molecular Nanoparticles Are Unique Elements for Macromolecular Science: From "Nanoatoms" to Giant Molecules. *Macromolecules*, (2014).

203. P. Mialane, A. Dolbecq, F. Secheresse, Functionalization of polyoxometalates by carboxylato and azido ligands: macromolecular complexes and extended compounds. *Chem. Commun.*, 3477 (2006).

204. A. Proust *et al.*, Functionalization and post-functionalization: a step towards polyoxometalate-based materials. *Chem. Soc. Rev.* **41**, 7605 (2012).

205. B. Xu, Y. Wei, C. L. Barnes, Z. Peng, Hybrid Molecular Materials Based on Covalently Linked Inorganic Polyoxometalates and Organic Conjugated Systems. *Angew. Chem. Int. Edit.* **40**, 2290 (2001).

206. X. Yan, P. Zhu, J. Fei, J. Li, Self-Assembly of Peptide-Inorganic Hybrid Spheres for Adaptive Encapsulation of Guests. *Adv. Mater.* **22**, 1283 (2010).

207. P. Yin *et al.*, Exploring the Programmable Assembly of a Polyoxometalate–Organic Hybrid via Metal Ion Coordination. *J. Am. Chem. Soc.* **135**, 13425 (2013).

208. Y. Yang *et al.*, Photo-Responsive Self-Assembly of an Azobenzene-Ended Surfactant-Encapsulated Polyoxometalate Complex for Modulating Catalytic Reactions. *Small* **8**, 3105 (2012).

209. Y. Yan *et al.*, Synthesis and redox-responsive self-assembly of ferrocene grafted Anderson-type polyoxometalate hybrid complexes. *Soft Matter* **8**, 1593 (2012).

210. J. Keggin, in *Proceedings of the Royal Society of London A: Mathematical, Physical and Engineering Sciences*. (The Royal Society, 1934), vol. 144, pp. 75-100.

211. S. Aoki, T. Kurashina, Y. Kasahara, T. Nishijima, K. Nomiya, Polyoxometalate (POM)-based, multi-functional, inorganic–organic, hybrid compounds: syntheses and molecular structures of silanol-and/or siloxane bond-containing species grafted on mono-and tri-lacunary Keggin POMs. *Dalton Trans.* **40**, 1243 (2011).

212. J. N. Israelachvili, D. J. Mitchell, B. W. Ninham, Theory of self-assembly of hydrocarbon amphiphiles into micelles and bilayers. *J. Chem. Soc., Faraday Trans.* **72**, 1525 (1976).

213. R. Freitag, F. Garret-Flaudy, Salt Effects on the Thermoprecipitation of Poly-(N-isopropylacrylamide) Oligomers from Aqueous Solution. *Langmuir* **18**, 3434 (2002).